2019

Organizing 6, 5-Carbon nanotubes on DNA origami arrays

Kathryn A. Pitton
kathrynpitton@gmail.com

ORGANIZING 6, 5- CARBON NANOTUBES ON DNA ORIGAMI ARRAYS

A thesis submitted to
the Graduate College of
Marshall University
In partial fulfillment of
the requirements for the degree of
Master of Science
In
Chemistry
by
Kathryn A. Pitton
Approved by
Dr. Michael Norton, Committee Chairperson
Dr. Bin Wang
Dr. Scott Day

Marshall University
May 2019

APPROVAL OF THESIS

We, the faculty supervising the work of Kathryn Ann Pitton, affirm that the thesis, *Organizing 6,5- Carbon Nanotubes on DNA Origami Arrays*, meets the high academic standards for original scholarship and creative work established by the Chemistry Department and the Graduate College of Marshall University. This work also conforms to the editorial standards of our discipline and the Graduate College of Marshall University. With our signatures, we approve the manuscript for publication.

4/24/19

Dr. Michael Norton, Department of Chemistry — Committee Chairperson — Date

4/24/2019

Dr. Bin Wang, Department of Chemistry — Committee Member — Date

B. Scott Day — 4/24/2019

Dr. Scott Day, Department of Chemistry — Committee Member — Date

ACKNOWLEDGMENTS

My first and most important acknowledgement is to my advisor, Dr. Michael Norton. He introduced me to carbon nanotubes and provided me an opportunity to work on a project and subject I am so passionate about. Through his guidance, I have developed skills in learning, writing, researching and thinking that I did not know I was capable of. Thank you, Dr. Norton for providing me with your valuable guidance. I would like to thank Dr. Bin Wang and Dr. Scott Day for agreeing to be on my committee and always open to any questions or concerns. Thank you to David Neff for two years of help with endless questions, helpful understanding, experimental design, and for continuous laughs throughout my years here. I would have been truly lost every day without you. I would like to thank Marshall University for giving me all the tools I need to advance my career. Thank you to the NSF and MURC for funding my research. Finally, thank you to my friends and family back in Florida.

TABLE OF CONTENTS

LIST OF TABLES

LIST OF FIGURES

ABSTRACT

Carbon nanotubes[1] are cylindrical carbon molecules and can be considered to be composed of one atom thick sheets of carbon called graphene. They have been at the forefront of nanochemistry due to their strength and multiple properties such as absorption, fluorescence, semiconduction, and light scattering capability. DNA Origami (DO)[2] has emerged as a novel domain for molecular design, resulting in the generation of numerous one, two, and three-dimensional structures that have provided platforms for the organization of organic species and inorganic nanoparticles through simple modifications. The use of DNA Origami to control the placement of single walled carbon nanotubes (SWCNT) with precise alignment,[3] purity and length would be a significant advance in controlled nanoscale organization.[4] G-quadruplex (G4) secondary structures are guanine rich ssDNA sequences which fold to create square planar guanine tetrads.[5] When G4 is introduced to Hemin, a (G4)/hemin-based DNA enzyme (DNAzyme) self assembles and possesses horseradish peroxidase (HRP)-mimicking catalytic properties.[6] In this work, multiple approaches for the immobilization of SWCNTs at precisely designated locations on cross shaped DNA origami[7] were implemented, and the results interpreted.

CHAPTER 1

REVIEW OF DNA ORIGAMI, SINGLE WALLED CARBON NANOTUBES, AND IMMOBILIZATION APPROACHES

With the increase of human dependence on technology, the need for smaller, more effective tools is of the highest importance. Scientists have been handed the task of creating compact, efficient instruments/tools at a nanoscale level. DNA origami and carbon nanotubes, both discovered and developed within the past thirty years, hold promise for the future of nanoscale technology both as platforms for arranging objects of interest and for performing nanoscale modifications. With recent nanoscale advancements, the pace of research has accelerated in many areas, including electronics, mechanics, medicine, and single molecule applications. The review presented here takes a closer look at these relatively new nanoscale components and their relevance to achieving the objectives of this project.

DNA Origami

With the invention of the scanning tunneling microscope and the synthesis of fullerenes in the 1980s,[8] came the birth of nanotechnology and nanotechnological applications. The beginning stages of nanotechnology focused on building complex structures through top down fabrication often involving etching processes. Engineering of these structures became increasingly more expensive, leading scientists to look for self-assembling materials, which would not only be cheaper, but easier to construct using methods now referred to as molecular nanotechnology. In 1982, Nadrian Seeman published *Nucleic Acid Junctions and Lattices* and is credited as the inventor of DNA nanotechnology.[9] This revolutionary paper used the principles of simple DNA base pairing to enable construction of three-dimensional shapes. In 2006, Paul K. Rothemund employed this idea to fold one long single stranded DNA sequence using small

"staple strands" to direct this self-assembly, creating what is now generally known as DNA Origami (DO).[2] DO is a powerful tool for the design and assembly of nanomaterials on platforms programmed to adopt a variety of functional shapes. Both "soft" (organic) and "hard" (inorganic) materials can be organized into patterns with close proximity and high resolution on these DNA based origami substrates. Since its initial invention, DO has evolved into applications involving but not limited to drug delivery systems[10] and platforms for placement of single molecules.[11]

DO can be described as scaffolded self-assembling, bottom up nanostructures created through the folding of a long ssDNA backbone (commonly the M13 viral genome) directed by ~200 short synthetic oligonucleotides, or "staples" when reacted via a decrementing temperature gradient. Their shape is dependent on the staples' sequence [2] allowing for different shapes to be formed depending on which would be best suited for a particular function. The predictability of the base pairing of DNA allows for the ability to organize nanostructures through simple staple modifications. The DO construct used in this research is aptly named Cross Origami-01 (CO-01),[7] and consists of two mutually orthogonal overlapping rectangular strips forming the cross structure shown in Figure 1. The size, ease of self-assembly, and simplicity of staple modifications makes CO-01 an ideal platform for the immobilization of carbon nanotubes.

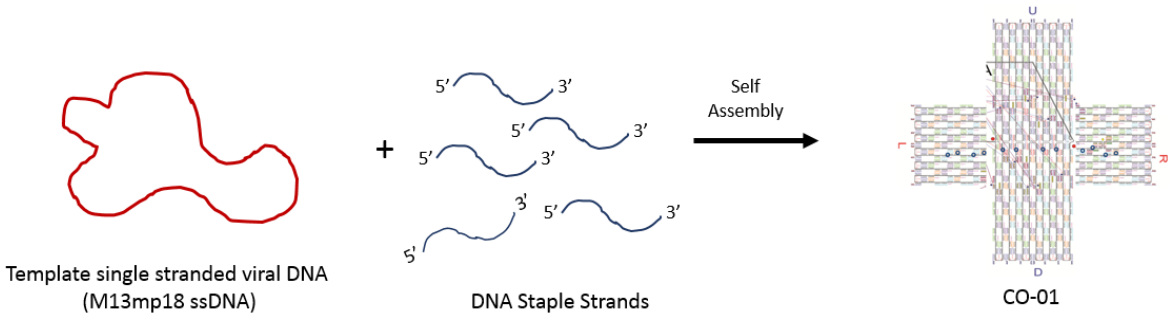

Figure 1. Self-Assembly of DNA Origami
Figure 1 depicts how a single stranded circular viral M13 DNA plasmid is reacted with ~200 synthetic oligonucleotides measuring ~32 bases long, and self-assembles into the cross shaped DO, CO-01.

0D and 1D Linear Arrays

Just as monomer molecular units are combined to make polymers, Cross Origami can be arranged in a variety of arrays such as 0D, 1D, and 2D with 0D being one single cross origami (monomer) and 1D being a linear array of monomer units. 0D Origami are produced as single, free floating crosses created in solution. 1D origami is constructed using two extra components: A) staples modified with sticky ends and B) terminating ends. A second, lower temperature annealing process is applied. As shown in Figure 2A, the modified staples, or "sticky ends," present three base overhangs designed for the left and right arms of CO-01 whereas the terminating staples provide the terminating CO-01 (CO-01TR) with six overhangs of 5 Ts on the right arm (Figure 2B). The sticky ends are integrated into the CO-01 origami at their left and right arms to concatenate the structures. A 1:7 ratio of terminating structures to CO-01 ideally forms a 7-10-monomer linear array of 1D CO-01 (Figure 3). 2D origami would be a planar array and although in ideal form it could improve organization, in practice it has proven to be more difficult to synthesize.

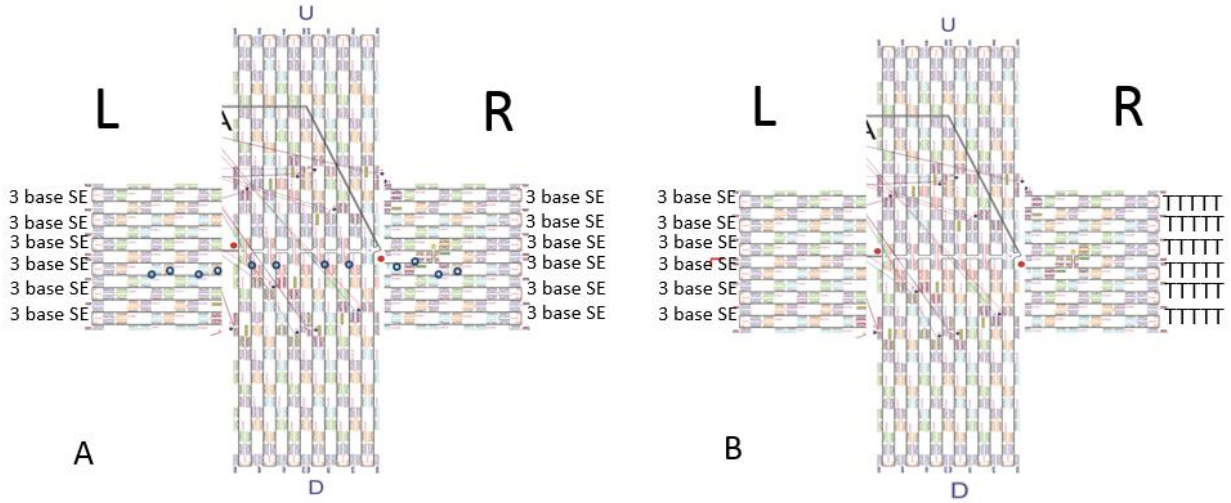

Figure 2. CO-01 modified to form 1D linear arrays
The two components that form 1D linear arrays of CO-01. (A) Shows the 3 base sticky ends that bind to the left and right arms of CO-01 so the 0D CO-01 can bind through their left and right arms. The linear growth is stopped by terminating with CO-01TR, (B) shows the six locations of the 6 $(PolyT)_5$ (not to scale). The terminating CO-01 structure does not include any additional modifications (i.e. docking sites or biotin tethers).

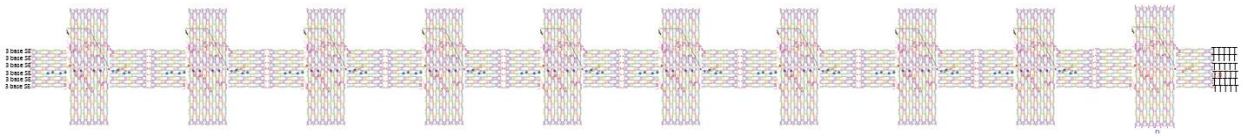

Figure 3. 1D linear array of CO-01
Figure 3 depicts a 10-monomer linear array of CO-01 predicted to result from a 1:9 terminating end to monomer origami ratio. The left arm on the far-left origami shows the three base sticky ends unbound. The far right CO-01 shows the six locations of the 5 poly Ts, which terminate the linear growth.

Introduction to 6, 5-Single Walled Carbon Nanotubes

Carbon nanotubes were discovered in the early 1990s[1] and have become one of the allotropes of elemental carbon with exceptionally high interest due to their incredible strength, unique fluorescence, absorption, light scattering, and electrical properties.[12] Because they are comprised entirely of sp^2 and pi bonds formed between individual carbon atoms, they are known for being the strongest materials discovered in terms of tensile strength. A length to diameter ratio of up to 132,000,000:1 has been observed.[13] Single walled carbon nanotubes (SWCNTs)

are members of the fullerene structural family and can be considered to be single layer graphene sheets rolled into hollow cylindrical tubes with their edges joined. Due to the wide range of CNT properties and the possibilities of highly efficient controlled nanoscale devices, combined functionalization of CNTs and DO have gained interest with researchers. Figure 4 shows the basic structure of an example SWCNT.

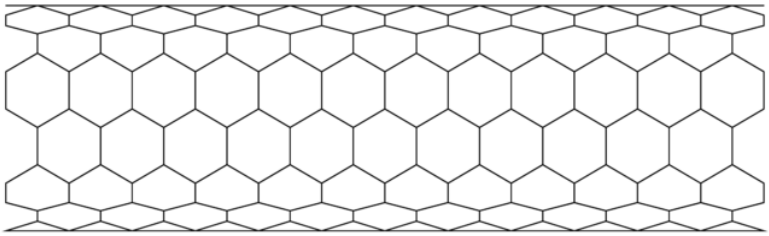

Figure 4: 6, 5-Single Walled Carbon Nanotube Structure[14]
A computer-generated model depicting the 6, 5- single walled carbon nanotube.

CNT synthesis is most often performed through catalysis in two ways; high pressure carbon monoxide (HiPco) and cobalt molybdenum catalysis (COMOCAT).[15] The importance of using a gas phase catalytic method is to ensure the solid catalyst can be tailored to maximize the selectivity of controlled synthesis of SWCNTs of desired chirality. A Co-Mo/SiO_2 catalyst with 6 wt % total metals and a Co:Mo molar ratio of 1:2 showed the highest selectivity towards SWNTs. The 1:2 molar ratio of cobalt and molybdenum is heated in the presence of hydrogen to 500°C, then further heated in the presence of helium to 700°C. Once optimal temperature is reached, carbon monoxide (CO) is introduced at a rate of 100 cm^3/min and the nanotubes grow on the catalyst particles to form these hollow cylinders. While this is the common method of synthesizing CNTs, it is only approximately 40% effective for giving the desired chirality (6,5),[15] therefore enhancing the synthetic efficiency is of scientific interest. This procedure is performed commercially and was not performed in our laboratory.

Since the discovery of SWCNTs, their unique properties have captured the attention of scientists and engineers in research and industry alike. While many applications require short,

monodisperse nanotubes as small as ~100 nm in length, in their raw form, CNTs are of uncontrolled lengths, up to micrometers in length and entangled with each other much like woven rope. DO with modifications could provide a solution to control placement, alignment and enable modification of CNTs. Previous work has achieved alignment of CNTs on the outer arms of cross shaped CO,[3] but enabling origami functionalization with CNTs placed along their central axis could provide greater versatility in controlling spatially defined interactions.

Nanotubes can be utilized for applications in a variety of fields including, but not limited to, electronics, medicine, with scientific applications including FRET based sensors. An interesting application currently being studied is cancer sensing utilizing CNT's fluorescent properties.[16] Biocompatible nanoparticles produced in a layer-by-layer manner, and incorporating, DNA, RNA, diagnostic agents and drugs are currently being tested in approaches directed at the treatment of ovarian cancer. CNTs are also being applied to electronics as a way to maximize battery efficiency. A group at the Georgia Institute of Technology is applying SWCNTs as nets anchored to battery material through poly[3-(potassium-4-butanoate) thiophene] (PPBT). The carboxylate groups and the thiophene backbone interface with the SWCNTs to create an electron flow through the nanotube nets and battery materials.[17] Another application of CNTs involves Nano sensing based on fluorescence resonance energy transfer (FRET) between graphene based quantum dots and CNTs for DNA detection with high sensitivity and selectivity.[18]

Carbon nanotubes come in two different categories in terms of graphene layers; single walled carbon nanotubes and multi-walled carbon nanotubes. This work focuses on single walled carbon nanotubes, or more specifically, 6, 5-SWCNTs because of their semiconducting, fluorescent capabilities. Each type of SWCNT has a unique set of characteristics, defined by

layer number, chirality, and chiral angle θ. The chiral vector of specific CNTs are defined by their vector values, n, m. The n and the m specify two unit vectors that are required for two carbon-carbon bond axes in the planar lattice to wrap and create their signature seamless hollow tube, further defining d and θ.[19] The specific n values give insight to how the carbon-carbon bonds orient if the tube were bisected, leading to information on their electron conduction properties. Through hypothetical bisections of C_{60}-derived carbon nanotubes (fullerene), axis folding of graphene can determine whether a nanotube is "armchair" or in "zigzag" conformation.[20] These axes are classified referring back to the vector values. For example, (n, 0) means the carbon-carbon bonds are parallel to the tube axis (zig-zag conformation), (n, n) value indicates that some carbon-carbon bonds are perpendicular to the tube axis (armchair conformation), and the (m, n) values indicate a chiral conformation containing species with either left or right-handed twists (Figure 5).

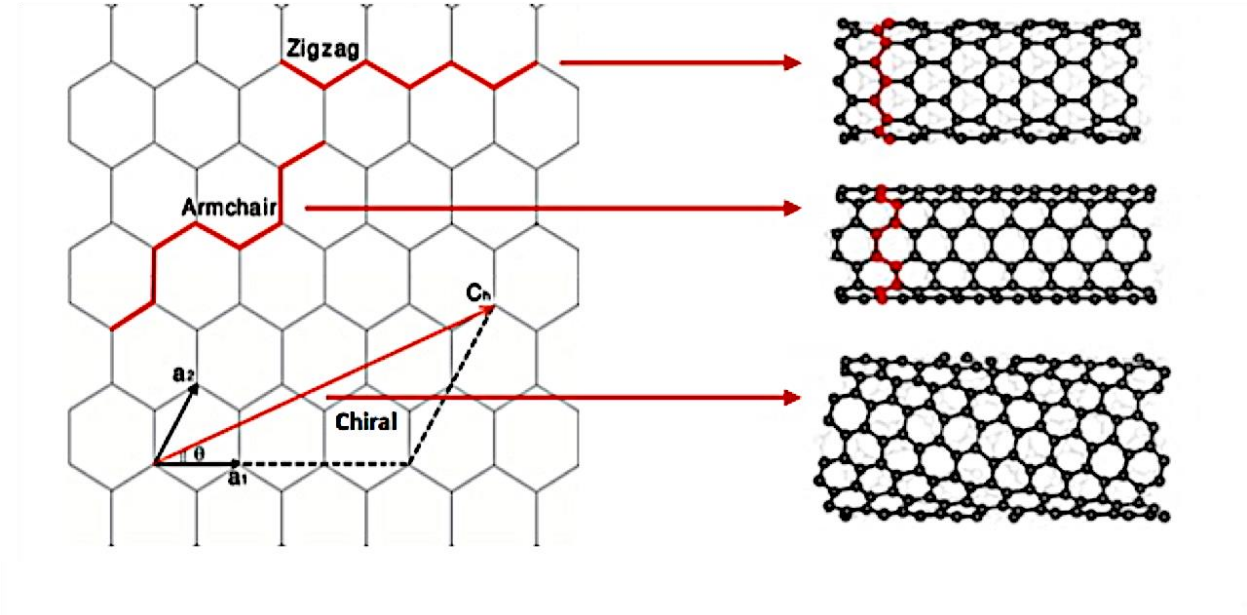

Figure 5: Zigzag, Armchair and Chiral Twists of SWCNTs
Depicting the different vector values a_1 and a_2 and the chiral angle θ. [21]

Armchair conformations possess metallic properties whereas zig-zag and chiral tubes possess semiconductive properties. The classifications of CNTs names defining chiral and conductive properties are tabulated in a way known as the periodic table of carbon nanotubes shown in Figure 6.[22] Calculations for chiral angles and diameters are provided in the supplementary information (Appendix C). Referring to Figure 6, it is relatively easy to infer that the 6, 5-SWCNTs have an n, m value of 6, 5, making it a chiral tube possessing semiconductive properties.

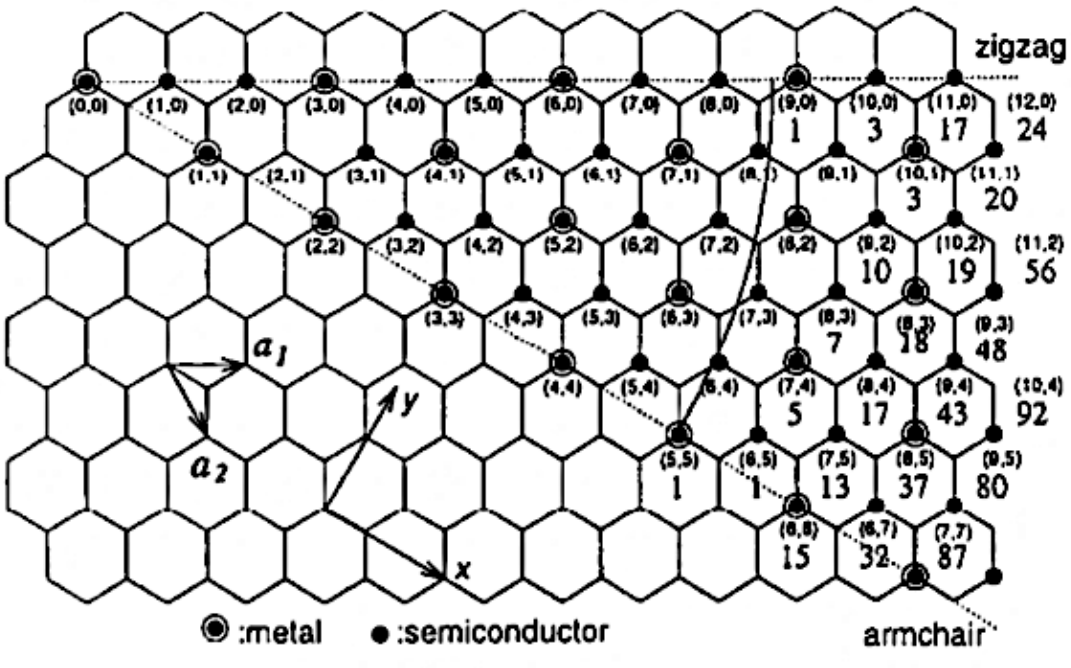

Figure 6. Periodic Table of Carbon Nanotubes
A two-dimensional graphene sheet illustrating the vectors that specify the different chiralities and properties of carbon nanotubes. The numbers in parenthesis indicate the (n, m) values and further define the zigzag and armchair conformations of the tubes. The circles and dots denote the electronic properties of each type of CNT. [22]

Solubilization of Carbon Nanotubes

CNTs in their natural state are hydrophobic, insoluble in water, and due to industrial COMOCAT synthesis being only ~40% selective for specific chiralities, many samples of SWCNTS need a separation of tubes into a single chirality to ensure the desired nanotube is

being used for downstream methods/further research. To solubilize nanotubes, a method of using short DNA sequences (40 bases and 18 bases) known as recognition sequences[23] which have periodic purine-pyrimidine patterns, can bind to or encircle selectively nanotubes of a defined chirality to enable both solubility in water and a first pass purification technique. This interaction is often called wrapping, because it provides a coating of DNA that allows for the selection of specific chiralities and enhances solubility in water, which is useful for further processing in aqueous solutions. Referring to Tu, [23] et al. and Mangalum, et al. [3] 6,5-SWCNTs can bind with some selectivity to a $(TAT)_4$ sequence and non-selectively to T_{40}.[24] Wrapping nanotubes in DNA sequences is performed through a sonication and centrifugation process.

Prior Immobilization Designs

Due to the relative novelty of the observation of nanotube and DNA interactions, an opportunity has been provided to review a large portion of the existing literature on the subject.

In 2010, *Self-assembly of Carbon Nanotubes into Two-Dimensional Geometries Using DNA Origami Templates* was published.[24] The approach was to align nucleic acid-labelled SWNTs along lines of complementary ssDNA "hooks" within the DNA origami. A rectangular origami template was modified with a pattern of hooks that projected from the origami in a cross shaped fashion. The SWNTs were exposed in solution and presumably wrapped in a solution of 40 base poly T domains and 20 base labeling domains which were complimentary to the DNA Origami template "hooks." Toeholds on the SWNT allowed binding on a hook, causing release of a protection strand, and leaving a CNT in a crosslinked form that was judged to be selective based on the SWNT's conducting or semiconducting properties.

Following Rothemund, in 2011 *Assembly of Single-Walled Carbon Nanotubes on DNA-Origami Templates through Streptavidin-Biotin Interaction* was published.[25] This approach

used the well-known interaction between streptavidin and biotin to initiate immobilization on origami surfaces. The nanotubes were wrapped in ssDNA modified with biotin molecules, and the DNA Origami was modified with biotin docking sites, allowing for interaction of the two reagents upon introduction of the multivalent streptavidin.

In 2013, *Site-Specific Immobilization of Single-Walled Carbon Nanotubes onto Single and One-Dimensional DNA origami* was published.[3] 6, 5-SWCNTs were wrapped with ssDNA and self-assembled onto various origami constructs such as single rectangular origami, single cross origami (0D CO-01), and one dimensional cross origami arrays (1D CO-01). CO was modified for CNT interactions by removal of some staples to leave ssDNA rich M13 domains prepared to immobilize SWCNTs at site specific locations.

As previously mentioned, discrete lengths of nanotubes are of scientific interest, resulting in the publication of *DNA Origami Templated Self-assembly of Discrete Length Single Wall Carbon Nanotubes*.[4] This work utilized triangular shaped DNA Origami modified with ssDNA probes emerging from the periphery. Size exclusion HPLC isolated uniform lengths of nanotubes, which were then wrapped with ssDNA that possessed two domains; one for nanotube binding, and a capture domain selected for recognition by the ssDNA probes on the origami surface. This process led to origami with an "outline" composed of nanotubes surrounding the triangle.

CHAPTER 2

PROPOSED APPROACH AND DESIGN

Although the tools described are interesting in their own right, one may ask why DNA Origami and Carbon Nanotube hybridization studies are significant. Due to their diverse range of properties, carbon nanotubes are of interest for developing a variety of applications as mentioned earlier. However, because of the natural state of nanotubes (tangled ropes and solubilization issues), scientists currently have poor spatial control, making them difficult to utilize for practical applications. Utilizing DNA Origami based alignment of carbon nanotubes would offer a gateway to long term applications in the previously described areas, as well as allow for multiply functionalized origami systems.

We propose that placement of one CNT down specially designed staple modifications, also known as docking sites, along a ~10 monomer 1D linear array CO-01 could provide a desired placement. Using base sequence changes, several staple sequences in the CO design were modified to enable CNT immobilization down a central line of a linear array of DNA Origami (Figure 7).

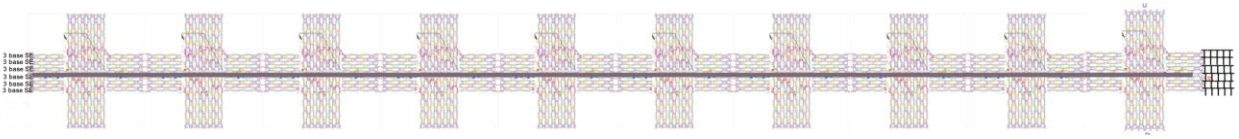

Figure 7. Immobilization Design of a Linear Array of CO-01 with a Single Carbon Nanotube Immobilized Down the Center.
Figure 7 depicts the proposed basic design of SWCNT and CO-01 immobilization through a 1D linear array of CO-01 averaging 7-10 monomer units, with one single 6, 5-SWCNT located down the center of the full array, reflecting controlled placement.

This design is expected to enable linear placement of carbon nanotubes, and present the tubes such that they can be readily observed, measured and analyzed. The impact of different deposition techniques on imaging and analysis of CNTs on the origami surface is also an

important consideration. With nanotubes docked in a controlled position, the applications of further modification on the CNTs and/or the origami were also investigated.

CHAPTER 3

DNAZYME COMPLEX

One reason to develop successful approaches for the immobilization of CNTs onto the surface of origami, is that such localization is a necessary step toward developing techniques to cut CNTs at controlled sites. Immobilization of CNTs onto origami surfaces would not only allow fabricating CNTs with precisely defined lengths, which are required for some transistor applications,[26] but would also enable the production of defects at precisely defined locations. Cutting nanotubes is done by cleaving the carbon-carbon bonds within the sp^2 lattice and since CNTs have been proven to be unusually strong, this mechanical method appears to be impractical. Although CNTs are highly resistant to degradation, they have been biodegraded using myeloperoxidase, a very strong oxidation bio-catalyst.[27] Cutting nanotubes has also been previously demonstrated using piranha solutions on tubes synthesized through the HiPco method;[28] however, this poorly controlled approach would presumably oxidize all organics in the reaction volume, not specific locations designated by the DNA origami. To provide localized degradation, DNAzymes have emerged as a new solution for cutting nanotubes without harming the DNA substrates.

DNA enzymes (DNAzymes), or deoxyribozymes are catalytically active molecules similar to other biological enzymes such as RNA enzymes (ribozymes) or proteins.[29] In the early 1990s, a variety of ribozymes had already been identified in biological systems, so interest in development of DNA as an enzyme increased in popularity because DNAzymes would be less expensive, easy to label, and more stable against heat.[30] In 1994 the first DNAzyme was developed by Breaker and Joyce[31] with identification of a DNA catalyst that displayed linkage in vitro. There have been no naturally occurring DNAzymes discovered so chemical synthesis is

the only method for DNAzyme formation to date.[32] Currently, the majority of DNAzymes that have been characterized fall under the category of RNA cleavage, but DNAzymes have shown catalytic properties of ligation, dimer repair, horseradish peroxidase mimicking activity, and there are reports of various bond-forming DNAzymes.[30,33] Using the catalytic properties of a DNAzyme, one can react the carbon-carbon bonds of a carbon nanotube with oxygen through peroxidase mediated oxidation.[34] The two specific types of DNAzyme used in this research are each formed from two components; G-quadruplex DNA (G4) and Hemin, but there have been other methods to break the bonds of carbon nanotubes. In 2009, using oxygen to break carbon-carbon bonds in a nanotube was achieved by "unzipping" nanotubes into graphene nanoribbons. Using permanganate in acid, manganate esters are formed and further oxidation creates diones. The creation of diones along with the continued oxidation causes strain on adjacent bonds, which helps facilitate the creation of ketones, causing an "unzipping" effect on the nanotube, where it structurally changes from a seamless, hollow cylinder, to a "ribbon," or sheet of graphene. This technique is outlined in Figure 8 from the paper "*Longitudinal unzipping of carbon nanotubes to form graphene nanoribbons.*"[35]

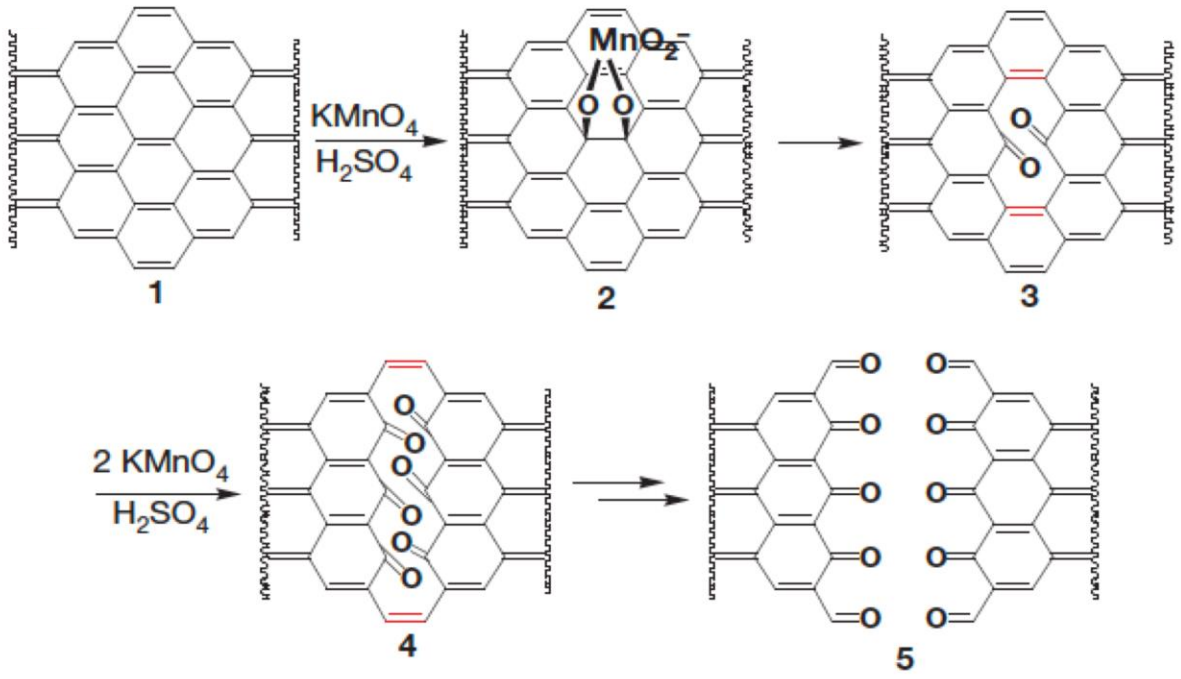

Figure 8: Proposed Chemical Mechanism of Oxidative Nanotube Unzipping[35]
Upon introducing the nanotube carbon-carbon pi bonds to potassium permanganate in the presence of an acid, a manganate ester is formed, creating strain on the adjacent pi bonds. Further oxidation and strain on the pi bonds drives continued ketone formation, causing the eventual unzipping of a nanotube.

Introduction to G-quadruplex DNA and Hemin

Since the 1960s, it has been known that guanines self-associate to form four-stranded helical structures.[36] Subsequently it has been observed that some DNA sequences found in telomeres form G-quadruplex structures in vitro.[37] G-quadruplexes are secondary structures formed by guanine rich nucleic acid sequences that form guanine tetrads. Through Hoogsteen hydrogen bonding, four guanine bases are capable of forming a square planar structure, and two or more tetrads can stack on top of each other to form the general G-quadruplex (G4) design.[5] The tetrad structure is stabilized by the presence of a cation, most commonly potassium or sodium, which sits in the center channel of each tetrad, through chelated K^{+}-$O^{\delta-}$ coordination

(Figure 9).[5, 38]

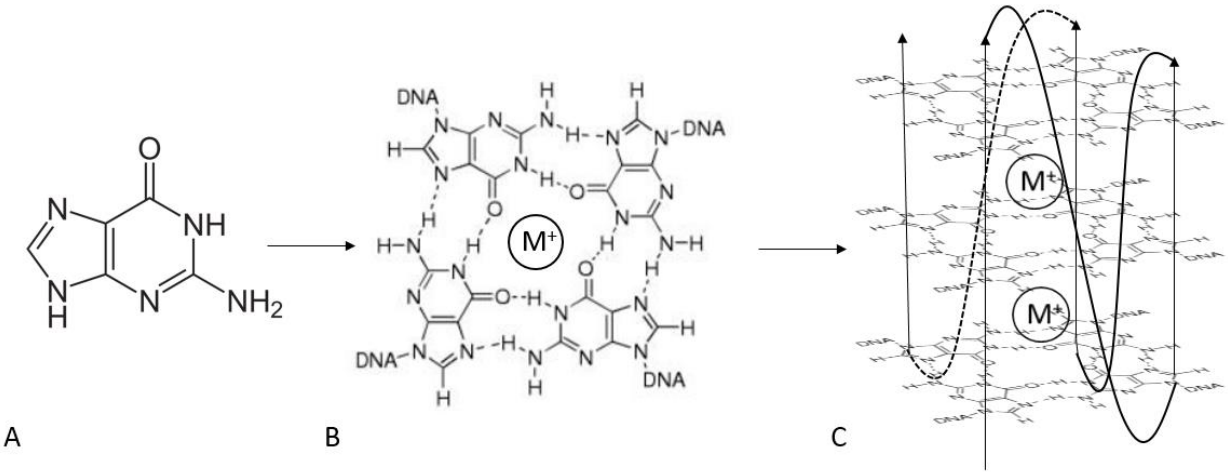

Figure 9: Structure of G-Quadruplex DNA
A) Structure of a single guanine. B) Four guanines hydrogen bond to make a single square planar structure. C) Through the addition of a cation, two or more of the square planar structures form a tetrad generally known as G4. The arrows depict the loop conformation typical of an intramolecular parallel Gquad design from 5' to 3'.[39]

The strands that form the tetrads can adopt a number of loop configurations forming parallel or antiparallel topologies as well as intra and inter-molecular folds, making them highly polymorphic, and allowing for varying strength of enzyme like activity.[5, 40] Unlike DNAzymes, which are a complex, an individual guanine rich DNA strand is capable of forming in the human genome naturally; however, the specific function of many of these natural G4 structures is not entirely understood or categorized. There is some evidence that G-quadruplexes function in DNA replication, telomere function and gene expression.[41] G4 can associate with hemin at high affinities to form peroxidase-mimicking G4 DNAzymes, sometimes called hemin-binding aptamers (HBAs).[42] These catalytic HBAs mediate the reaction between H_2O_2 and several substrates, including 2, 2'-azino-bis(3-ethylbenzothiazoline-6-sulfonic acid)diammonium salt (ABTS), 3, 3'-diaminobenzidine (DAB), and a number of other fluorescent, colorimetric, and chemiluminescent substrates. [43-44]

Hemin, found in the hemoglobin of human blood, is an iron-containing porphyrin with a central Fe^{+3} ion and a coordinating chloride ligand. Hemin is protoporphyrin IX, which is one of the most common organic porphyrins in nature and contains a ferric iron (Fe^{3+}) shown in Figure 10.[45] The affinity of hemin binding to G-quadruplex DNA is determined by the topology and loop conformation of the G-quadruplex sequence. Previous research has indicated that parallel loop conformations provide the highest hemin binding affinity,[43] therefore one parallel G-quadruplex sequence and one mixed type hybrid sequence (three parallel and one anti-parallel orientation) were prepared for this work. Both parallel and hybrid mixed orientations were used based on their k_{cat} number, or the number of times each enzyme site converts substrate to product per unit of time (s^{-1}).[48]

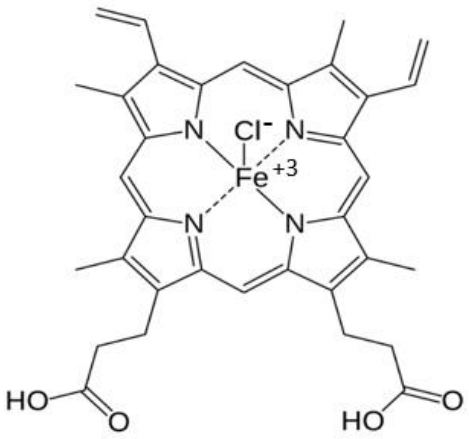

Figure 10: Structure of Hemin[45]
Image of the structure of the hemin compound found in nature.

When hemin is introduced to G-quadruplex structures in the presence of one of the cations mentioned previously, the hemin is able to bind to the external guanines in a quadruplex complex through end stacking.[46] This binding mimics the His residue[47] of a horseradish peroxidase (HRP) enzyme, displaying much higher peroxidase like activity than hemin alone. A

schematic of the interaction of Hemin and a G-quadruplex to form a DNAzyme is shown in Figure 11.

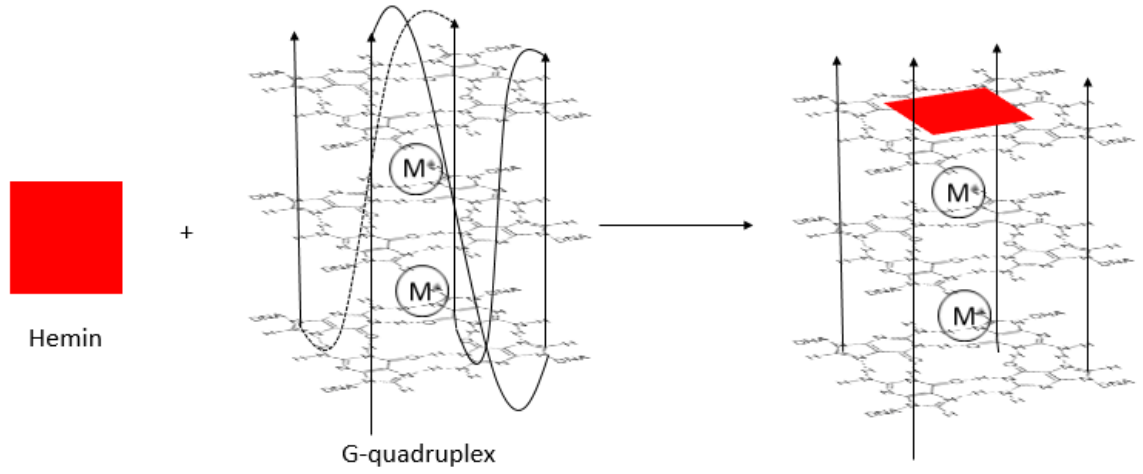

Figure 11. Complexation of G-quad with Hemin to Create a DNAzyme
The interaction between a hemin molecule and a folded G-quadruplex to make a DNAzyme. For simplicity and visibility, the hemin has been depicted as a red square. Upon interaction with a G-quadruplex, the hemin's iron loses its chloride and forms an axial coordination with the G-quadruplex.

DNA Origami Modifications for G-quadruplex DNA Insertion

Each G-quadruplex sequence was modified with a staple sequence which addressed the G-Quad to a specific location on the origami. For the CO-01 construct with twelve central $(TAT)_{10}$ docking sites, one staple on the left arm was modified with the G-quadruplex sequence EAD2[48] in line with the docking sites. These placements will cause the G-quad to be aligned with the docking sites, landing the CNT within direct or in close proximity to the G-quad. After oxidative cutting, the locations of the G-quad (thereby the potential cut sites) will yield ~100 nm distances between the ends of the CNTs on a 1D linear array of CO-01 (Figure 12). For the CO-01 construct with eight central Biotin docking sites, two staples (one on the left and one on the right arm) were modified to carry the PS2M[48] G-quadruplex staple. Due to the CO-01 biotin constructs being in a 0D formation, having two G-quads would allow for cutting on both arms to

create a single CO-01 construct with an individual CNT functionalized down the center at a calculated distance of approximately 83 nm (Figure 13).

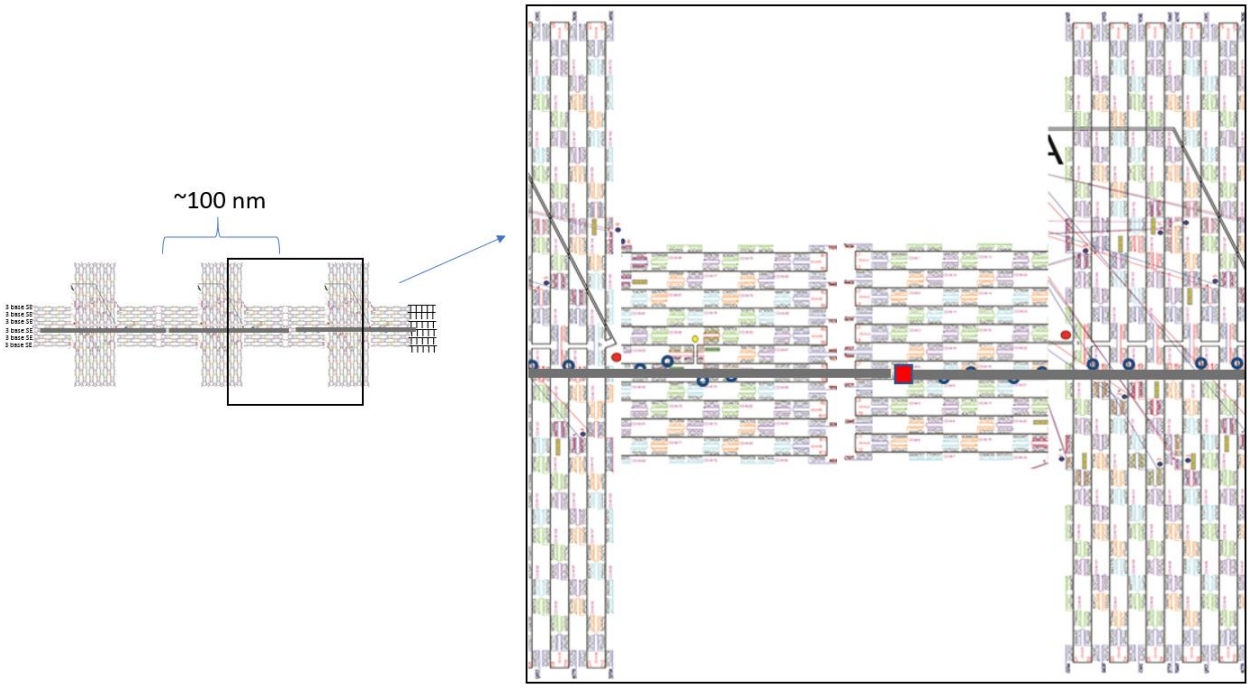

Figure 12: Schematic of Cuts on a CNT Aligned Along a 1D Linear Array of CO-01
A depiction of a linear array of CO-01 with twelve central $(TAT)_{10}$ docking sites per origami with cuts where HRP mimicking peroxidase activity would occur using EAD2 G-quadruplex DNA on the left arm to create ~100 nm long CNTs.

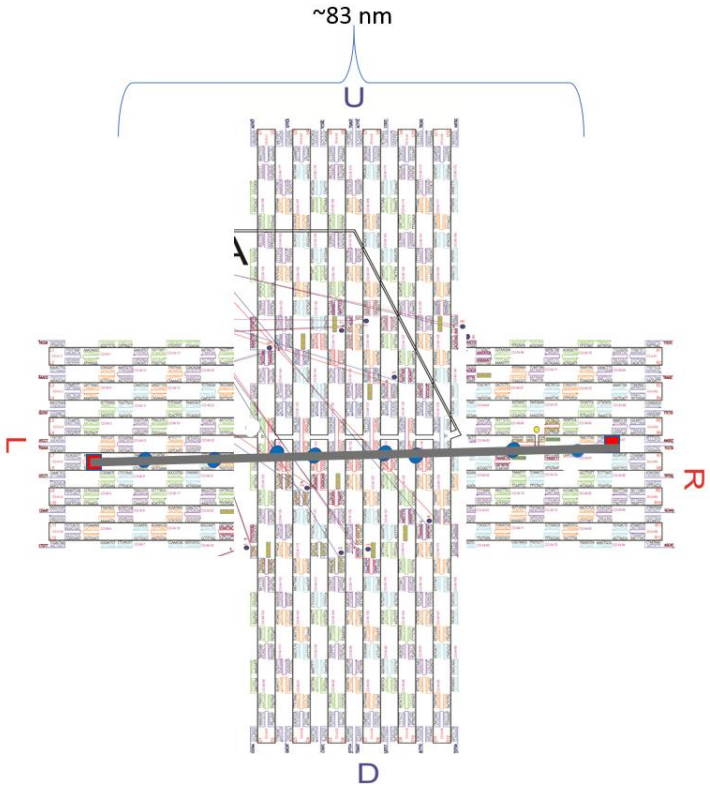

Figure 13: Schematic of Cuts on CNTs through a 0D CO-01 with a Biotin-Streptavidin Interaction.
Depiction of the ideal 0D CO-01 with eight central biotin docking sites with cuts where HRP mimicking peroxidase activity would catalyze CNT oxidation. The PS2.M G-quadruplex DNA on the left and right arms (red squares) would create ~83 nm long CNTs on individual origami.

Utilizing DNAzymes HRP mimicking peroxidase activity would allow CNTs of specific length to be achieved. Through modification of the surface of DNA origami with DNAzymes, then immobilization of the 6, 5-SWCNTs, along the central line, length control of precisely positioned CNTs could be achieved.

Catalysis of 3, 3'-Diaminobenzidine Reaction

Producing uniform length CNTs requires that all DNAzymes perform identically. To test these DNAzymes, the catalytic reaction between H_2O_2 and a precipitating substrate, which should generate a product observable with AFM, was implemented. 3, 3'-Diaminobenzidine (DAB) is an organic compound derivative of benzidine with the formula $(C_6H_3(NH_2)_2)_2$. It is a water soluble tetrahydrochloride that is commonly used for reactions involving staining of

nucleic acids and proteins. In the presence of hemoglobin, or a derivative such as hemin, DAB is oxidized by H_2O_2 to give both colorimetric and precipitating products.[49] In the beginning stages of DNAzyme tests on CO-01, DAB's ability to form a precipitate provided an ideal detection method to test the activity of individual DNAzymes. Imaging with a Bruker MM8 AFM was utilized to visualize any precipitate resulting from the reacting DAB and H_2O_2 catalyzed by the G-quad EAD2 located on the left arm of CO-01 which had also been modified with twelve central $(TAT)_{10}$ docking sites.

Catalysis of Tyramide Reaction

Tyramide refers to a tyramine molecule functionalized via an amide bond (Figure 14). In this work, biotin or AlexaFluor Dye are the functional groups attached via this amide bond, and is a type of detection method that is commonly used with an antibody conjugated to HRP for fluorescent immunocytochemistry.[50-51]

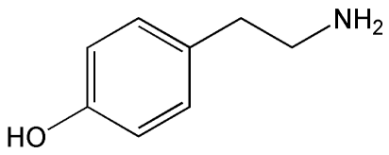

Figure 14: Tyramine Structure
General structure of an unmodified tyramine.

Tyramide labeled with Alexa Fluor™ 546 (ThermoFischer Scientific) was interacted with CO-01 containing active G-quadruplex EAD2 on the left arm, to attempt detection of G-quadruplex activity on single origami via fluorescence. It has been suggested that Tyramide can bind to the C8 position of individual guanine molecules (Figure 15), leading to possible reactions of Tyramide with nonspecific areas of the G-quadruplex or the remaining CO-01 structure.[52-53]

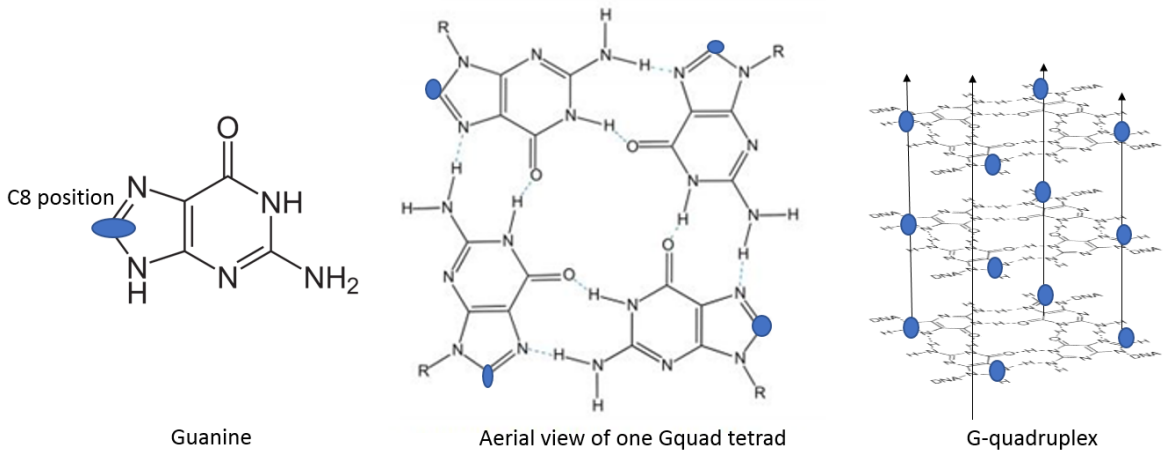

Figure 15: C8 Positions on a Single Guanine, Gquad Tetrad, and a G-quadruplex
Highlighted locations of the C8 position on a single guanine, Gquad tetrad, and a G-quadruplex to show the suggested areas where Tyramide can react.

Oxidative Cutting

Peroxidase mimicking DNAzyme has been of interest due to its advantages over the protein enzyme it mimics, horseradish peroxidase; these advantages include small size, easy assembly, and allosteric control.[43] The basis of the HRP mimicking peroxidase activity is the pi-pi stacking of ferric hemin on the G4 scaffold to activate 1 or 2-electron oxidation.[54] It has been suggested that DNAzymes follow a catalytic mechanism similar to protein peroxidases.[43] A mechanism for HRP mimicking peroxidase activity is shown in Figure 16. During this reaction, the hydrogen peroxide bonds to the vacant octahedral position on the ferric iron, which gives an enzymatically active intermediate. Interaction of H_2O_2 with a DNAzyme active center produces a highly oxidizing species, a ferryl Oxo $^{+4}$Fe and a porphyrin pi radical cation. Heterolytic cleavage of H_2O_2 would result in degradation of SWCNTs.

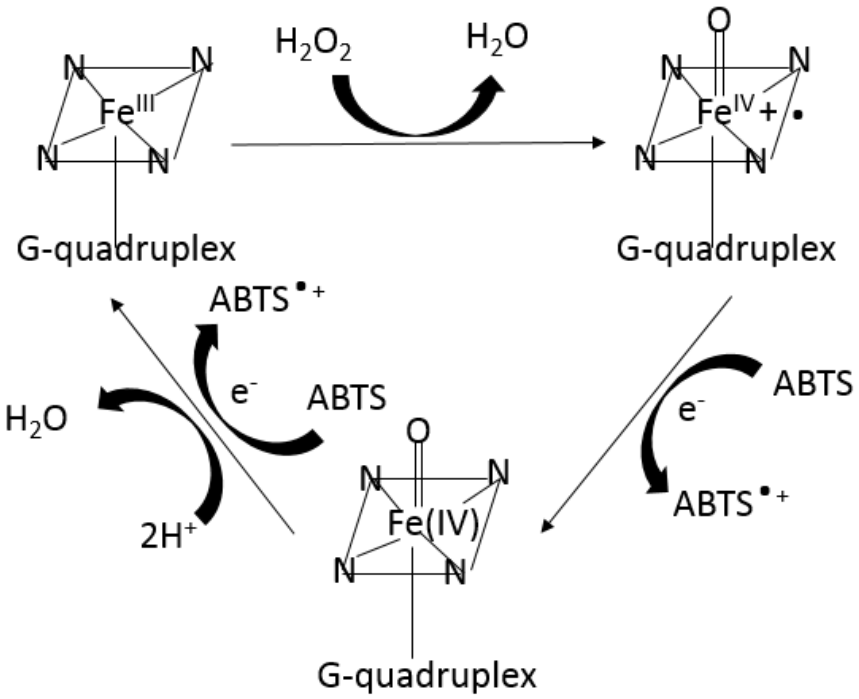

Figure 16: Proposed Mechanism for Action of HRP Mimicking Peroxidase on ABTS
The proposed mechanism for an HRP mimicking peroxidase acting on a general reducing substrate.[55]

In this work, there are two different G4 sequences used for the HRP peroxidase mimicking reactions with the CNTs. The first one, named EAD2, has the following sequence 5'-$CTG_3(AG_3)_3A$-3' and is designated as an intramolecular parallel sequence.[42] The second sequence, named PS2.M[44] has the following sequence 5'-$GT(G)_3TA(G)_3C(G)_3TTGG$-3' and was used by Atsumi and Belcher[34] during their G-quad studies, and is a coexisting or mixed type hybrid hemin aptamer. A coexisting G-quad means the ssDNA sequence is pathway dependent on the cation present. When PS2.M is in the presence of Na^+ or Pb^+, it tends to form an anti-parallel loop conformation, whereas in the presence of K^+, it forms either a parallel or hybrid mixed structure.[57]

CHAPTER 4
MATERIALS, METHODS, AND PROTOCOL DEVELOPMENT FOR AFM AND FLUORESENCE CO-SWCNT IMMOBILIZATION, OXIDATIVE CUTTING, AND SURFACE IMAGING

AFM Analysis

Atomic Force Microscopy (AFM) is a type of high-resolution scanning probe microscopy that measures the forces between the probe and the sample, offering high resolution without a vacuum, which is required for most electron microscopes. Piezoelectric elements facilitate tiny, accurate, and precise movements to obtain images at a nanoscale level. In an AFM, a cantilever has a small silicon nitride tip located on the end. During sample imaging, the motion of the cantilever transduces the interaction between the tip and the sample in the form of a measured deflection value. This deflection measurement is read by a detector that sends the intensity signal to be integrated with XY coordinates such that one is presented with a color-coded topography map. AFM is the optimal imaging technique for visualizing the CNT/CO interactions because of its mechanical and topographic abilities to measure size, structure, and thereby to visually quantify yield of immobilization. Inphase imaging is another feature in AFM that allows for high contrast viewing of material differences in a sample. Commonly used for analyzing polymers, composites, and surface coatings [58] the phase imaging should be able to differentiate between the mica surface, carbon nanotubes, and DNA origami. Seeing the materials difference between the CNT and CO may be challenging due to the fact that the CNTs are wrapped in DNA, with the result being that the materials coming into contact with the tip are the same substance; DNA. Phase shifts in an AFM image are registered as lighter and darker regions of similar color, reflecting the phase advance, or retardation in oscillation of the tip. AFM was the main technique used throughout this work for imaging. A comparison of a height

and an inphase image of CO-01 is shown in Figure 17. Significantly notable in the inphase image a deeper brown color appears, at locations where the CO-01 are present, indicative of a substance with a different composition than the imaging surface.

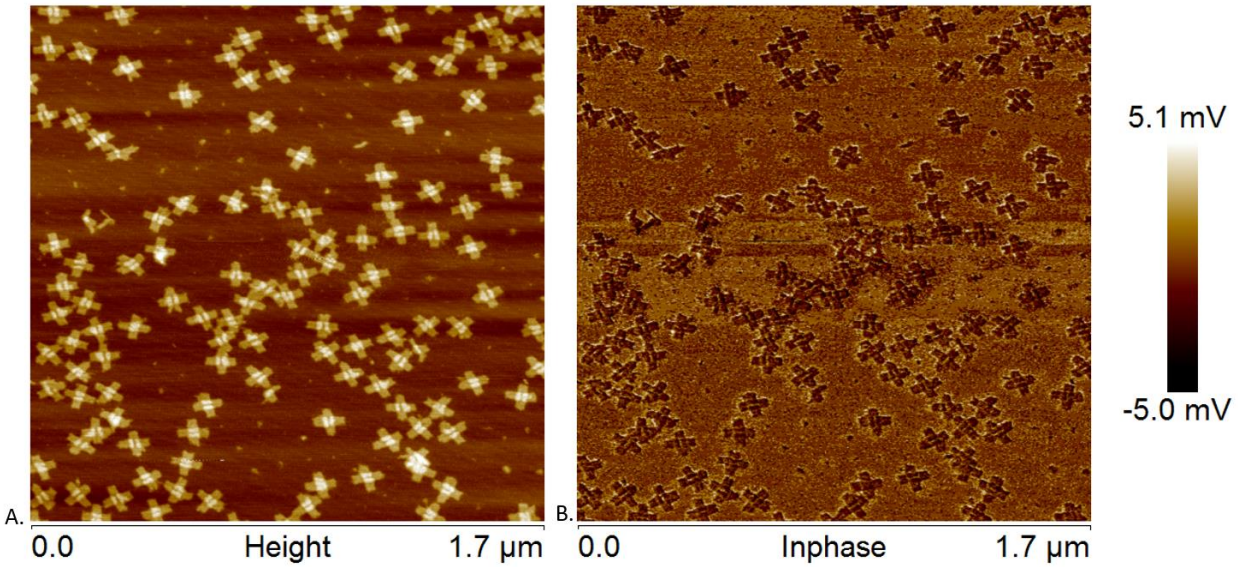

Figure 17: AFM Height Image and Inphase Image Comparison for 0D CO-01
(A.) Height image of 0D CO-01 and the right (B.) Inphase image of the same 0D CO-01.

In preparation for AFM imaging, the sample must be fixed to a surface because an AFM tip can dislodge sample components, potentially leading to an empty and/or blank surface. Mica was used as the substrate of choice for all samples since it is an atomically flat, hydrophilic aluminosilicate which provides a clean, planar surface for origami to adhere to. Cleaved mica possesses a negative charge, which could be a disadvantage for DNA imaging as DNA is usually negatively charged. This issue is overcome by putting a cation (typically Mg^{+} from $MgCl_2$) either on the mica surface, or in the DNA containing buffers. For this work, all DNA was kept in a buffer of 40 mM Tris-acetate, 20 mM acetic acid and 1 mM EDTA /12.5 mM $MgCl_2$ buffer (COB) at a pH of 8.0.

All AFM imaging was performed using a Bruker Multimode 8 (MM8) in scanasyst-air mode, using peakforce tapping (Figure 18). Peakforce tapping is a non-resonant, 2000 Hz

tapping imaging mode employing silicon nitride tips with a nominal radius of about 2 nm. Commonly, 2 µL of sample is mixed with 8 µL of COB on the mica surface and left to rest for a specific period of time depending on sample reagents as described in supplemental information, followed by rinsing with 400 µL of ddH_2O, then dried with a steady stream of argon gas. Essentially, dilution factor and deposition time are empirically determined and largely based on CO concentration and ionic environment. For optimum visualization and elimination of salt or other cations, multiple rinses may be needed. Since water can denature dsDNA, care must be taken to ensure minimum interaction time of origami and water. When imaging on the MM8, images were typically taken with x-y scans of 5 µm, 1.7 µm, and 550 nm with X and Y offsets initially set to 0 and a scan rate of 1 Hz.

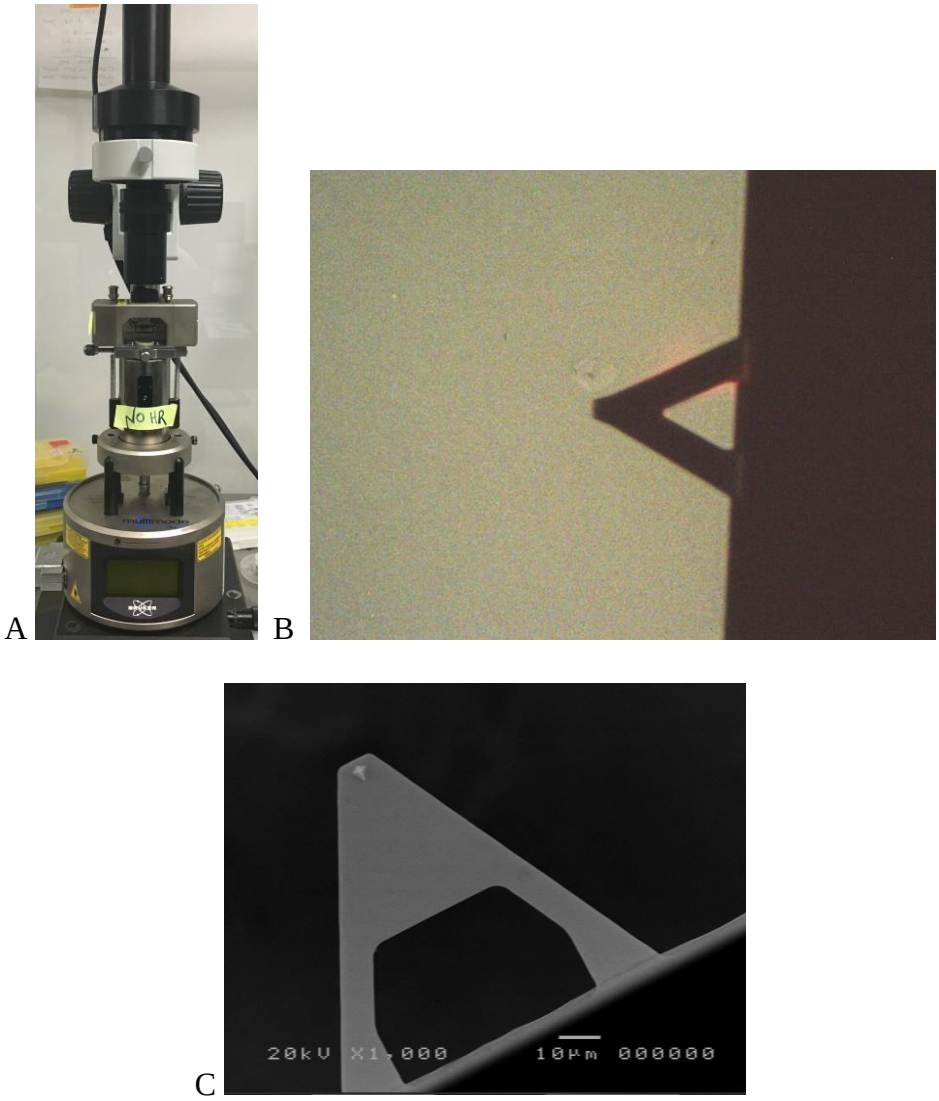

Figure 18: Bruker Multimode 8 and Cantilever
Bruker Multimode 8 (A) and (B) an optical image of the MM8 cantilever in focus on a mica sample. (C) SEM image of an MM8 cantilever and tip at 1000X.

Fluorescence Imaging and Absorbance

Semiconducting SWCNTs emit near-IR light upon photoexcitation known as fluorescence.[59-60] It is suggested that SWCNTs have stable, uninterrupted emissions.[60] To assist in further characterizing the purified CNTs, optical fluorescence microscopy was performed. 6,5-SWCNTs possess an emission wavelength max of 976 nm.[61] They also have a green excitation maximum,[15] hence the purified nanotubes were exposed to a 561 nm laser at 20 mW

and imaged using an 830 nm long pass filter. Using these parameters, fluorescence properties of the DNA wrapped SWCNTs should enable efficient excitation and measurable fluorescence in the IR region of the electromagnetic spectrum. Our attempts to image the fluorescence shows promising preliminary results for future work involving optical characterization of CNT/CO interactions.

CNTs were imaged on specially treated coverslips to remove adventitious fluorescence. To treat them, they were first scratched lightly to produce an indicator for focusing the microscope. Next, they were sonicated in a bath sequentially with EtOH then acetone, then blown dry with argon gas, then they were exposed for 15 minutes to short wave UV light, and the resulting ozone. This preparation ensured that no organics, dust, or other particulate with possible fluorescence was present on the coverslip. 10 µL of electrodialysis and drop dialysis purified T_{40} wrapped CNTs and 5 µL of MilliQ H_2O were then deposited on the cleaned coverslip. Because of the laser's sharply defined spectral output, no excitation filter was used in this process. A 561 nm laser set to 20 mW excited the CNT emissions, which were collected through an 830 nm long pass emission filter. An image stack consisting of 365 frames was collected at a rate of one frame per second, and twenty of those frames were selected to form a time stack image. In ImageJ, a data analysis software,[67] a 3D drift plugin[68] was employed to help stabilize shifting between frames within a substack and an intensity projection was performed to increase visibility, over background and noise, of individual nanotubes. These image modifications allow one to view the entire (or part of the) time course in a single image known as a z axis projection. This treatment increases contrast dramatically.

DNA ORIGAMI

Preparation and Annealing Protocol

For self-assembly of CO-01, a 7249-base single stranded M13mp18 DNA (Bayou Biolabs) (Final concentration 10 nM) is mixed with a solution of complementary synthetic staple sequences averaging 32bp long (IDT) (50 nM) in a Tris-Acetate-EDTA/$MgCl_2$ buffer at a pH 8.0 and 20 mM KCl. These reagents were annealed in a PCR system (Biorad T100 Thermal Cycler) ramped from 95° C to 20° C linearly over a period of 6 hours. During the thermal annealing process, the DNA origami self-assemble, folding into the shapes designated by the staples sequence designs. The single CO-01 designs exhibited in Figure 19 are 97 nm wide and long and each individual arm measures 32 nm wide. Concentration determinations of CNTs and CO were performed on a NanoDrop ND-1000 Spectrophotometer. For each reading, a concentration reading of ng/µL is recorded. CO-01 and Terminating end CO-01 reagents are presented in Table 1 and Table 2.

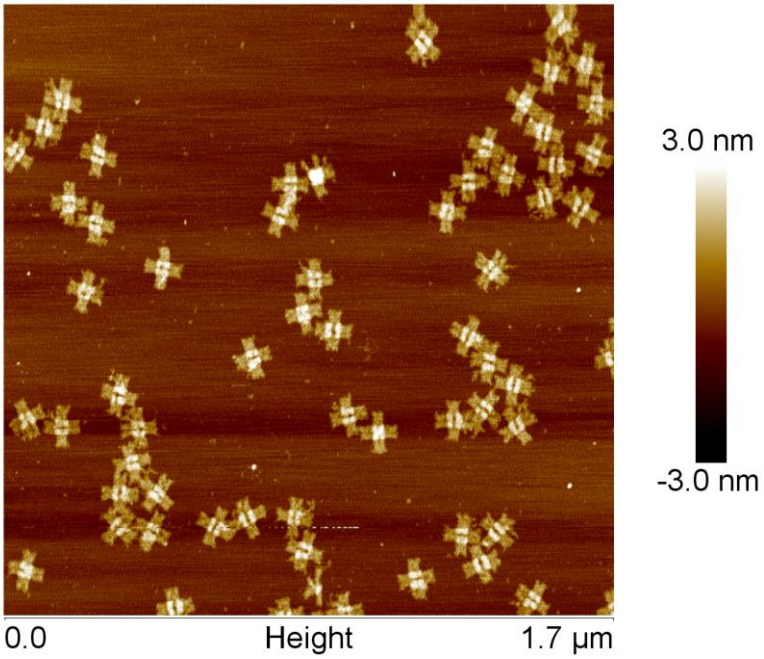

Figure 19: A 1.7-Micron Wide AFM Image of Unmodified, 0D CO-01.
AFM height image of unmodified CO-01 viewed on a Bruker MM8. Each origami measures ~100 nm in length.

1D CO-01 assembly requires a second annealing procession, separate from the initial annealing temperature gradient and before the excess staple removal from the initial anneal. As described in detail later, in order to prepare the 1D CO constructs, terminating ends are included in a second temperature anneal separate from the original synthesis at a 7:1 CO-01 to terminating end ratio from 45-20 degrees cycled four times, 15 minutes per cycle for one-hour total. An image of purified 1D is shown in Figure 20. The protocol for the annealing process for CO-01 with CNT immobilization modifications and CO-01 terminating ends as well as the annealing protocol for 1D CO-01 at a 1:7 terminating end to CO-01 ratio is followed by a reagents list in Table 3.

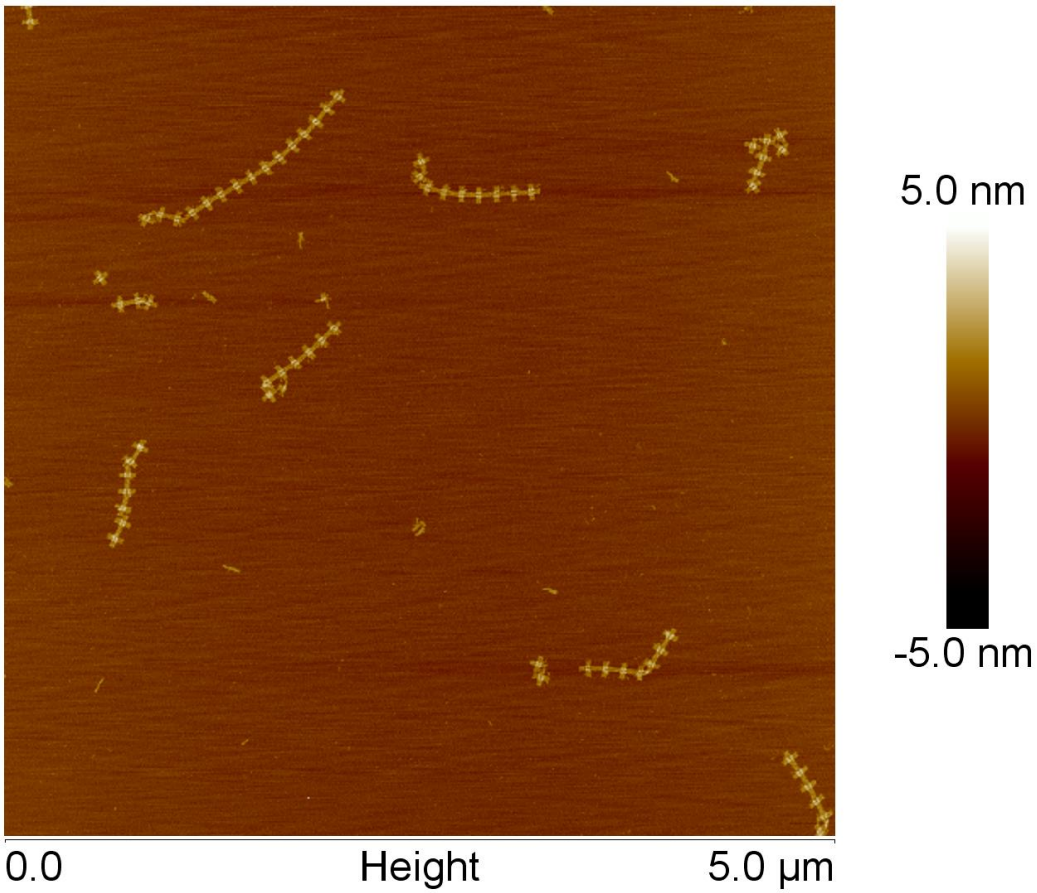

Figure 20: 1D Linear Array of CO-01
Five-micron wide AFM height image of 1D CO-01. A small distribution of lengths of arrays that can occur during even a well calculated 7:1 ratio of CO-01 to terminating ends is shown here, with arrays ranging from 2 monomer units to 12 monomer units.

0D and 1D Origami Annealing Protocols:

Preparing CO-01 0D with modified sites for CNT immobilization and G-quad. 100µL, 10nM.

1. ssM13 (10 nM final concentration) is mixed at a 1:5 concentration ratio with 10X COB, unmodified CO-01 staples, G-quadruplex DNA modified staples, CO-01 modification staples [$(TAT)_{10}$ docking sites or TAT-biotin wrap)], CO-01 up and down arm single base C terminated staples (50 nM final concentration), KCl (20 mM final concentration) and water to a final volume of 100 μL
2. Reagents shown in reagent list (Table 1) are annealed from 95 -20 degrees over 6 hours
3. Samples are stored at 4 degrees

	Working Concentration	Volume	Final Concentration
M13	0.1 µM	10 µL	10 nM
COB	10 X	10 µL	1 X
CO-01 CORE missing 12 central and G-4 Staple	0.5 µM	10 µL	50 nM
G-quad docking sites	0.5 µM	10 µL	50 nM
Staple modifications for CNT immobilization	0.5 µM	10 µL	50 nM
KCl	1M	2 µL	20 mM
UP and Down Arm staples	0.5 µM	10 µL	50 nM
H_2O	-	48 µL	55.6 M

Table 1: Reagent list for CO-01 0D with modified sites for CNT immobilization and G-quad. 100 µL, 10 nM

Synthesis conditions for formation of CO-01 with modifications for CNT immobilization. Since there are G-quads in this solution, 20 mM KCl was included in the annealing process. These monomers include a series of six- single base cytosines on the up and down arms, to prevent the CNTs from having a higher affinity to the open ends of CO-01 versus the center. After the reagents are mixed in a 200 µL PCR tube, they are annealed from 95-25 degrees over a period of 6 hours.

Preparing CO-01 0D Terminating ends (CO-01TR). 100µL, 10nM.

1. ssM13 (10 nM final concentration) is mixed at a 1:5 concentration ratio with 10X COB, unmodified CO-01 staples, CO-01 modification staples [$(TAT)_{10}$ docking sites or TAT-biotin wrap), six sequences of $PolyT_5$ on the right arm (5TR) (50 nM final concentration) and water to a final volume of 100 μL
2. Reagents shown in reagent list (Table 2) are annealed from 95 -20 degrees over 6 hours
3. Samples are stored at 4 degrees

	Working Concentration	Volume	Final Concentration
M13	0.1 µM	10 µL	10 nM
COB	10 X	10 µL	1 X
CO-01 CORE missing 12 central and G-4 staple	0.5 µM	10 µL	50 nM
CO-M-4	0.5 µM	10 µL	50 nM
Staple modifications for CNT immobilization	0.5 µM	10 µL	50 nM
5TR	0.5 µM	10 µL	50 nM
H_2O	-	30 µL	55.6 M

Table 2: Reagent list for CO-01 0D Terminating Origami (CO-01TR). 100 µL, 10 nM
Synthesis conditions for formation of CO-01 with terminating ends. These monomers include 5TR which are six sequences of $(PolyT)_5$ to terminate the linear growth of 1D CO-01 constructs. After the reagents are mixed in a 200 µL PCR tube, they are annealed from 95-25 degrees over a period of 6 hours.

Annealing 7:1 ratio origami to terminators 10 nM

1. CO-01 0D with modified sites for CNT immobilization is introduced to clean, sample tube (10 nM final concentration)
2. CO-01TR introduced to sample tube at a 7:1 ratio CO-01: CO-01TR (1.42 nM final concentration)
3. Reagents shown in reagent list (Table 3) are annealed from 45-20 degrees cycled four times 15 minutes each cycle for 1hour total
4. Samples are stored at 4 degrees

	Working Concentration	Volume	Final Concentration
CO-01 0D twelve central $(TAT)_{10}$ docking sites	10 nM	50 µL	10 nM
CO-01 0D Terminating ends	10 nM	7.1 µL	1.42 nM
LRSE	0.5 µM	5 µL	50 nM

Table 3: Reagents list for Annealing 7:1 ratio origami to terminators 10 nM
Synthesis conditions for formation of 1D linear array of CO-01 at a ratio of 7 monomers per 1 terminating end origami. After the reagents are mixed in a 200 µL PCR tube, they are annealed from 45-20 degrees cycled four times for one hour total, or 15 minutes per cycle.

Purification Techniques

For the removal of excess staple strands for both 0D and 1D CO-01 constructs, the CO is filtered using 30 kDa MW centrifugal filters (Millipore 30 kDa filters). The unpurified CO is added to filtration cartridges that pass smaller, individual staples with 400 µL of 1X COB for two cycles of 5 minutes at 14,800 RCF. After two cycles, the filter is inverted into a clean sample tube and centrifuged further for 2 minutes at 930 RCF, transferring the purified CO-01 into the clean sample tube. The concentrations were analyzed using the NanoDrop ND-1000 UV VIS Absorbance Spectrophotometer to obtain an ng/µl concentration by evaluating the absorption peak at 260 nm. Samples were stored at 4°C.

Preparation and Modifications of DNA Origami for Optimal Immobilization

In the work described here, two designs of DNA Origami CO-01 were used to achieve functionalization with SWCNTs. The first functionalization method takes advantage of 6, 5-

SWCNT's affinity for TAT sequences to immobilize CNTs onto twelve $(TAT)_{10}$ docking sites arranged across the horizontal center of the origami construct.[23] The second functionalization method uses the well-known streptavidin-biotin interaction to secure a CNT across the center of a CO. Binding is accomplished through eight 3' biotin modified staples positioned down the center of the DNA origami.[12]

Design of $(TAT)_{10}$ Docking Sites

Docking strands are single-stranded sequences of DNA composed of two parts, one part which integrates into the origami and another part that projects from the origami structure. Using simple base pairing rules, when the docking strand encounters a complementary DNA sequence in the origami construct, they interact to bind to the CO-01, exiting in the upper surface. Tu, et al.[23] carefully categorized DNA sequences that showed the highest specificity to each of a variety of SWCNT chiralities. Twelve locations spanning from the center of the left arm, through the central axis, and ending in the center of the right arm were chosen based on co-linearity with each other, and where the double helix of the staple terminus was facing "up," or on the same surface of the origami. While Tu, et al.[23] determined $(TAT)_4$ was optimal for 6, 5s, $(TAT)_{10}$ docking sequences were used to provide more reach into solution toward the CNTs. The hypothesis is that when the $(TAT)_{10}$ docking strand interacts with the T_{40} wrapped CNT, the affinity of the TAT sequences for the 6,5-SWCNT will cause displacement of the T_{40} strand in that location, allowing for the CNT to remain solubilized but enabling docking of the CNT down the center of the DO. The final design for the twelve $(TAT)_{10}$ docking sites on CO-01 is shown in Figure 21. Upon mixing the origami solution with a solution of T_{40} wrapped, electrodialysis purified nanotubes, a temperature ramp is implemented, cycled four times to allow the

displacement of T_{40} in the locations the $(TAT)_{10}$ docking sites are intended to bind, directing a single nanotube to bind down the center of a CO-01 origami.

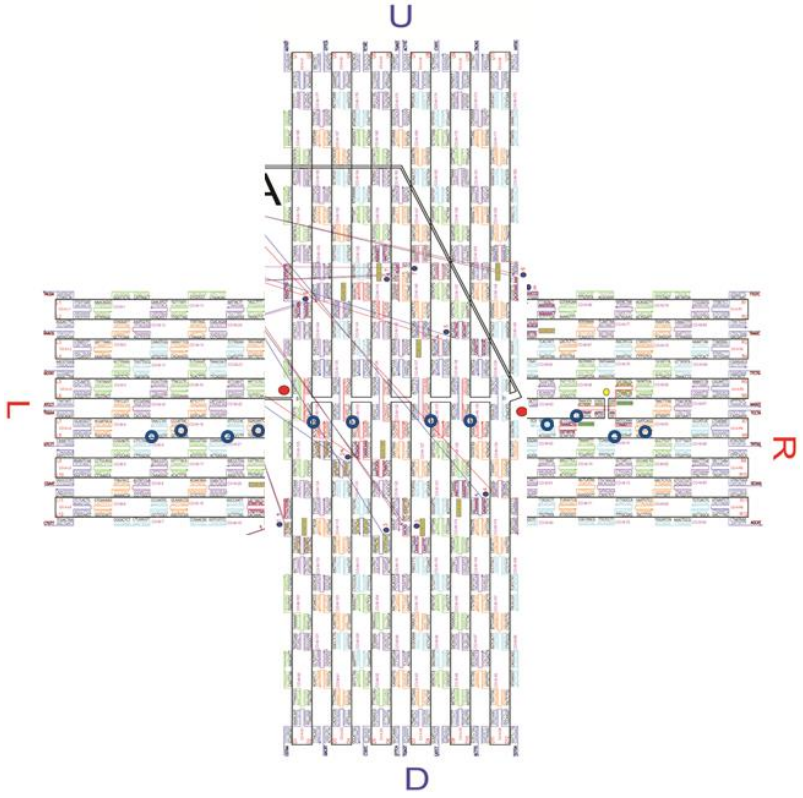

Figure 21: CO-01 with Twelve Docking Sequence Locations for $(TAT)_{10}$
Diagram of CO-01 with its twelve carefully designed locations for $(TAT)_{10}$ sequences (blue circles) spanning the center of the construct.

To construct the CO with central docking sites, twelve staples modified with extensions consisting of $(TAT)_{10}$ were included in the initial annealing process at a 1:5 M13 to staple ratio. When designing the locations of the $(TAT)_{10}$ docking sites, the ~32 base sequence is followed from 5' to 3' until a desired location is found; a location where a modification in the double helix would point out of the upward surface of the CO-01. This approach avoids having modifications on different sides of the CO which could get sandwiched between the CO and mica during imaging. In cases where a staple must be broken, the remainder of the bases in the original staple are incorporated into the immediately adjacent staple sequence. An example of this design process is shown in Figure 22.

A

Original staple sequence: CO-M-9 5'-GTGCCAAGGAAGATCGACATCCAGATAGGTTA-3'
Modified staple sequence: CO-M-9 (TAT)10 5'-GTGCCAAGGAAGATCGACATCCAGATATATTATTATTATTATTATTATTATTAT-3'
Original staple sequence: CO-M-10 5'-CGTTGGTGTAGCTATCTTACCGAATTGAGCGC-3'
Sequential modified staple: CO-M-10 Extension 5'-TAGGTTACGTTGGTGTAGCTATCTTACCGAATTGAGCGC-3'

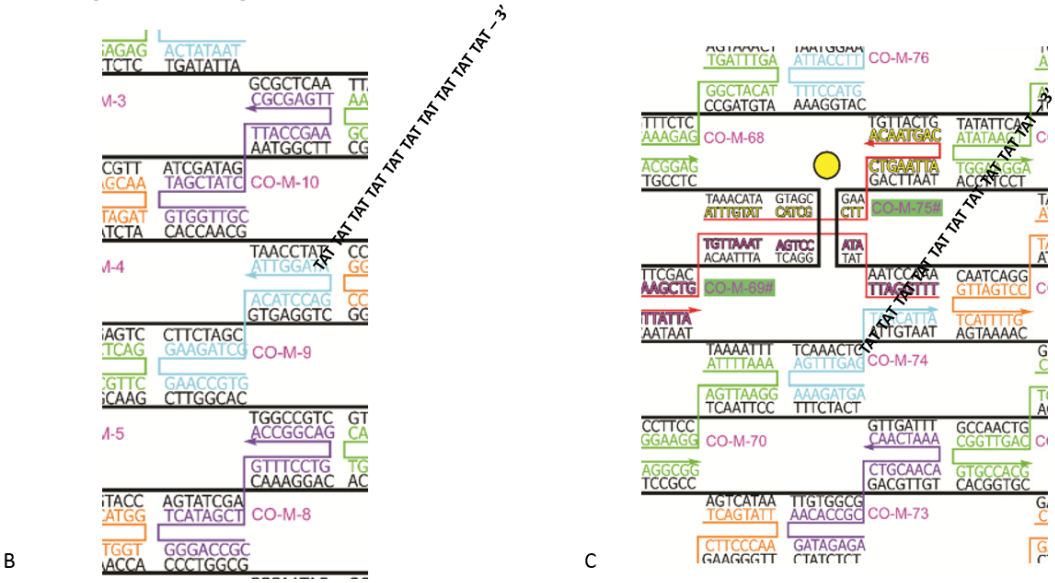

B C

Figure 22: Design of TAT Docking Sites onto CO-01
Above are shown two locations on the surface of CO-01 where $(TAT)_{10}$ docking sites were designed A) staple sequences before and after modification. B) Schematic of a section of CO-01 reflective in the staple sequence shown in (A). The original staple, CO-M-9 can be traced from 5'-3'. The modified CO-M-9 (TAT)10 can be followed from 5' then continues as a TAT sequence until the 3' end. CO-M-10 short follows the remaining staple in the original sequence of CO-M-9 and flows into the following staple originally named CO-M-10. (C.) Another example of $(TAT)_{10}$ modification on a section of the surface of CO-01.

Design of Streptavidin-Biotin Docking Sites

Streptavidin, a protein, is extremely effective at non-covalently binding to biotin molecules. Eight locations on CO-01 spanning the same area as the $(TAT)_{10}$ docking sites (Figure 22B) were replaced with a $(PolyT)_4$ spacer, and terminated with a biotin molecule, measuring a total of 2.46 nm above the origami surface consistent with two previous designs.[24,12] When streptavidin is introduced into a solution with both CO-01 and CNTs wrapped in TAT sequences flanked with biotins, the streptavidin-biotin interactions will take over and dock a nanotube approximately 8.5 nm above the origami surface (Figure 24). An advantage of this technique is that no temperature annealing is needed for immobilization, but this includes a disadvantage of placing the nanotubes at a height of ~8.5 nm above the origami surface, which

can lead to some variation in the alignment and observability of the CNT on the CO surface. The design for the locations of the eight biotin docking sites is shown in Figure 23.

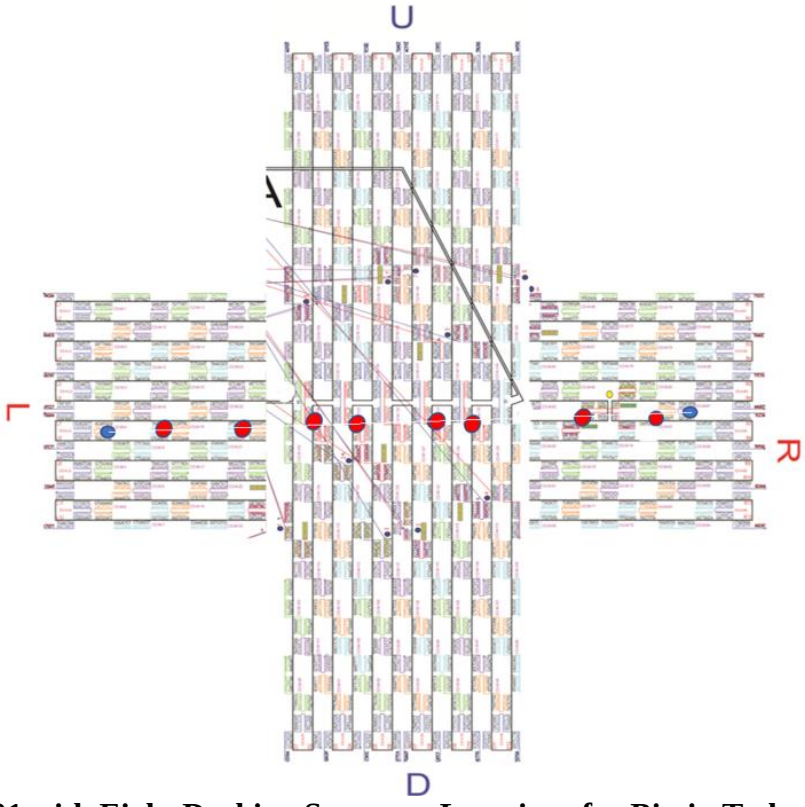

Figure 23: CO-01 with Eight Docking Sequence Locations for Biotin Tethers
CO-01 with 8 carefully designed locations of biotin docking tethers (red circles) spanning the center of the construct.

To construct the CO with central docking sites in preparation for a biotin-streptavidin immobilization, eight staple modifications consisting of a $(polyT)_4$ spacer followed by a biotin (IDT)[12] molecule measuring ~2.46 nm above the origami surface were included in the thermal annealing process at the same 1:5 M13 to staple ratio. Designing the locations for the biotin tethers followed the same process as for the $(TAT)_{10}$ locations. Height is an important factor in modeling the biotin mediated immobilization because the CNTs will essentially be lifted off the surface of the CO-01 versus directly bound to the origami as in the $(TAT)_{10}$ design. Therefore, we consider that biotin has a height of ~1.1 nm,[62] and the $(polyT)_4$ spacers have a height of 1.36 nm following the general rule that individual bases stack at a .34 nm distance from each other.[63]

Including the addition of a streptavidin molecule, an additional ~5 nm[64] (modeled in close relation to the crystal structure of Avidin) is added to the height of the tether, bringing a total height of ~7.48 nm at full extension and with the inclusion of biotin molecules bound to CNTs, a full extension total height of 8.5 nm. (Figure 24)

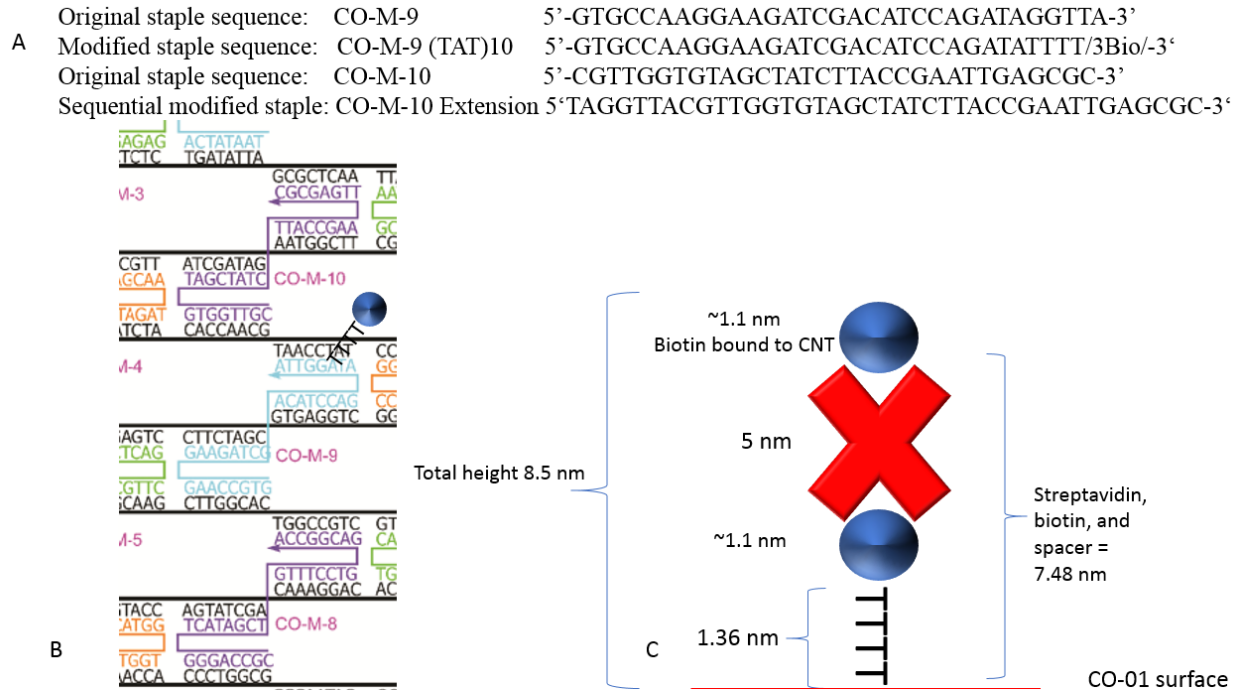

Figure 24: Design of Biotin Tether Docking Sites on the Surface of CO-01
Using the same location on the CO-01 surface as shown in Figure 23 previously, this set of staples (A) and diagram (B) show the locations of a biotin tether consisting of a $(polyT)_4$ spacers and a biotin molecule. (C) Shows the design for modeling the height of the biotin tethers on the surface of CO-01.

G-quadruplex Design and Docking sites

Designs integrating the G-quadruplex DNA modified staple into CO were generated in similar fashion to the design of docking sites. For CO-01 $(TAT)_{10}$, one G-quadruplex was used on the left arm of CO-01 (Figure 25). The G-quadruplex used in this construct was EAD2 (IDT), discussed previously,[48] and was integrated on the end of a CO-01 staple in a location colinear with the horizontal $(TAT)_{10}$ docking sites. This staple did not contain a spacer to present the DNAzyme as close to a functionalized CNT as possible to facilitate future nanotube cutting.

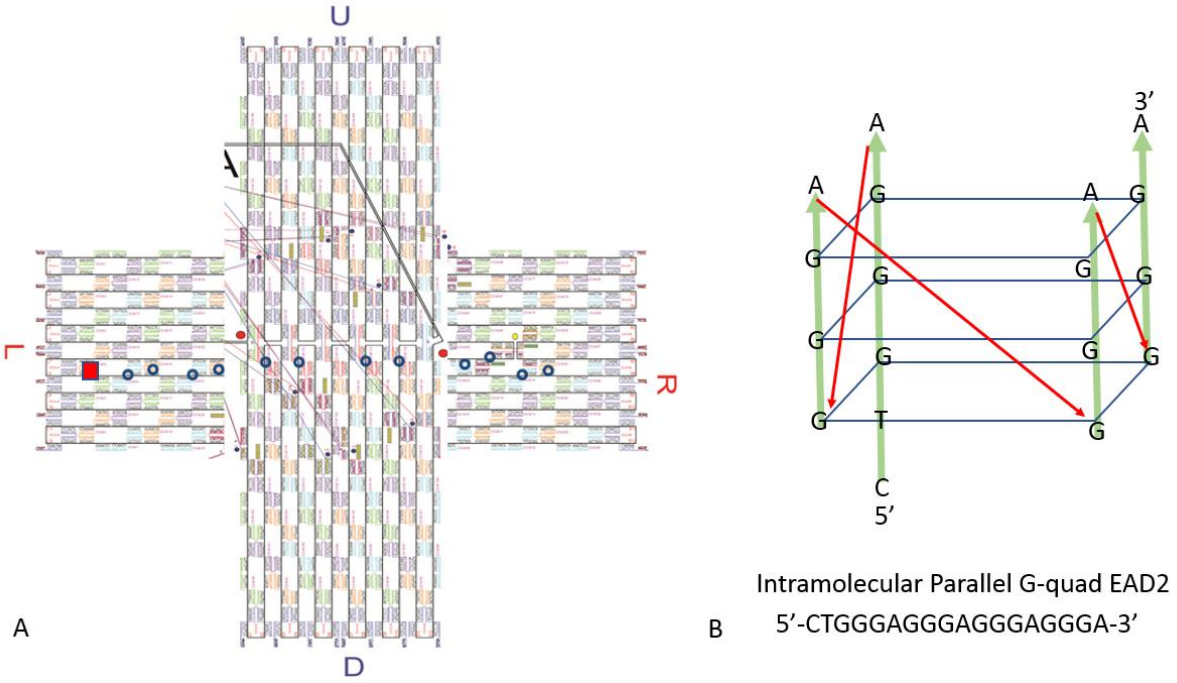

Figure 25: EAD2 Location and Design
A) Location of the G-quadruplex EAD2 (denoted by red square) on the left arm of CO-01 as well as B) a diagram of the single stranded guanine rich DNA sequence demonstrating how it folds into the quadruplex formation upon introduction of potassium followed by heating to 95 degrees Celsius and cooling to room temperature.

For the CO-01 construct with eight biotin docking tethers, because of potential CNT functionalization between 7-10 nm above the origami surface, the G-quadruplex sequence could not simply be integrated in a staple. The design includes a $(polyT)_{11}$ spacer followed by a $(TAT)_5$ sequence, followed by the G-quadruplex sequence PS2.M,[12,48] measuring ~10 nm high. The reason for the height is to allow for plenty of range for the DNAzyme to be in close proximity to a functionalized CNT held above an origami surface by the biotin tethers and streptavidin. Two DNAzymes are positioned with one on the left arm and one on the right arm (Figure 26), to facilitate cutting of a nanotube in two locations measuring approximately 80 nm apart.

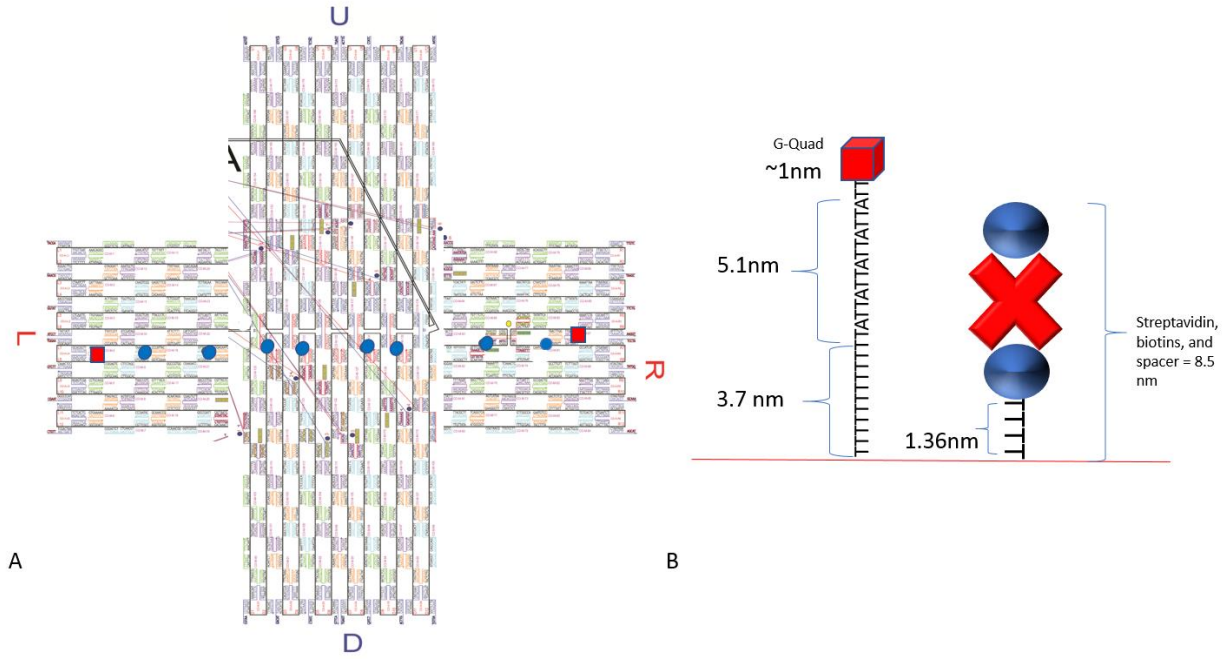

Figure 26: Biotin G-quadruplex Location and Design
A) Locations of the two G-quadruplex DNA sequences on CO-01 are outlined by red squares that measure ~10 nm above the CO-01 surface on the left and right arms in parallel with the eight central biotin tether docking sites. B) Depiction of the height difference between the biotin tether docking sites with a bound streptavidin and the G-quadruplex staple on the surface of CO-01.

For assembly, the staples are mixed with the M13 at a M13: staple ratio of 1:5, and thermal annealing is performed from 95-20 degrees Celsius over six hours as described previously, producing the origami ready for functionalization with CNTs.

6, 5-SWCNT

Preparation and Modifications of Carbon Nanotubes for Optimal Functionalization

In the work described here, there are two types of wrapping, one with T_{40} ssDNA[18] and one with a $(TAT)_4$ sequence flanked by two biotin molecules[12] used to prepare the CNTs for two different approaches to functionalization as discussed with the two different types of docking sites.

To wrap the CNT with DNA, equal volumes of CNT (Sigma) (80 µL) (2.5 mg/mL) and ssT_{40} (IDT) (80 µL) (300 µM) or $(TAT)_4$ with flanking biotin (B-DNA TAT wrap) (300 µM)

(IDT) with 100 mM final concentration NaCl in 400 µL final volumes were sonicated for 90 minutes in ice water then left to rest at room temperature for 30 minutes. After 30 minutes at room temperature, samples are centrifuged for 1 hour at 20,000 RCF. Centrifugation forms a pellet at the bottom of the sample tube and a grey supernatant. The supernatant is removed and stored at 4^{o} C while the sample pellet is discarded into an appropriate, covered, waste container. Images taken at different steps in the process of the solubilizing 6,5-SWCNT in the T_{40} solution described in Table 4 are shown in Figure 27. Figure 28 presents an AFM image of 6,5-SWCNTs solubilized in $(TAT)_4$ with flanking biotin (B-DNA TAT wrap). Figure 29 presents an AFM image of TAT wrapped CNTs. The solubilized nanotubes are then ready for purification.

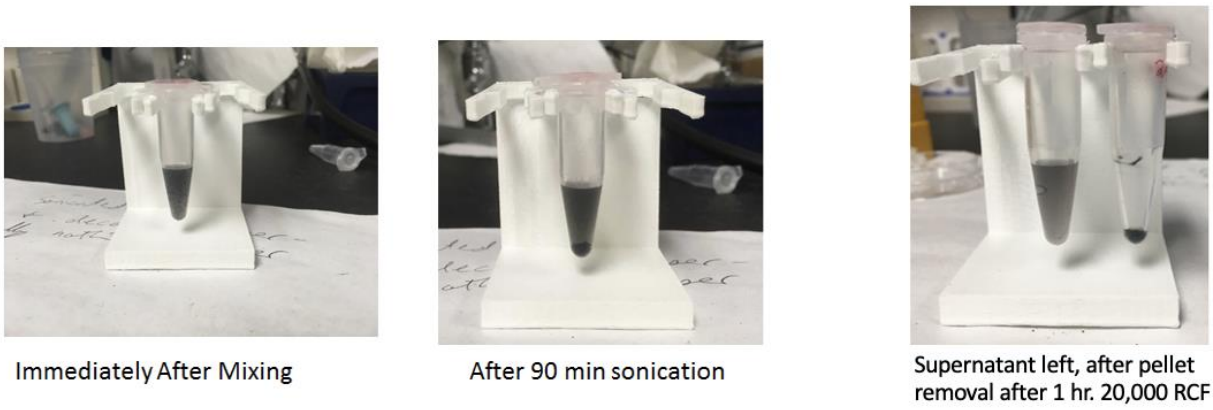

Figure 27: **Solubilization of Carbon Nanotubes in DNA**
Three steps showing the process of making CNTs soluble in H_2O. Image on the far left depicts the CNTs immediately after being mixed with T_{40} containing solution. Center shows how the CNTs and DNA appear after 90-minute sonication in ice water and 30 minutes of rest at room temperature. Right shows the supernatant of the CNTs after 1-hour centrifugation at 20,000 RCF, leaving a pellet of non-soluble CNTs at the bottom of the original sample tube.

Solutions used in CNT solubilization protocol	Working concentration	Volume	Final concentration
CNT/H_2O	2.5 mg/ml	80 µL	7 nm equivalents of 100 nm
NaCl	1 M	40 µL	100 mM
T_{40} ssDNA OR B-$(TAT)_4$	300 µM	80 µL	60 µM
H_2O	-	200 µL	55.6 M

Table 4: Solution composition for solubilization of 6, 5-SWCNTs
This table provides the solution components for the solubilization of 6, 5-SWCNTs in ssDNA. Protocol is the same whether the sample is wrapped in the T_{40} DNA or the $(TAT)_4$ DNA flanked with two biotins.

CNT solubilization protocol:

1. Combine solutions described in table 4
2. Sonicate the solution in a 1.5 mL PCR tube in an ice bath for 90 minutes
3. Let sit at room temperature for 30 minutes
4. Centrifuge for one hour at 20000 RCF
5. Retain supernatant and dispose of pellet

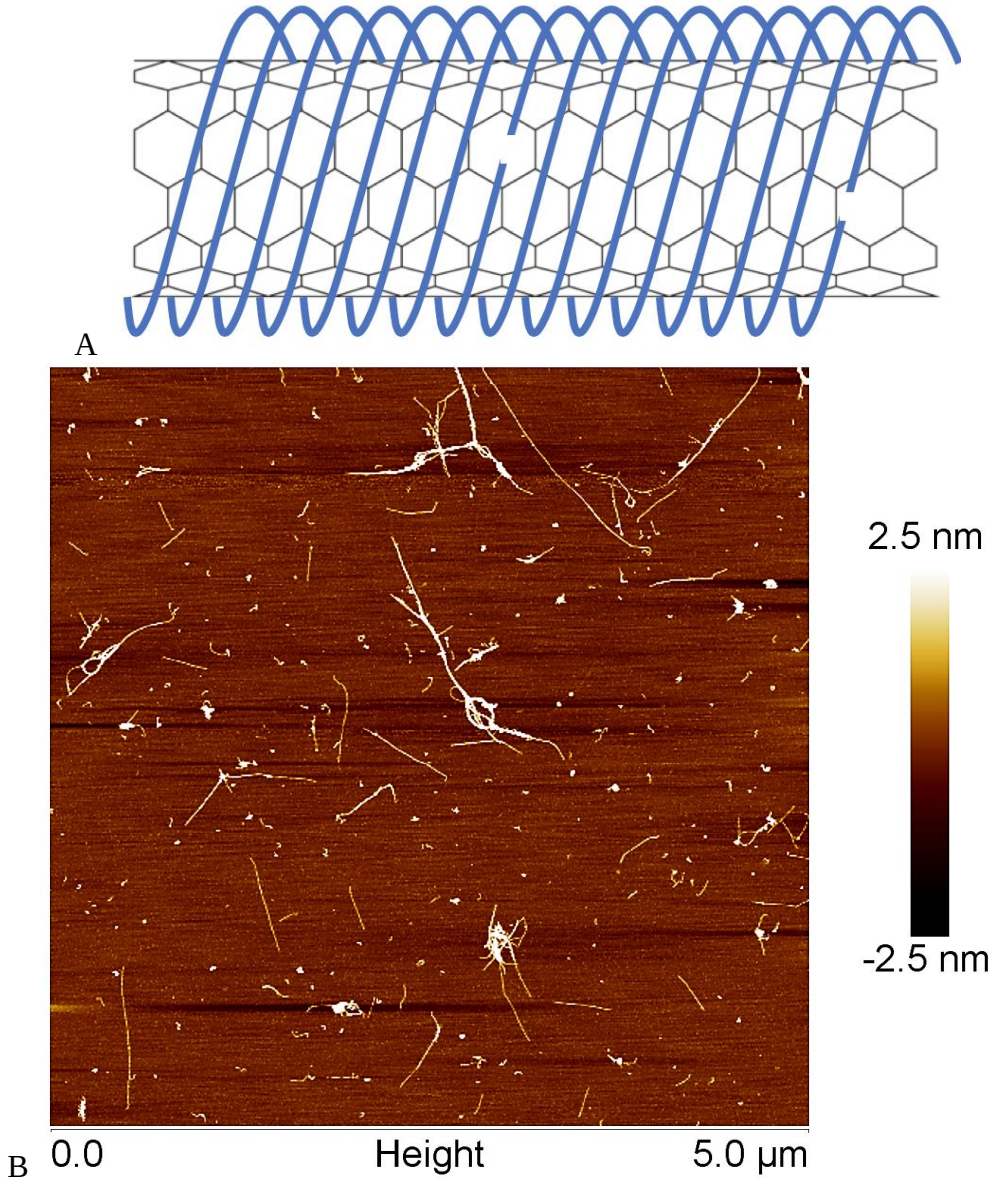

Figure 28: Schematic of 6, 5-SWCNTs Wrapped in T_{40} ssDNA and a Low Magnification AFM Image of T_{40} Wrapped 6, 5-SWCNTs before Purification

A digital rendition of a CNT wrapped in T_{40} ssDNA (A) where the blue lines are indicative of T_{40} and (B) an image of T_{40} wrapped 6,5-SWCNTs. These 6, 5-SWCNTs have been wrapped in T_{40} to prepare for introduction to CO-01 with $(TAT)_{10}$ docking sites.

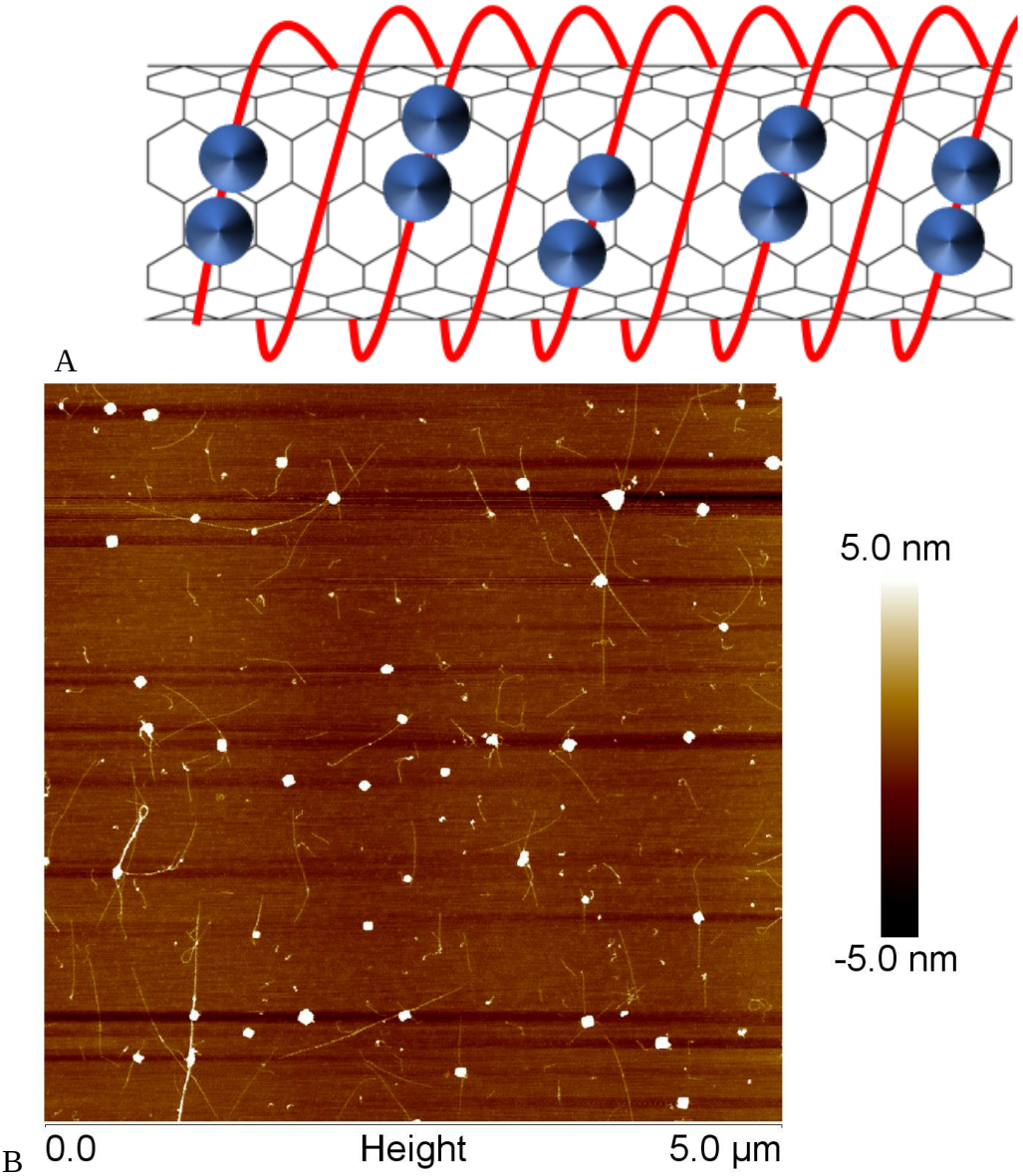

Figure 29: Schematic of 6, 5-SWCNTs Wrapped in B-DNA TAT Wrap and AFM Image of B-DNA TAT Wrap 6, 5-SWCNTs

A graphic rendition of a CNT wrapped in B-DNA TAT wrap (A). The blue spheres are indicative of the biotin molecule while the red lines depict the TAT wrap. B) AFM image of 6, 5-SWCNTs which have been solubilized in B-DNA TAT wrap to prepare for introduction to CO-01 biotin-streptavidin docking sites. As evident in the white particulate matter scattered throughout the image, there is a high concentration of NaCl still in the sample, which can interfere with imaging.

Concentration Determination of DNA Wrapped 6, 5-SWCNT

Concentrations are determined through a process using 100 nm CNT equivalents as the unit "CNT molecules." In 2011, Schöppler et al.[65] stated that there are 88 Carbons per nm of 6,

5-SWCNT. If there are 88 carbon atoms in 1 nm, there will be 8800 in 100 nm. An absorbance at A_{575} of 1 cm path length equals 60 μM of carbon atoms, which is equivalent to 7 nM of 100 nm CNT equivalents. Figure 30 shows an example nanodrop ND 1000 display indicating the absorbance peak of interest. Example calculations are provided in the supplementary information.

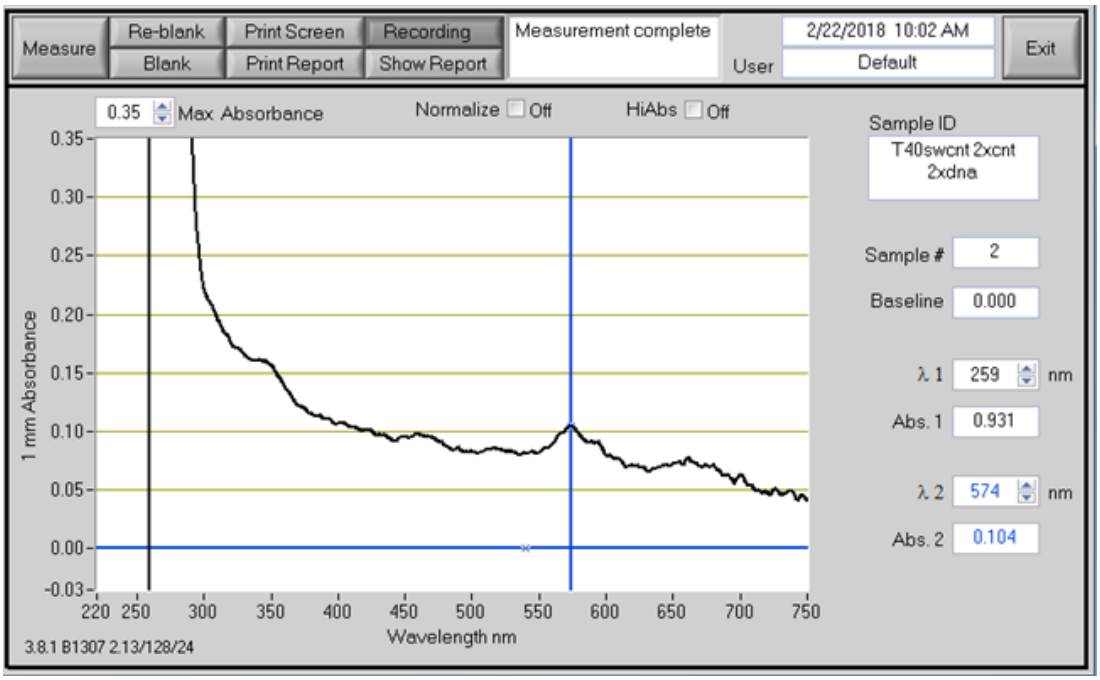

Figure 30: Nanodrop Absorbance of Solubilized CNTs Used to Determine Concentration of CNTs
Nanodrop absorbance analysis performed on unpurified ssT_{40} wrapped 6, 5-SWCNTs shows an absorbance peak at 574 nm.

Purification and Buffer Exchange Techniques

After solubilizing the carbon nanotubes, several types of impurities remain, including carbon "soot" and excess DNA which was not utilized in the solubilization process. To remove these, an electrodialysis procedure was implemented using Harvard Apparatus (HA) Electroprep tanks. The newly solubilized carbon nanotubes are subjected to a small electric current of 20 mA for two hours, switching electrodes each hour (Figure 31A).[24] Electrodialysis is followed by drop dialysis to exchange the sodium phosphate buffer used in electrodialysis with the same

buffer used for CO-01. This solution exchange process employing a drop dialysis procedure is illustrated in Figure 31B.

A 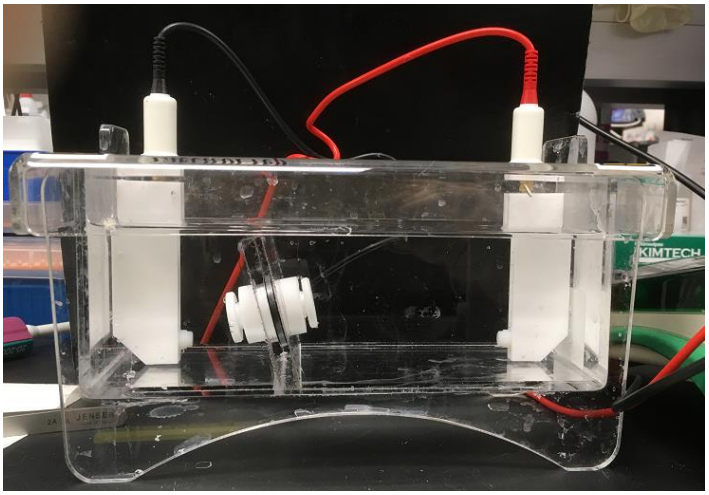 B 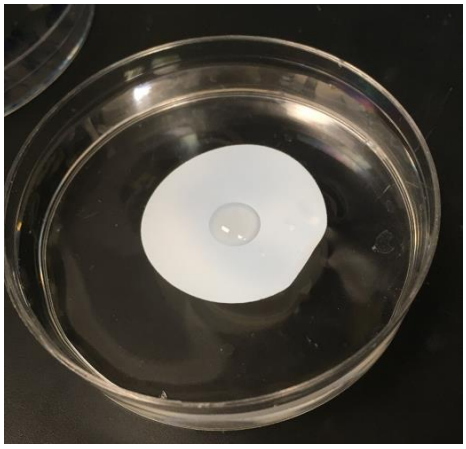

Figure 31: Harvard Apparatus Electroprep Dialysis Design and Drop Dialysis of Electrodialysis Treated 6, 5-SWCNTs
(A) The Harvard Apparatus set up is used for electrodialysis purification. (B) Image of a drop during drop dialysis processing of electrodialysis treated 6, 5-SWCNTs. Drop is placed on a 0.025 μm pore size membrane to exchange sodium phosphate buffer with COB.

Equal volumes of DNA wrapped 6,5-SWCNTs (100 μL) (7 nM of 100nm CNT equivalents) and 0.1 M Na_2HPO_4 Buffer Solution (100 μL) [25] are introduced to a fast dialyzer chamber and two 50 kDa membranes (HA) are cut to size using an 8 mm biopsy punch (Ted Pella Inc.) and placed over each opening of the dialysis chamber. The dialysis chamber was placed in the HA Electroprep tank filled with buffer to the fill line and the material migrates under the influence of a small current of 20 mA (Biorad Powerpac) for one hour. After one hour, electrodes are flipped and the current is run through the sample for an additional hour. After two hours total, the chamber is removed from the tank, the membranes are removed (Figure 32) and the solution inside the chamber is collected into an empty sample tube. The sample is still slightly gray, but the appearance of gray/black particulate on the membranes indicates that much of the gray particulate material was removed from the sample through the electrodialysis

procedure. Through AFM imaging, a decrease in coverage density of CNTs as well as aggregates of CNTs was observed (Figure 33).

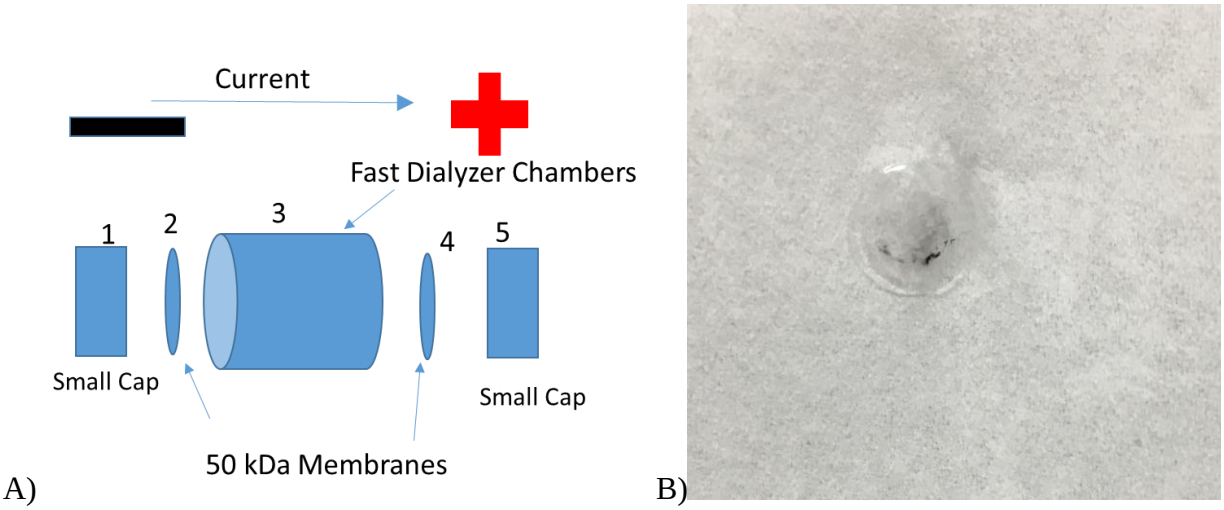

Figure 32: A) Harvard Apparatus Electroprep Dialysis Design and B) Used 50kDa Membrane after Dialysis Procedure

A) A schematic depicting the design of the electrodialysis capsule using 50 kDa membranes, two small caps, and one large fast dialyzer chamber that holds the sample. Current flows from anode to cathode, then chamber is reversed at mid-point in 2 hour total reaction time. B) 50 kDa membrane after the electrodialysis procedure is discolored by black "soot" or impurities bound to the membrane that have been removed from the sample.

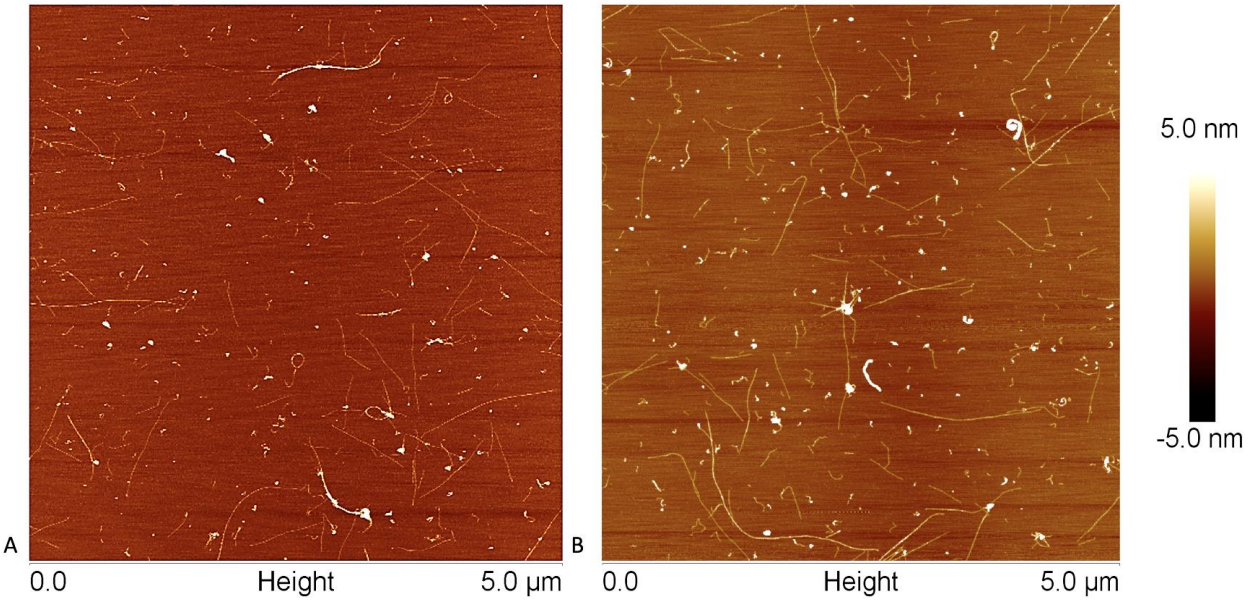

Figure 33: 5-Micron Wide Images of T_{40} and TAT-Biotin Wrapped 6, 5-SWCNTs after Electrodialysis Treatment

Two 5-micron wide images of the T_{40} wrapped CNTs (A) and TAT-biotin wrapped CNTs (B) after being solubilized and treated using electrodialysis with 20 mA current for a total of two hours.

After electrodialysis treatment of DNA wrapped 6, 5-SWCNTs, they are now contained in a solution of Na_2HPO_4. As an additional purification step a buffer exchange is performed via a drop dialysis procedure. 18 mL of COB is added to a 5.8 cm diameter polystyrene dish and a 0.025 μm pore size membrane (New England Biolabs) is floated on the surface of the COB, and allowed to equilibrate for 5-minutes before introducing 34 μL of electrodialysis treated DNA wrapped 6, 5-SWCNTs to the center of the membrane, followed by equilibration for one hour. As collected, these nanotubes are ready for immobilization onto the surfaces of DNA Origami. AFM imaging displays an even greater decrease in aggregation (Figure 34).

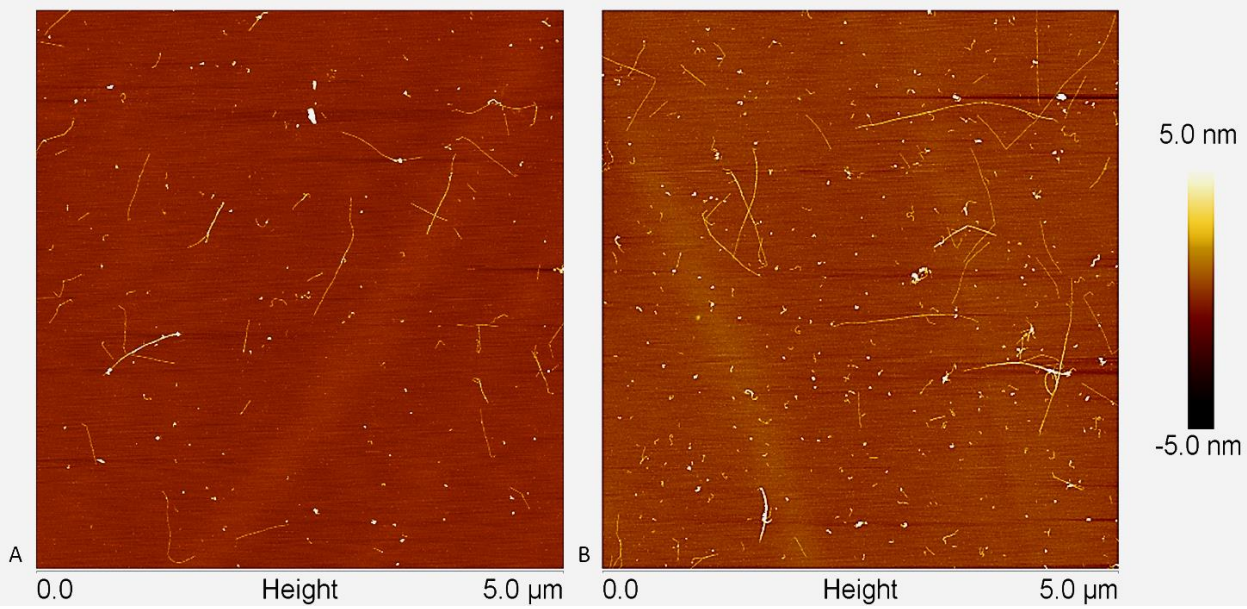

Figure 34: Two 5-Micron Wide Images of T_{40} and TAT-Biotin Wrapped 6, 5-SWCNTs after Electrodialysis and Drop Dialysis Buffer Exchange
AFM image of 6, 5-SWCNTs that have been wrapped in T_{40} ssDNA (A) and TAT-biotin (B) then electrodialysis treated for two hours followed by an hour of drop dialysis/buffer exchange.

Immobilization of Carbon Nanotubes on DNA Origami

After the CNTs are wrapped in ssDNA and the CO is modified to the desired specifications, functionalization of CO with CNTs is performed both in a solution approach and via a sequential surface deposition approach. Functionalization was performed using

electrodialysis then drop dialysis treated carbon nanotubes and CO-01 with excess staples removed. To test the optimum capabilities of different origami arrays with functionalized carbon nanotubes on their surfaces, eight different deposition and modification approaches were investigated, as shown in Figure 35. Both 0D and 1D CO-01 with $(TAT)_{10}$ and biotin docking sites were functionalized with carbon nanotubes both in solution and on the mica surface to study a full array of functionalization approaches.

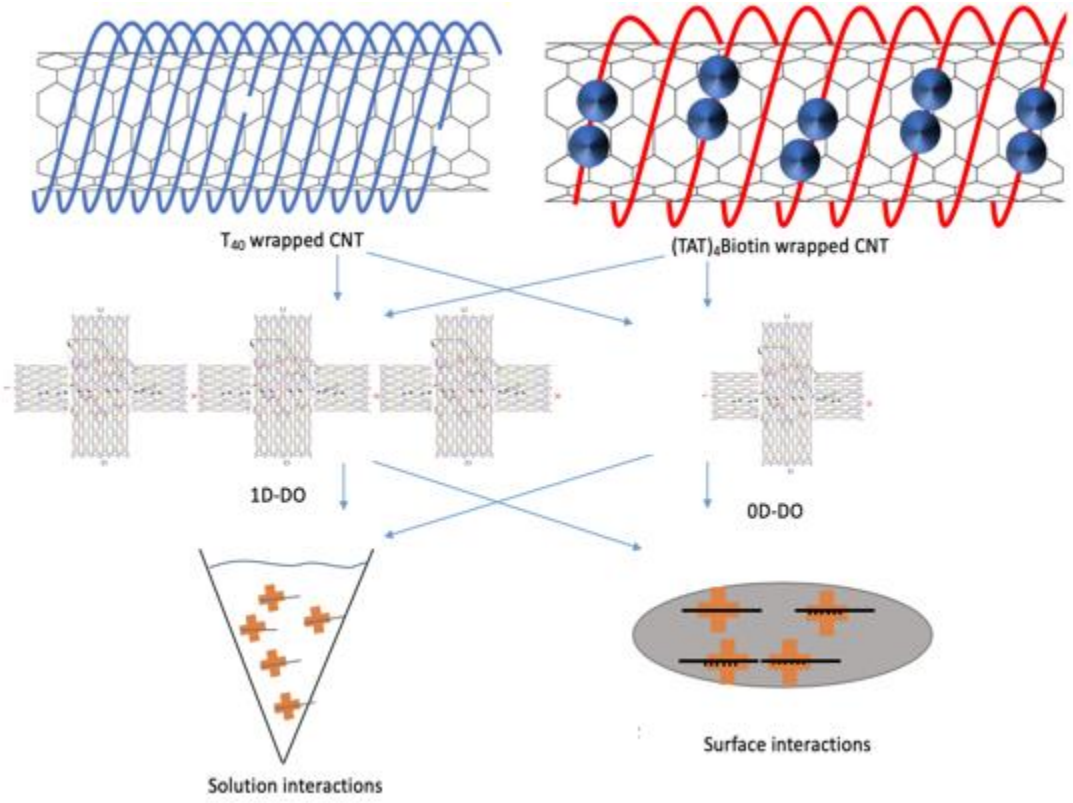

Figure 35: Schematic of the Different Functionalization Procedures Performed
Schematic of the different experimental procedures performed. T_{40} wrapped CNTs or $(TAT)_4$-Biotin wrapped CNTs are bound to 1D CO-01 arrays and 0D origami via specific docking sites in solution or on mica surfaces utilizing pre-immobilized origami. (Eight experimental designs in total).

$(TAT)_{10}$ Docking Sites

Immobilization of CO-01 with $(TAT)_{10}$ docking sites and CNTs were performed and studied in both a solution and a surface technique for both 1D and 0D CO-01. In solution, for

proper functionalization of the T_{40} ssDNA wrapped CNTs on the CO-01 with twelve central $(TAT)_{10}$ docking sites (both 0D and 1D), equal volumes CO (6 µL) (10 nM) and solubilized CNT (6 µL) (~70 nM of 100 nm CNT equivalents) plus 0.6 µL 10X COB was annealed from 45°C to 20 °C over a period of 25 hours in the PCR system followed by sample storage at 4 °C.

For surface functionalization of 0D CO-01 and 1D CO-01 modified with $(TAT)_{10}$ docking sites, with electrodialysis and drop dialysis treated T_{40} wrapped CNTs, 0.25 µL of CO-01 (10 nM) was adsorbed onto a prepared mica surface which had been cut to fit within a 200 microliter PCR sample tube (Figure 36). To enable maximum coverage, the CO-01 was allowed to dry on the mica surface, then the mica was placed into an empty sample tube. The mica sample with CO-01 pre-immobilized on it was then covered with a 10 µL of drop dialysis treated CNTs (~70 nM of 100 nm CNT equivalents) in 90 µL 1XCOB for a final volume of 100 µL. Sample was ramped to 45° C then cooled to 20 ° C over a period of four hours, then incubated overnight at 20 °C. Samples were stored at 4 °C.

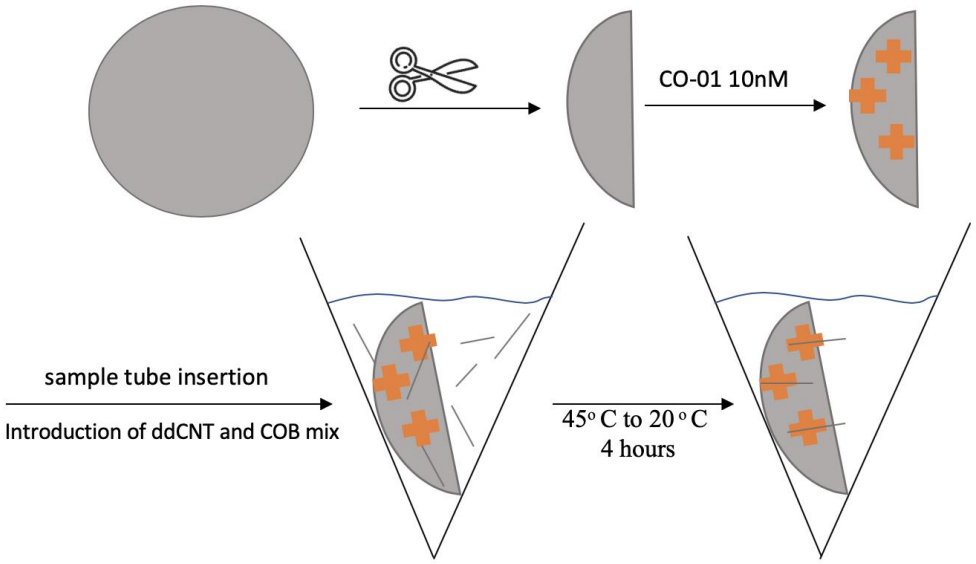

Figure 36: Schematic Depiction of Surface Functionalization of CO-01 with T_{40} Wrapped CNTs
A plain mica slide is cut to fit into a 200 µL sample tube. It is then coated in 10 nM CO-01. Mica slide is inserted into sample tube which is then filled with ed-ddCNT/COB solution until mica slide is covered. Sample is annealed for four hours, stored at 4 °C, and then imaged on Bruker MM8 AFM.

Streptavidin-Biotin Docking Sites

For functionalization in solution of 0D CO-01 and 1D CO-01 containing biotin tethers with electrodialysis and drop dialysis treated TAT-biotin wrapped CNTs onto, equal parts CO-01 (6 µL) (10 nM) and solubilized CNT (6 µL) (~70 nM of 100 nm CNT equivalents), plus Streptavidin (8 µL) (100 nM), plus 0.6 µL Tris-Acetate-EDTA/$MgCl_2$ buffer were incubated overnight at 20 °C and stored at 4 °C.

A surface deposition technique utilizing the biotin-streptavidin interactions was performed on mica surfaces prepared for AFM imaging. A mica surface was first pre-treated with 10 nM diafiltered CO-01 to immobilize them, then the surface was exposed to 8 µL of 100 nM streptavidin at an 8:1 ratio streptavidin: CO-01, then incubated on the mica for 30 minutes in a humidity chamber to prevent drying of the sample. After 30 minutes, excess streptavidin is rinsed away with COB and 2 µL of ~70 nM 100 nm CNT equivalents of electrodialysis then

drop dialysis treated $(TAT)_4$-biotin wrapped CNTs were introduced to the mica surface for at least two hours (Figure 37).

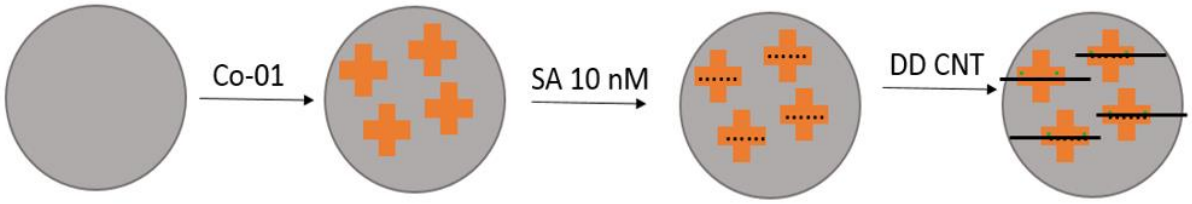

Figure 37: Schematic of Stepwise Surface Reaction Performed on Mica Surfaces
Using a mica surface prepared for AFM imaging, all reactions were kept in a humidity chamber to prevent drying of the sample, and reagents were added stepwise as depicted here

3'3-Diaminobenzidine (DAB) as substrate for DNAzyme

CO-01 0D 10 nM presumed to carry G4/hemin was deposited onto a prepared mica slide, incubated for 5 minutes, rinsed, and then blown dry with argon gas. The immobilized CO-01 was reacted with 5 µL 0.1% DAB (ThermoFischer) and 1 µL 0.3% H_2O_2 for one minute. The mica was then rinsed and imaged with Bruker MM8. This reaction process is described in Figure 38.

Figure 38: DNAzyme Peroxidase Activity Monitored Using DAB as a Precipitating Indicator
Scheme depicting the steps taken to observe precipitate formation catalyzed by the DNAzyme on the left arm of CO-01. The red square represents the location of the DNAzyme and the small blue circles are representative of the locations of $(TAT)_{10}$ docking sites. After introduction of DAB and H_2O_2, for one minute, a localized precipitate forms on the DNAzyme location.

H_2O_2 Mediated Oxidative Cutting of Carbon Nanotubes

Following immobilization of carbon nanotubes onto DNA origami surfaces by the various methods described above, along with DAB studies which ensured the DNAzyme was active, H_2O_2 was used to initiate oxidative cutting of nanotubes on locations previously chosen through G-quad location selection. For CO-01 with twelve central $(TAT)_{10}$ docking sites and T_{40} wrapped CNTs that were prepared in solution, the sample was absorbed to a prepared mica slide by the same method used to prepare samples for AFM imaging. Samples were prepared from a solution of 2 µL 1D CO-O1/CNT and 8 µL 1X COB for a final CO-01/CNT concentration of approximately 2 nM based on the origami concentrations. Hemin was prepared for sample introduction by being initially dissolved in DMSO and then further diluted in 1X COB to give a final concentration of 10 nM Hemin. The sample was exposed to 2 µL of 10 nM hemin at an approximate 1:1 ratio CO-01 to hemin for 30 minutes, assuming the CO-01 is 2 nM based on assumed dilutions and inferring one DNAzyme per origami. The sample was reacted with 1 µL of 3 mM final concentration H_2O_2 for a total of 2 hours before it was rinsed with 400 µL of H_2O and imaged with AFM.

Solution phase reaction of the biotin-streptavidin CNT/CO constructs with H_2O_2 was performed but not studied in depth; instead efforts were directed toward study of the sequential surface functionalization technique. For sequential surface depositions and immobilization of CO-01 and CNTs facilitated by streptavidin-biotin interactions, the sample was reacted with 2 µL of 10 nM hemin representing a ratio of 2:1 hemin: CO-01, for 30 minutes, then the sample was reacted with 1 µL of 3 mM H_2O_2 solution for a total of 2 hours before it was rinsed with 400 µL H_2O and imaged with the MM8 AFM.

CHAPTER 5
RESULTS AND DISCUSSION

Fluorescence and Absorbance Analysis of CNTs

Using the fluorescence protocol described previously, the length of individual emitters were measured based on the optical image in Figure 39. Of 20 measurements selected from eight different regions from eight modified substacks, the total average measured length of 6, 5-SWCNTs observed was 0.9 microns, with a standard deviation of 0.3 microns, which closely coincides with manufacturer's specified values of the average length of CoMoCAT synthesized 6,5-SWCNTs purchased from Sigma.[14, 15]

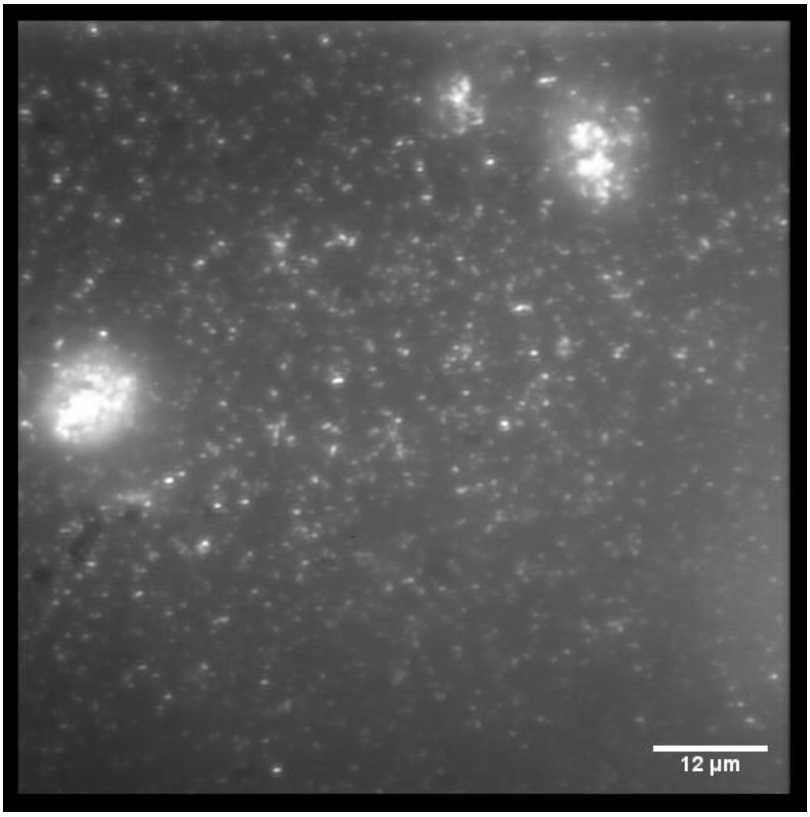

Figure 39: Example Image of Fluorescent Purified 6, 5-SWCNTs
Average fluorescence intensity projection image derived from70 frames (substack) of a time course video of 6, 5-SWCNTs that have been purified via electrodialysis and drop dialysis. 20 emitters were randomly chosen and the average length of long axis measurements was observed to be 0.9 microns with a standard deviation of 0.3 microns.

To confirm the presence of an enriched population of 6,5-SWCNTs after electrodialysis purification and chirality selection via solubilization, an absorption spectrum was acquired (Figure 40) then correlated with early literature[59,66] reports and values observed for purified CNTs by DuPont researchers and reported in the publication "*DNA sequence motifs for structure-specific recognition and separation of carbon nanotubes."*[23] The values here were in good agreement with DuPont experimental values but about 10 nm longer in wavelength than the previously reported literature values.

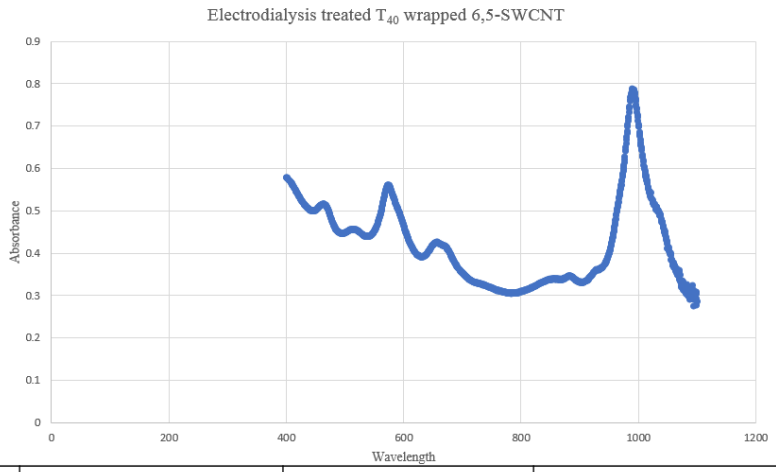

Chirality (n, m)	E11 (nm)			E22 (nm)			E33 (nm)			E44 (nm)		
	Lit[59,68]	DP obs[23]	MU obs	Lit[59,68]	DP obs[23]	MU obs	Lit[59,68]	DP obs[23]	MU obs	Lit[59,68]	DP obs[23]	MU obs
6,5-SWCNT	976	988	992	566	571	574	344	346	N/A	302	N/A	N/A

Figure 40: Absorption Spectrum and Peak Comparison Observed Versus Literature Values for 6, 5-SWCNTs
This figure shows the absportion spectrum captured of T_{40} wrapped 6, 5-SWCNTs that have been treated with electrodialysis for two hours. MU observed E11 and E22 transitions as collected in the absorbance data. DP observed shows the values reported in *DNA sequence motifs for structure-specific recognition and separation of carbon nanotubes.*[23] Lit refers to DuPont's E transition values found through two reviews of SDS wrapped SWCNTs.[59,66]

DNA Origami

AFM images were obtained at each step of each reaction to confirm structure and function of both CO-01 and CNTs. Since the $(TAT)_{10}$ staples are not visible through standard

peakforce feedback AFM, the appearance of a normal, CO-01 cross structure was used to deduce the staples were integrated properly since missing staples would destabilize the structure. For CO-01 with biotin docking sites, while biotin itself is too small to be observed, streptavidin can be easily distinguished when imaged with AFM because of streptavidin's diameter and height difference from the origami surface. An image of streptavidin populated CO-01 structures is shown in Figure 41 followed by a quantitative population analysis in Table 5. Because streptavidin is multivalent for biotin (3-4 per streptavidin) a single streptavidin can bind to more than one biotin tether. Upon measuring the maximum possible surface area potentially swept by the biotin tethers (i.e. maximum reach) shown in Figure 42, and G-quad staple, it is not unreasonable that only between four and five streptavidins bind to each CO-01.

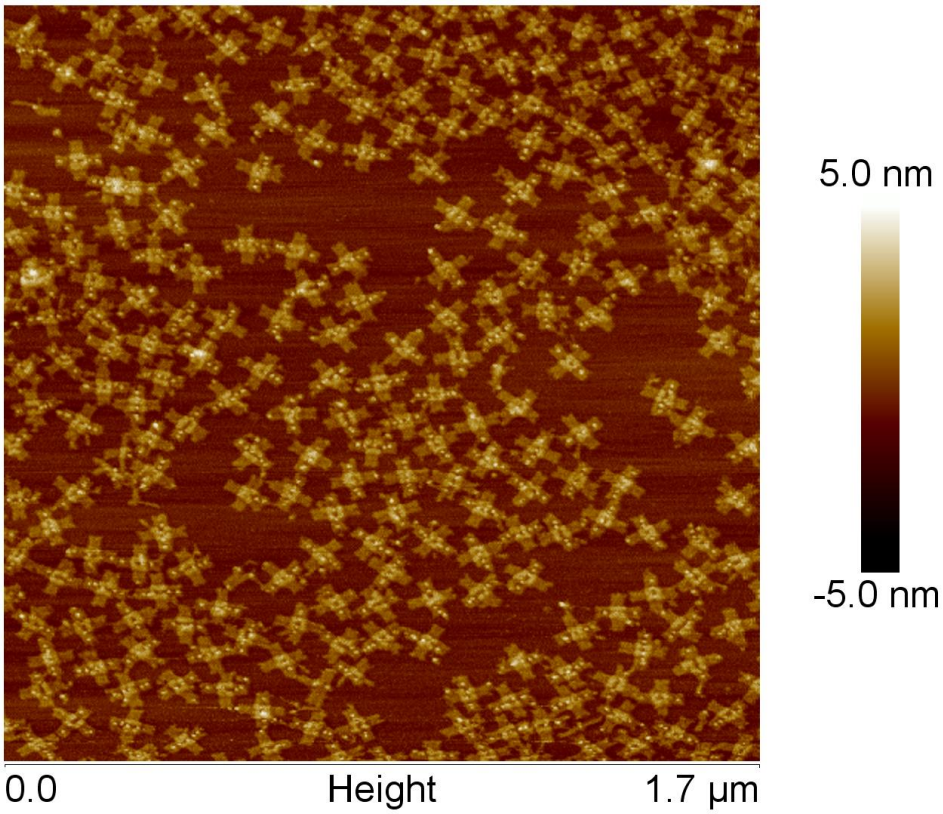

Figure 41: CO-01 with Biotin Docking Sites and Bound Streptavidin
This figure depicts a 1.7-micron wide height signal AFM image of biotin-streptavidin binding on CO-01. This AFM image shows an unpurified sample of CO-01 with streptavidin synthesized at a ratio of 1:10 CO-01: streptavidin. Each origami averaged 4 streptavidins per 8 docking sites, however there were instances of up to 7 streptavidin per origami.

# Streptavidin	Amount of CO-01 possessing SA #	% CO-01 with # SA
1	1	0.45 %
2	12	5.4 %
3	45	20.27 %
4	86	38.74 %
5	58	26.12 %
6	11	4.95 %
7	2	0.9 %
8	0	0 %
No streptavidin binding	7	3.15 %

Table 5: Streptavidin Binding Analysis of CO-01
Analysis of the image in Figure 41, 222 CO-01 with eight central biotin docking sites were counted excluding CO-01 partially in the image. 38.74% of CO-01 present possessed four streptavidin even though 8 biotin docking sites are available. 26.12% possessed five streptavidins.

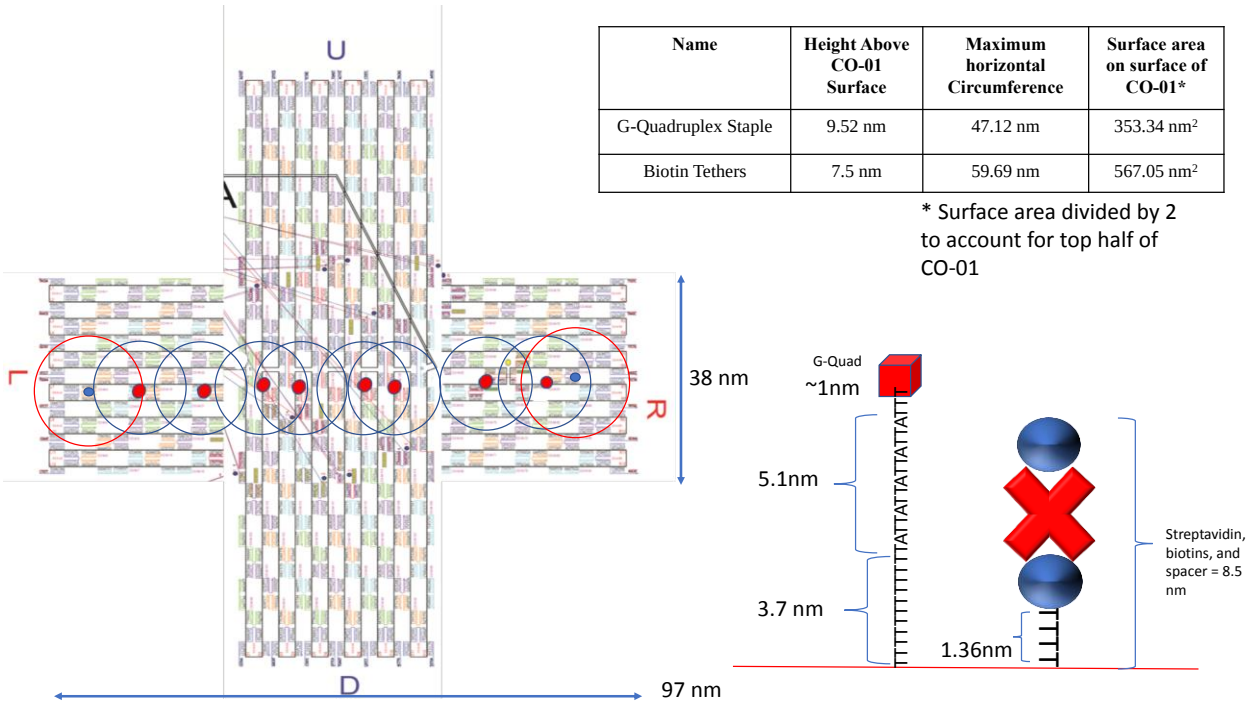

Name	Height Above CO-01 Surface	Maximum horizontal Circumference	Surface area on surface of CO-01*
G-Quadruplex Staple	9.52 nm	47.12 nm	353.34 nm^2
Biotin Tethers	7.5 nm	59.69 nm	567.05 nm^2

* Surface area divided by 2 to account for top half of CO-01

Figure 42: Circumference and Surface Area of G-quadruplex Staples and Biotin Docking Sites on CO-01

The red outlines correspond with the maximum horizontal distance the end of the G-quadruplex staple can travel. The blue outlines correspond with the maximum horizontal location the biotin tethers can reach. Looking at the overlaps on the surface, it is reasonable to assume not all eight biotin docking sites would have an individual streptavidin due to the multiple valency of streptavidin.

1D origami arrays were visualized and assembly was confirmed through AFM imaging (Figure 43). An analysis of twenty individual, 5-micron wide height scans provided the frequency of polymer length assemblies produced using a 1:7 terminating end to CO-01 ratio. Aggregations of 1D were not included in the count because the individual monomers cannot be clearly observed for counting, 1D CO-01 was counted and the instances of CO-01 ranging from 1-12 monomers per linear array were tallied. Throughout a calculated total of 195 instances of 1D CO-01, 25% remained in its 0D monomer form, 12% became sequences of three monomer arrays (3'mers), and only 3% of the linear arrays formed 8'mers, the designed 1:7 ratio of terminating ends to CO-01 (Table 6).

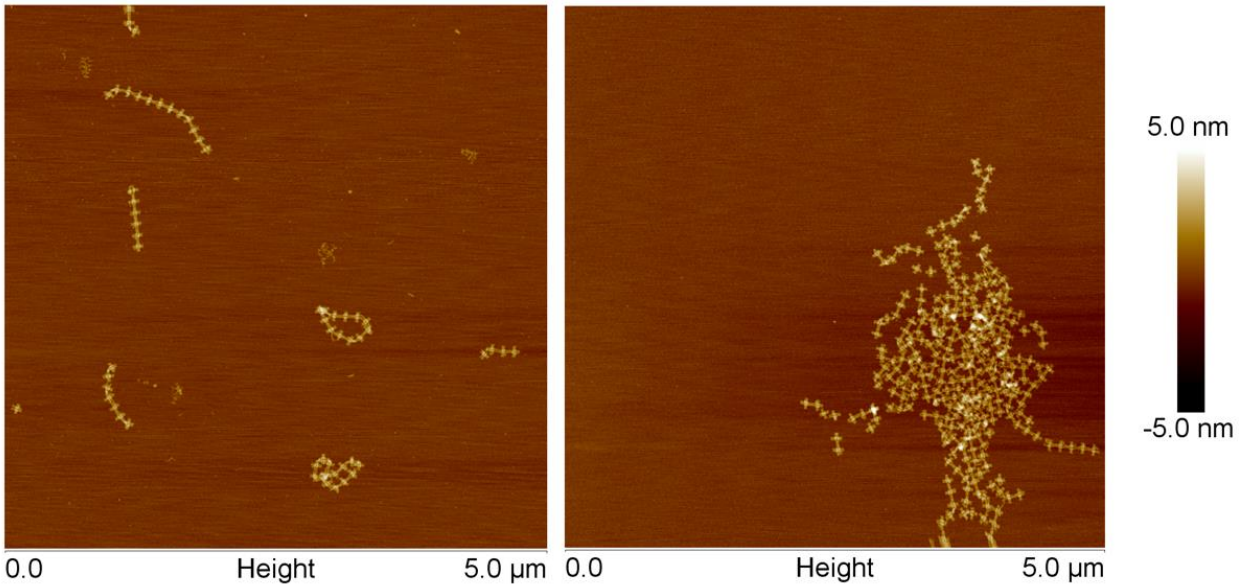

Figure 43: Example Images of 1D Linear Arrays of CO-01 and the Distribution of Lengths
Two AFM images showing the distribution of lengths of 1D linear arrays synthesized with a 1:7 terminating end CO: CO-01 ratio. Right shows an instance of "clumping" or aggregations that can arise even without the presence of CNTs, however, they are not as frequent or large in the absence of CNTs.

1D Linear Sequence Length	# instances of sequence length	Percentage Cases of defined lengths over 195 1D linear arrays
1	49	25%
2	39	20%
3	23	12%
4	15	7.7%
5	12	6.1%
6	6	3%
7	6	3%
8	6	3%
9	6	3%
10	5	2.5%
11	1	0.5%
12	4	2%
Longer/Aggregated	23	12%

Table 6: Distribution of CO-01 1D Linear Arrays Observed Lengths
1D CO-01 were counted, composed of 195 oligomers ranging in length from 0D (monomers) to 12 monomers linked to form a 1D linear array. Any 1D Co-01 arrays longer than 12 monomer units and/or aggregated, were not counted, but placed into a longer/aggregation row which constituted over 12% of the instances of origami.

Excess staple removal and purification for both 0D and 1D CO-01 was assayed via UV-Vis absorption spectroscopy using A_{260} measured using a Nanodrop ND 1000 spectrometer. Figure 44 presents spectra for two sets of 0D CO-01 constructs both before and after removal of excess staples. The red and green absorbance spectra are from the two origami solutions with excess staples present, and can be compared to the brown and bright green spectra representing the CO-01 solutions which have had all the excess staples removed. CO with excess staples removed have a much lower absorbance value, indicating a higher degree of purity. However, we find that a loss of intact CO also occurs such that the concentration is reduced to 1-2 nM after diafiltration.

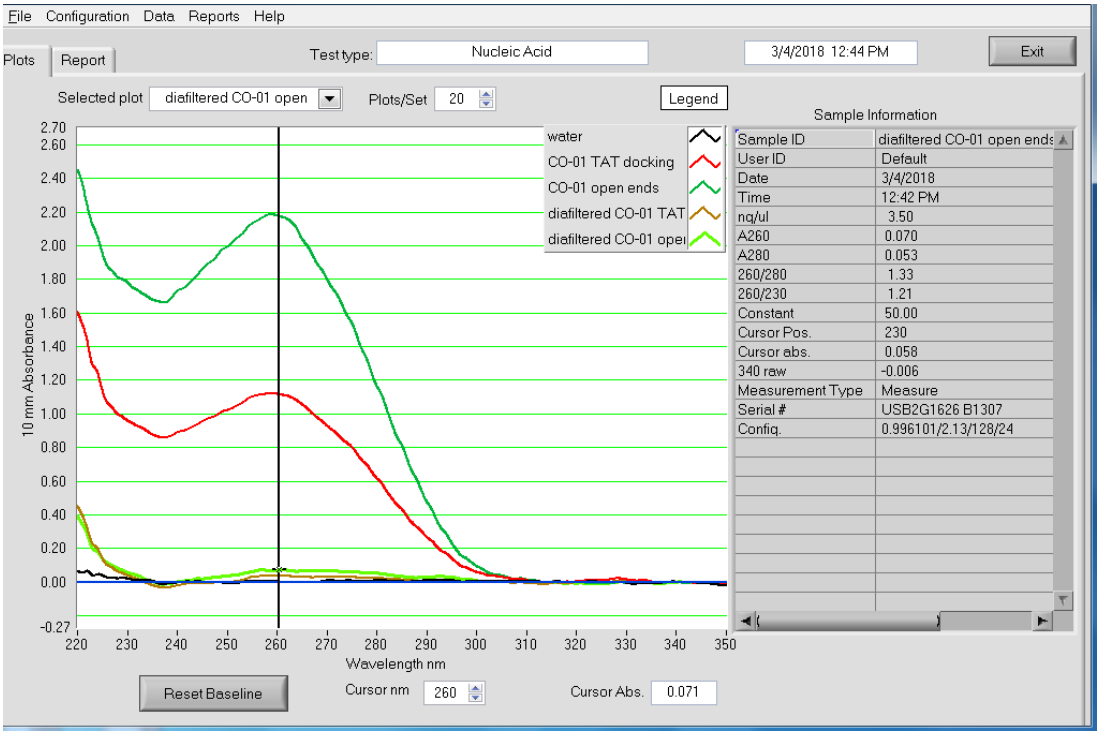

Figure 44: Nanodrop ND 1000 Absorption Spectra of CO-01 Solutions with and Without Excess Staples

Spectra of CO-01 solutions with 5X excess staples and after excess staple removal accomplished through 30 kDa Millipore filtration. The samples were two different CO-01 constructs, one with the $(TAT)_{10}$ docking sites and one with the left and right arms of the origami open with unpaired M13 bases used in prior studies.[4] The higher absorbance readings reflect the CO-01 with excess staples, whereas the low absorbance spectra reflect the absorbance of CO-01 after the removal of excess staples.

SWCNT Purification

Solubilized 6, 5-SWCNTs treated through electrodialysis and drop dialysis buffer exchange showed a decrease in tangling within each other through each stage of purification. After CNTs are initially solubilized, they are in a mixture containing excess DNA, NaCl, and H_2O, where both excess H_2O and NaCl can be damaging to DNA or prevent binding to mica. When the CNTs are run through the electrodialysis process, excess DNA not affiliated with a nanotube is filtered or caught in the 50 kDa membranes in the electrodialysis chamber and water is exchanged with a Na_2HPO_4 buffer. While the electrodialysis treated nanotubes show less aggregation and a more uniform appearance in length, they are still dispersed in a buffer that contains sodium chloride and does not serve as the best solution for deposition and integrity of CO. Drop dialysis appears to preserve CNT concentration while enabling exchange of COB for NaCl. Representative images of CNTs at each purification step are shown for the T_{40} wrapped CNTs in Figure 45. The B-TAT wrapped CNTs possess approximately the same appearance at each stage.

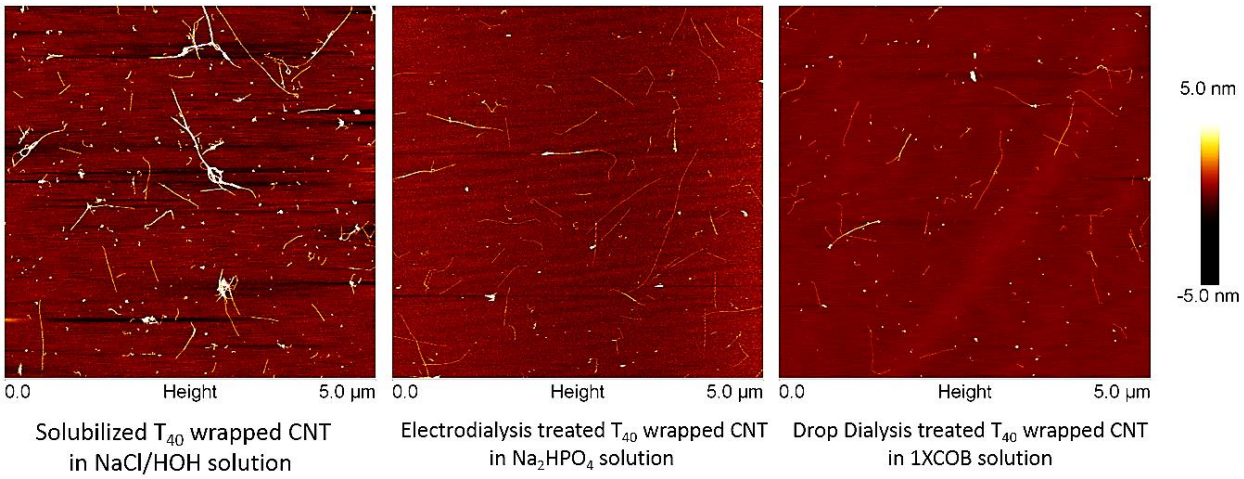

Figure 45: T_{40} Wrapped CNTs During Each Stage of Purification
From left to right, each AFM image visually depicts the increasing purity and uniformity of T_{40} wrapped 6, 5-SWCNTs.

SWCNT Immobilization

Carbon nanotubes immobilized onto DNA Origami arrays were imaged and confirmed through AFM analysis.

Solution Based 0D and 1D CO-01 $(TAT)_{10}$ Immobilization

Solution based functionalization of 0D CO-01 with CNTs via $(TAT)_{10}$ docking sites yielded samples with tangled aggregates of CNTS and CO. Commonly, ropes of CNTs oriented down the center or on the arms of individual monomers were observed. Immobilization of CNTs onto CO surfaces were present, but visualization and analysis was hindered due to the presence of aggregations and the binding of multiple CNTs onto COs (Figure 46).

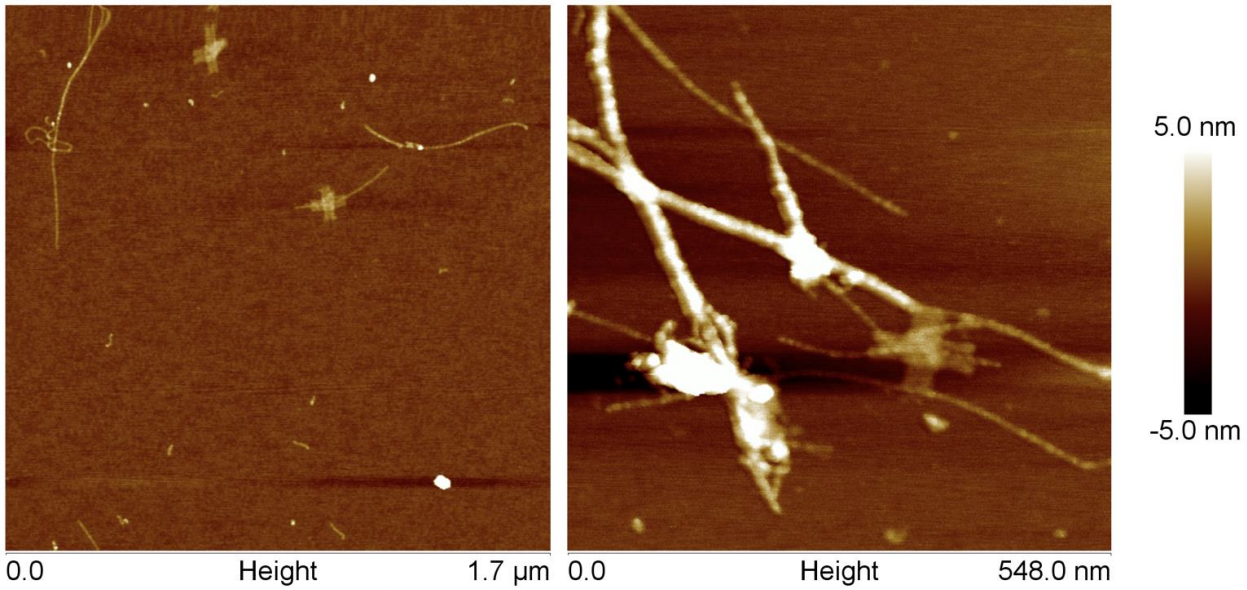

Figure 46: Solution Immobilization of CNTs onto 0D CO-01 via $(TAT)_{10}$ Docking Sites
Two AFM images demonstrate instances of functionalization of DNA origami with carbon nanotubes via homogeneous solution phase reaction. Some of the CNT/CO intertwine.

For constructs containing 1D CO-01 with $(TAT)_{10}$ docking sites and functionalized in solution with electrodialysis drop dialyzed T_{40} wrapped CNTs, the observed tangling between CNTs and 1D CO-01 led to difficulty in visualizing functionalization. Since CNTs tend to aggregate together and form ropes, many AFM results showed large masses of aggregations that

were only viewable at high magnification on the outer edges of the mass (Figure 47). Despite the size of aggregates, there was a large degree of functionalization displayed on these outer edges. It is therefore probable that there is also a large amount of functionalization within the aggregations as well, which are not visualizable through AFM. The outer edges of aggregates showing successful functionalization provided evidence that the TAT docking sites were binding properly, despite the tangling (Figure 48). Imaging the outer edges did provide some insight to functionalization outside the aggregates, but the regions with a high degree of aggregation could not be imaged, limiting the statistical information that could be obtained through studies of samples prepared in this manner. To decrease the presence of aggregations, sequential surface functionalization was implemented.

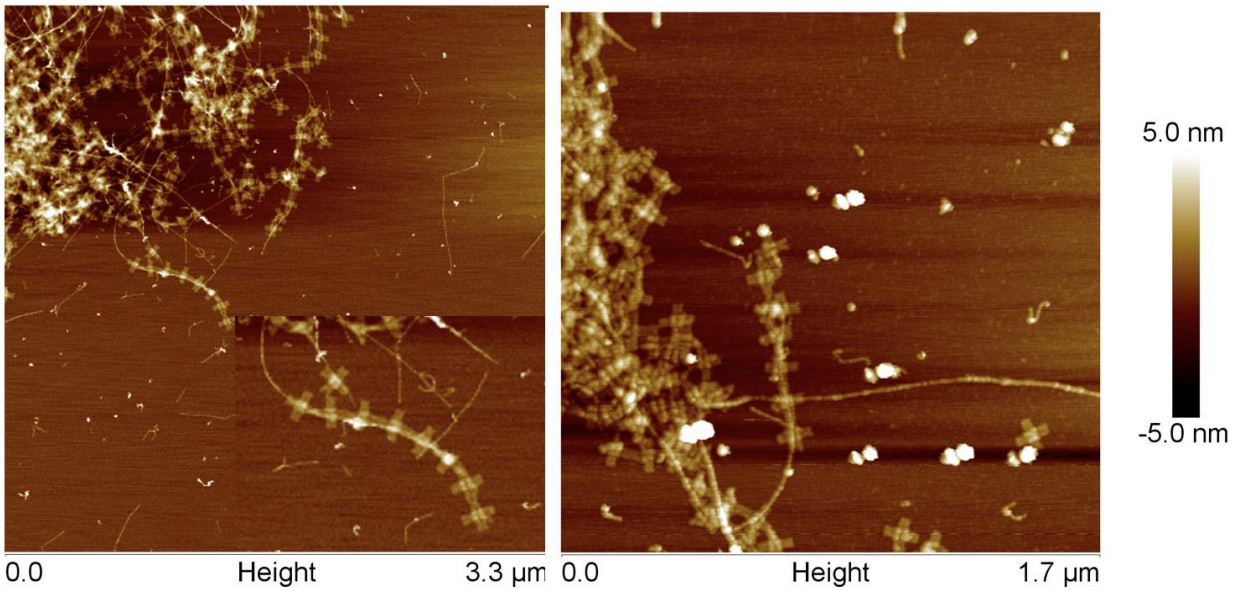

Figure 47: Immobilization of Carbon Nanotubes on 1D CO-01 through TAT Docking Sites
Two AFM images of the outer edges of large aggregates that display the high degree of CO-01 functionalization with CNTs. The inset provides a closer view of a 1D linear array 8 monomer units in length functionalized down the center with a CNT.

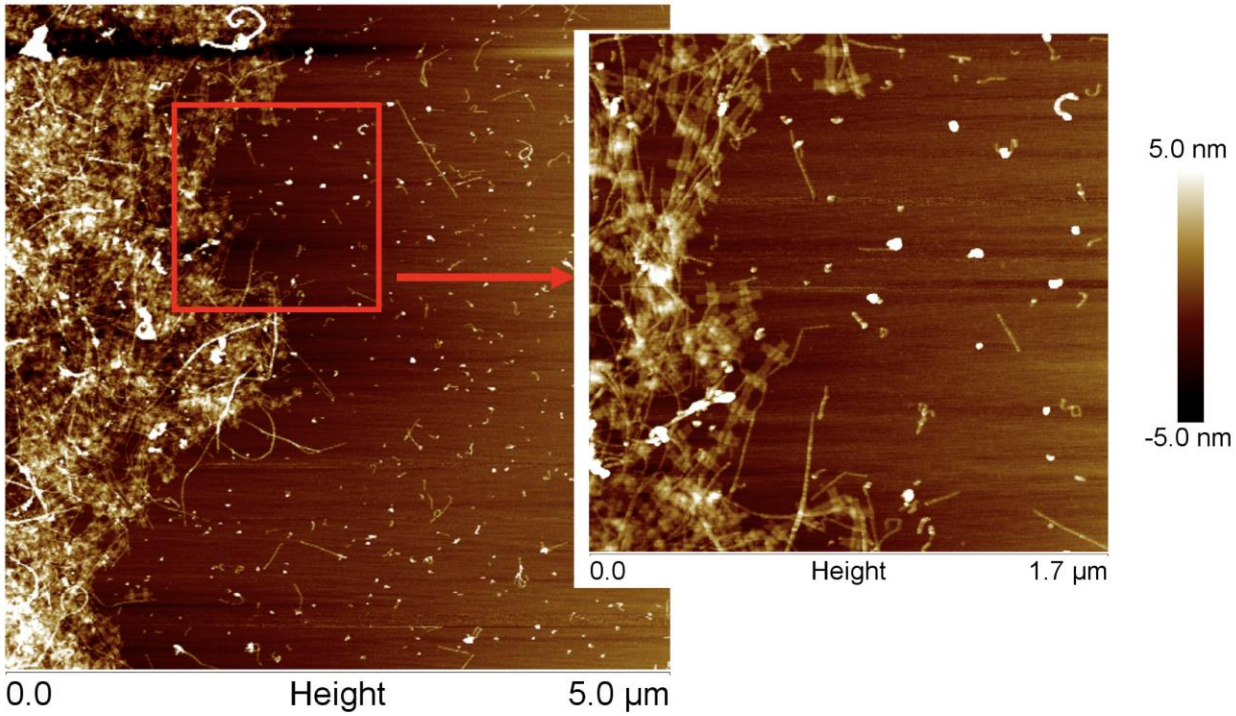

Figure 48: AFM Imaging of Aggregates and a Higher Magnification View of Functionalization Visible on the Outer Edges of Aggregates
A five-micron wide height mode AFM image of 1D CO-01 $(TAT)_{10}$ aggregation with T_{40} wrapped electrodialysis and drop dialysis treated CNTs. This is a good example showing how large these aggregates can become, making imaging of a large portion of the sample unrealistic. A zoom (right side) image of the outer edges of these aggregates provides a clearer view of the structures of the complex between CNTs and CO.

Surface 0D and 1D CO-01 $(TAT)_{10}$ Immobilization

Functionalization of surface bound 0D CO-01 with $(TAT)_{10}$ docking sites with electrodialysis then drop dialyzed CNTs on mica proved to remove the formation of aggregates, but also greatly decreased the degree of functionalization while increasing the appearance of an impurity tentatively identified as "carbon soot," or carbon originating during CNT synthesis and still remaining in the samples (Figure 49). Though greatly reduced, the occurrence of some successful functionalization on surfaces provides a beginning platform for future studies of surface modifications with DNA and CNT interactions through DNA binding.

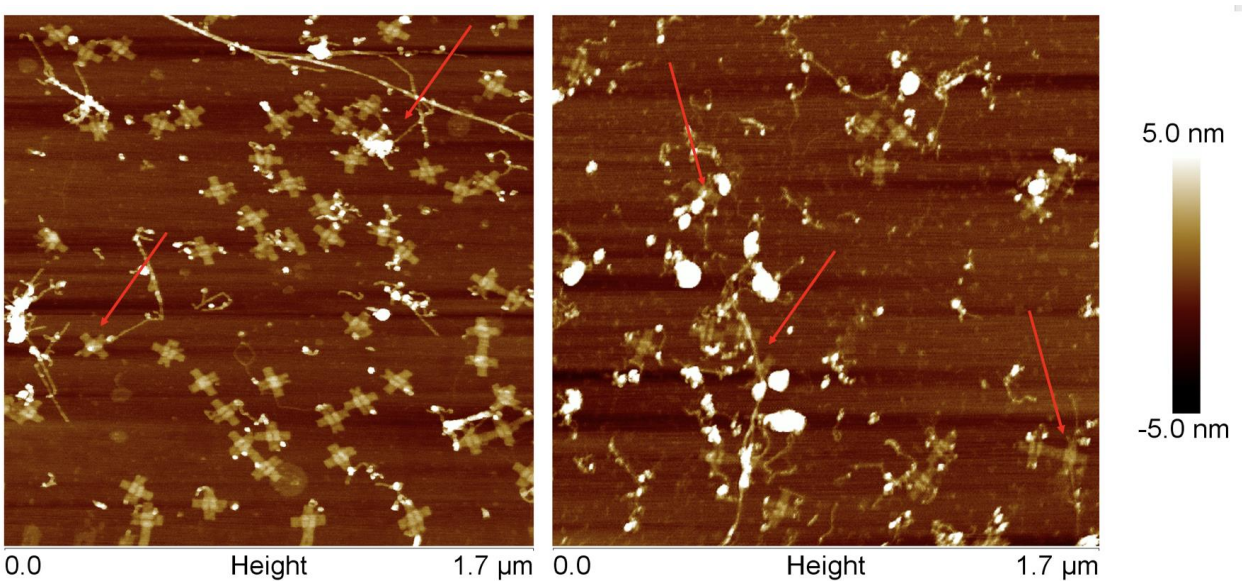

Figure 49: Surface Immobilized 0D CO-01 with Twelve Central $(TAT)_{10}$ Docking Sites Treated with Electrodialysis then Drop Dialyzed 6,5-SWCNTs

Two images of 0D CO-01 with twelve central $(TAT)_{10}$ docking sites first immobilized on mica then reacted with electrodialysis then drop dialysis treated T_{40} wrapped 6,5-SWCNT. There are several instances of CO functionalized with CNTs, however, the white "masses" on the origami surface appear to interfere with binding.

Stepwise surface functionalization of 1D CO-01 modified with $(TAT)_{10}$ docking sites involves pre-immobilization on mica and is followed by reaction with electrodialysis then drop dialyzed CNTs. This deposition technique proved to eliminate the formation of aggregations, but decreased the degree of interactions between the CO and CNTs, just as in the case of 0D CO-01 TAT. There was a high concentration of both CNTs and 1D CO-01 on the completed mica surface (Figure 50) suggesting a high probability of interaction.

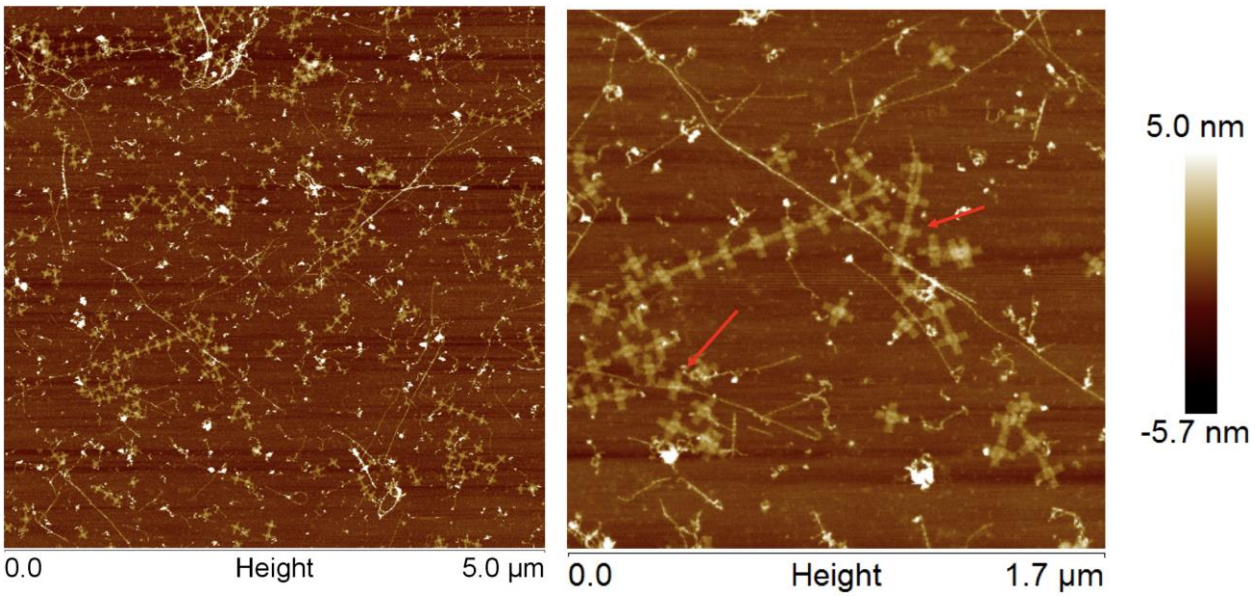

Figure 50: AFM Images of Products of the Reaction Between Surface Bound of 1D CO-01 with $(TAT)_{10}$ Docking Sites and T_{40} Wrapped CNTs
Two AFM height images of 1D CO-01 with $(TAT)_{10}$ docking sites and T_{40} wrapped CNTs. The number of CNTs and 1D CO-01 was approximately equal, but there was little complex construct formation. In the right image the two red arrows show regions of successful functionalization, with one of the instances of functionalization very faint and difficult to see (upper right quadrant).

Solution 0D and 1D CO-01 Biotin-Streptavidin Immobilization

As described earlier, reaction of 0D CO-01 with CNTs through biotin-streptavidin provided a high degree of functionalization, but retained the same problem seen with the T_{40} wrapped CNTs such as the aggregations. Figure 51 provides AFM images of two examples of CNT depositions which are very different in appearance. Figure 51A shows not only the aggregates of CNTs, but shows an apparent increase in the thickness of the CNTs, perhaps due to streptavidin binding to the CNTs. What is believed to be happening is, even with carefully calculated streptavidin to origami ratio, the streptavidin prefers binding the nanotubes together, creating ropes, aggregates, and causing difficulty in visualizing functionalization. Figure 51B is another AFM image of the same mica sample as in A. Figure 51B also shows the presence of aggregation, but the streptavidin appearance on the CNTs is minimal, while the origami is well

decorated. Since positional control of single isolated nanotubes is one of the purposes of this work, streptavidin-biotin immobilization of CNTs on CO in solution is not the most feasible option. Similar aggregations and variation in streptavidin binding results were observed for 1D CO-01 solution phase assembly (Figure 52).

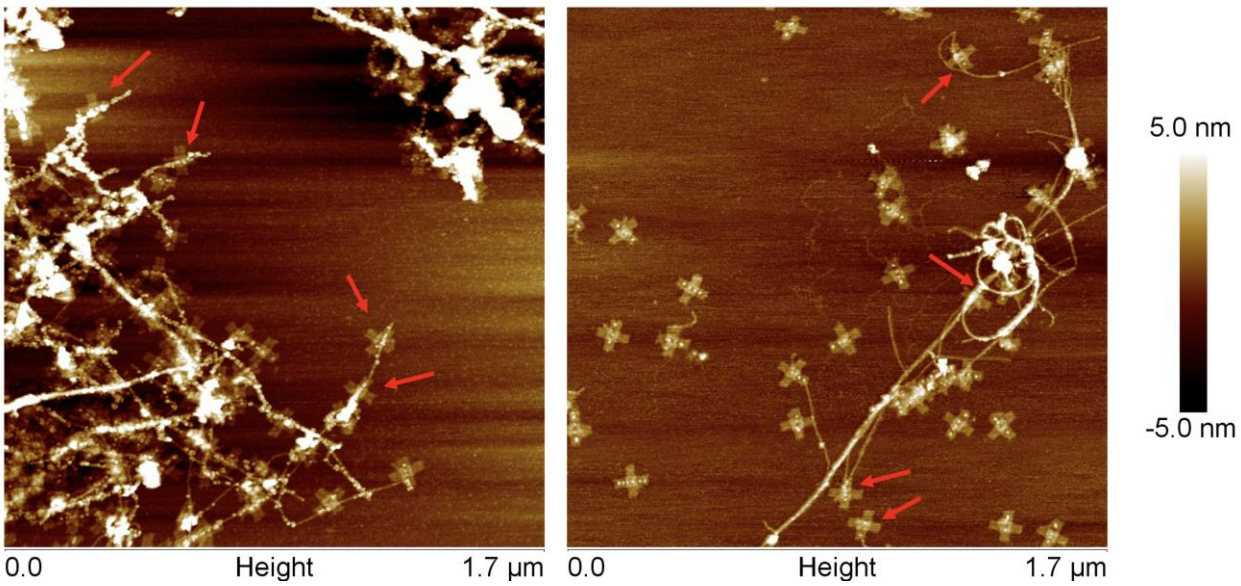

Figure 51: Solution Phase Immobilization of CNTs on CO Mediated Through Streptavidin-Biotin Interactions
Two AFM images from the same sample showing the variation that can occur through solution phase reaction of CNTs and CO. Red arrows indicate CNT modified constructs.

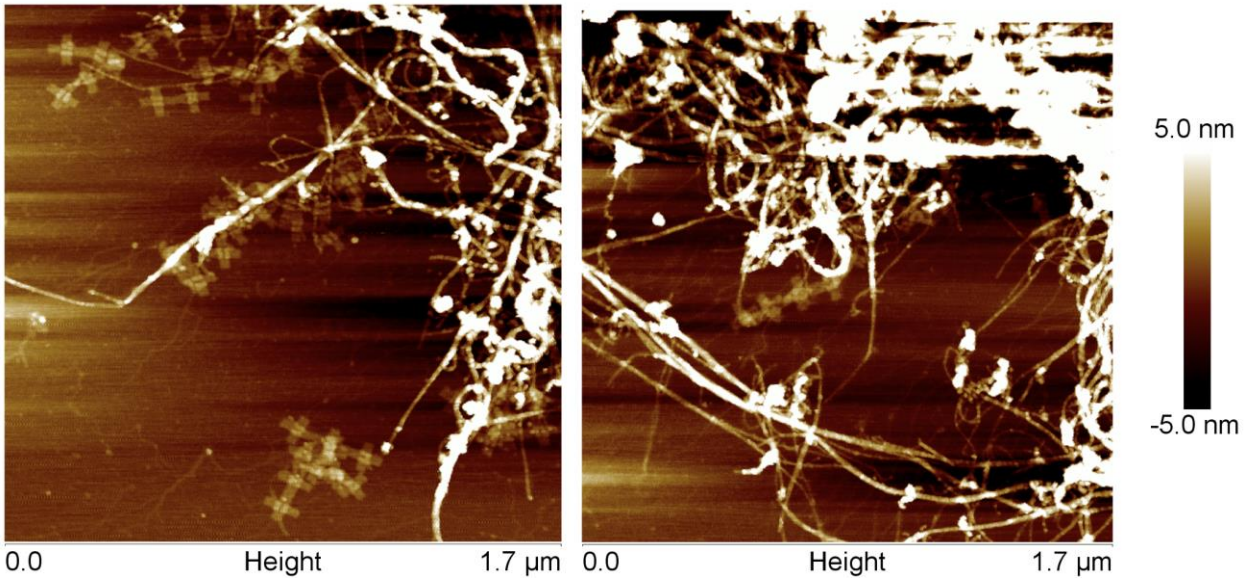

Figure 52: Solution Immobilization of CNTs onto 1D CO Moderated Through Streptavidin-Biotin Interactions
Two AFM images showing solution phase immobilization of CNTs onto 1D CO-01 mediated through biotin streptavidin interactions yielding large aggregates.

Surface Immobilized 0D and 1D CO-01 Reacted with CNTs Through Biotin-Streptavidin Mediation

Surface immobilization of CO-01 before reaction with streptavidin enables rinsing before reaction with $(TAT)_4$-biotin wrapped CNTs. This reaction was performed on a prepared mica slide, at room temperature, in a humid chamber to prevent sample drying. The reaction of surface immobilized CO with CNTs through streptavidin biotin bridges provided a high frequency of predicted CNT/CO constructs and eliminated the appearance of aggregates of CNTs. There were small quantities of impurities, but they were minimal in comparison to the solution binding solution processes. Figure 53 displays images at three different magnifications of the products of biotin mediated binding. Figure 54 shows two examples of successful surface immobilization in a 3-D perspective view, which provide a clearer view of the structures of the products. For 1D pre-immobilized constructs, in which CO-01 was first absorbed onto the mica, then reacted with streptavidin, then further reacted with CNTs, the CO did not appear to react to

the same extent as 0D, or as was expected. One hypothesis is that a high degree of rotation of the 1D arrays cannot occur, whereas the 0D constructs can possibly rotate on the surface. This rotation hinderance possibly explains why CNTs didn't immobilize on the 1D CO surface as well as they did on the 0D CO (Figure 55). It can also be hypothesized that the strength of rinsing the mica slides for AFM preparation can play a part in removing bound streptavidin or possibly bound CNTs from the CO, taking with them the streptavidin. Comparing the surface immobilization approaches, the streptavidin-biotin interactions provided the least amount of aggregations, required no heat, and could be performed within hours.

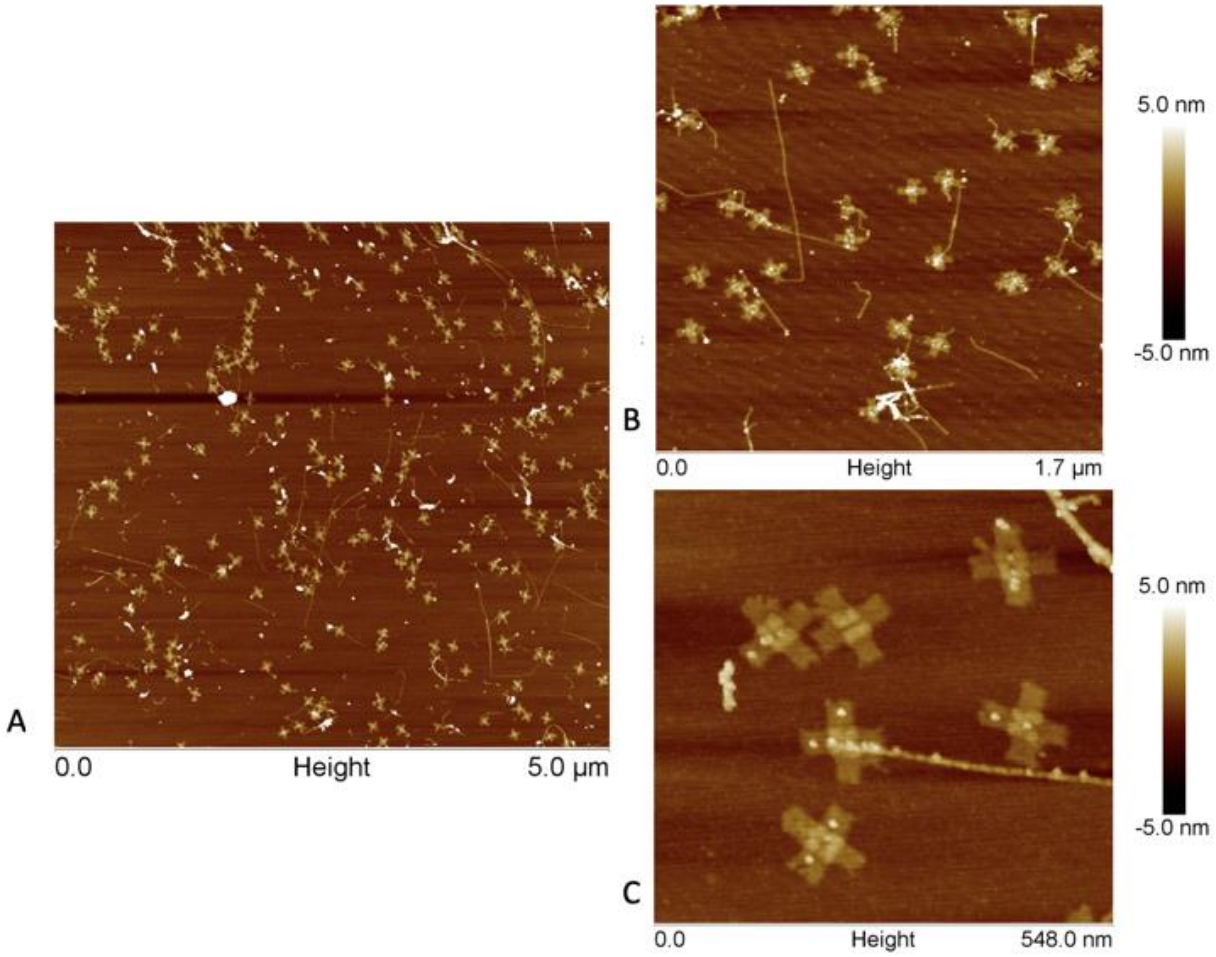

Figure 53: Images Acquired at Three Different Magnifications Presenting Surface Bound Origami Binding CNTs through Biotin-Streptavidin Interactions
A five-micron wide AFM image (A) shows a good stoichiometric balance of nanotubes to CO-01. (B) presents a higher magnification, 1.7-microns wide, which shows a few instances of surface bound origami functionalized with CNTs. In this image, only two full nanotubes can be seen which are not interacting with origami. (C) Displays a 548 nm wide AFM image of successful immobilization of a CNT down the center of a CO.

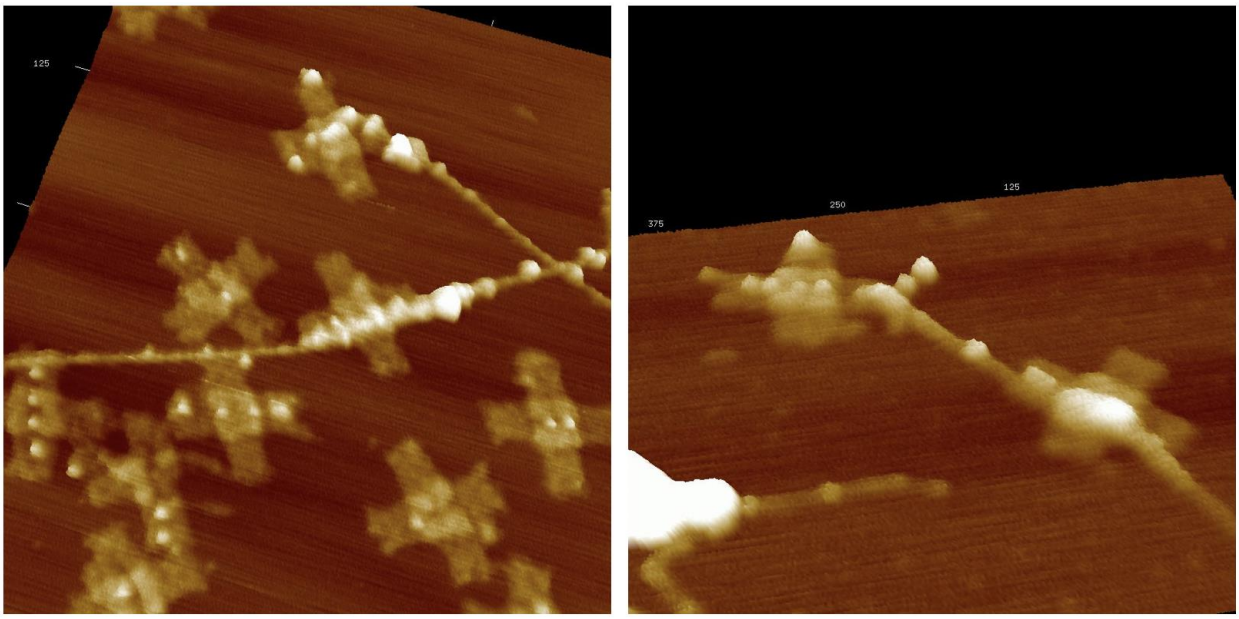

Figure 54: Two 3-D AFM Images of CNT/CO Constructs Bound through Biotin-Streptavidin Interactions

More instances of CNT immobilization on surface immobilized CO-01 through biotin-streptavidin interactions.

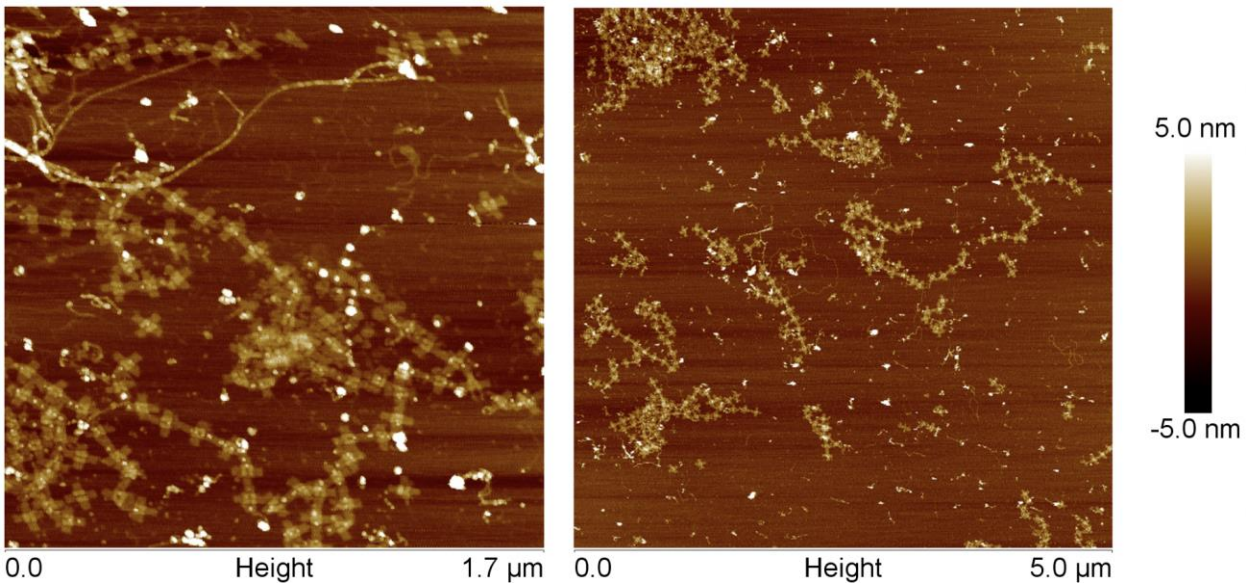

Figure 55: Surface Bound 1D CO-01 after Reactions with CNTs Mediated Through Biotin-Streptavidin Interactions

Two AFM images of 1D CO-01 pre-immobilized onto mica followed by sequential reaction with streptavidin, rinsing, then reacted with biotin wrapped CNTs.

DAB

DAB precipitation was monitored at several different time points during the reaction using AFM. The first attempt showed that a 1-hour reaction time was too long since the size of the polymerized precipitate was too large to be visualized through AFM, obscuring the origami. The reaction time was reduced to thirty minutes, with polymerization still too large for useful visualization. Precipitation products were still too large for reduced time points of 10 minutes and 5 minutes as depicted in Figure 56.

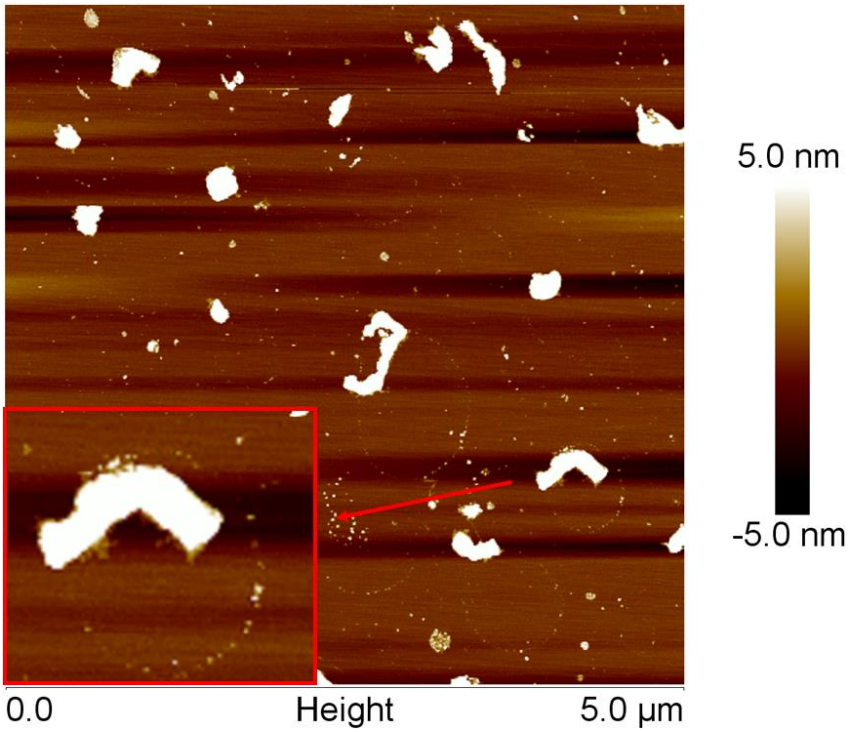

Figure 56: AFM Height Image of DAB Precipitation on CO-01 Surface over 5 Minutes This precipitation on the CO-01 surface was imaged at five minutes after introduction of DAB and H_2O_2. Looking closely, the outer edges of CO-01 are visible underneath the precipitation masses, indicating the effectiveness of the DAB precipitations at higher time points.

By modifying the concentrations of the reagents, the optimal timepoint for precipitation was brought to 10 seconds. Under these conditions the reaction was too rapid for any quantitative analysis (i.e. controlling the reaction for 9 vs. 10 seconds is too difficult). Further adjustments of concentrations resulted in a suitable, 1-minute polymerization that did not

obscure the origami. Table 7 shows the quantitative analysis of 128 origami spanning five samples, each at 1-minute precipitation times. Not including CO-01 that was within close proximity to each other i.e., where single CO-01 could not be counted separately, out of 128 CO-01, 109 or 87% had evidence of precipitate formation somewhere on the CO-01 surface. Out of the total CO-01 present, 84, or 65% had precipitate evidence on the presumed left arm of CO-01, the DNAzyme location, evidently indicating that approximately 65%, of CO-01 contained an active DNAzyme. Upon close inspection of AFM images (Figure 57), matter that appeared similar to the precipitate but which was not associated with origami was observed. This precipitate not associated with origami may be the result of non-catalyzed reaction of DAB and H_2O_2, or more likely, possible precipitation dislodged from its precise location due to AFM tip forces, or possibly catalyzed by excess DNAzyme staples that had bound to the surface of the mica.

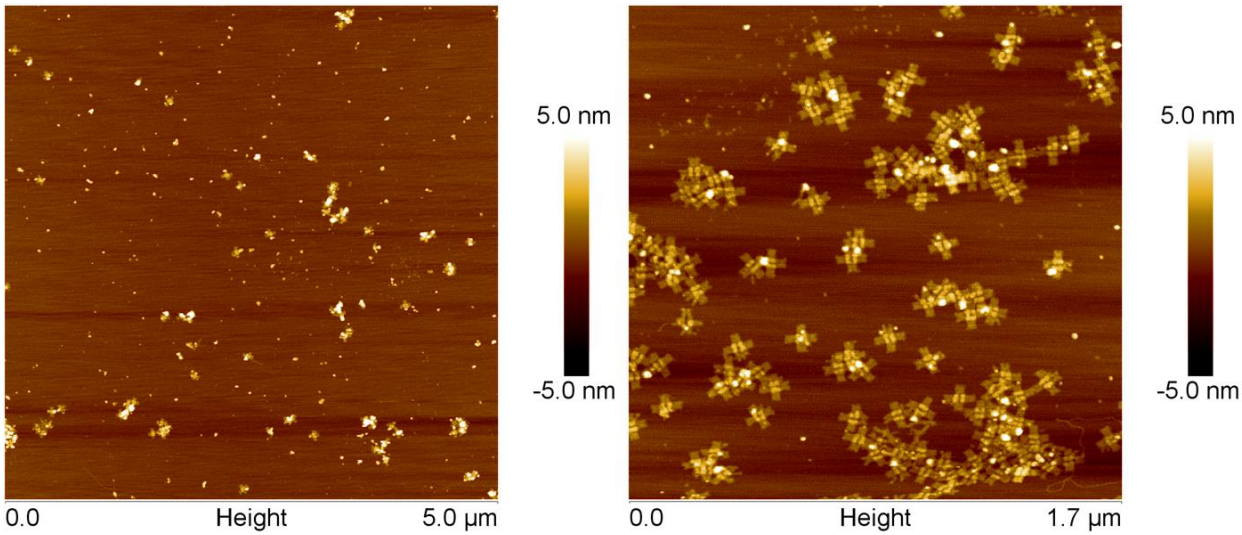

Figure 57: AFM Height Analysis Image of Localized DAB Precipitation on CO-01 Surface
Two 5-micron and 1.7-micron wide AFM topography images of the relation between the DAB precipitation and CO-01 0D. The white "specks," or precipitate, are clearly correlated with the CO-01, mostly on the left arm or location of the DNAzyme, with less appearances of precipitation on mica in the background, leading one to conclude that it is evidence of the predicted reaction mediated by the DNAzyme on the origami.

Quantitative Analysis of DAB precipitation on CO-01	# single origami	# origami with precipitate activity	# Origami with correctly localized G-quad Precipitate activity	% Origami with activity	% Origami with localized G-quad activity
Totals	128	109	84	87 %	65 %

Table 7: DAB Precipitation Observed on DNAzyme Modified CO-01 Upon Reacting with H_2O_2

This table shows the percentage of CO-01 with active DNAzymes that created a precipitate upon reaction with DAB and H_2O_2 for one minute.

Tyramide

A variety of experiments were performed using fluorescence imaging, AFM height analysis, agarose and polyacrylamide gel electrophoresis to test for the reaction of Tyramide with CO at precise locations. The studies of potential catalyzed results were inconclusive, but suggested Tyramide does not react exclusively with a DNAzyme, in contrast to the known reactivity of Tyramide.[52]

H_2O_2 Oxidation Fueled Reactions

All H_2O_2 based oxidation reactions were performed on mica slides already pre-functionalized with CNT/CO at room temperature under a humidity chamber to prevent sample drying. All reactions were performed with 3 mM H_2O_2 for a total of two hours and imaged with a Bruker MM8 AFM. Attempts were made to return to the very same constructs before and after H_2O_2 reactions. This approach was made difficult because of changes in configuration of adsorbed CO/CNTs during H_2O_2 exposure.

Solution 1D CO-01 $(TAT)_{10}$ Functionalized with T_{40} Wrapped CNTs

Due to the difficulties experienced in visualization of CNTs through aggregates, catalytic H_2O_2 oxidation was not thoroughly tested with the products of solution functionalization techniques. H_2O_2 tests were performed on 1D CO-01 with $(TAT)_{10}$ docking sites bearing CNTs. Figure 58 presents an area of possible cutting of a nanotube positioned down the center of a 1D

array of CO-01 (divots indicated by red arrows). Figure 59 displays the same apparently degraded CNT. The length measured between the "divots," which have the appearance of cuts on the CNT, is approximately 104 nm. Using accepted DNA metrics to calculate distances between DNA, there is ~6 nm length between the end of the left arm of CO-01 to the center of the G-quad location, and ~92 nm distance between the centers of the G-quad to the end of the right arm of CO-01. With the three base sticky ends measuring ~1.02 nm, addition of these lengths adds to 99 nm, leaving a 5 nm difference between measured divots and a calculated value of the distance between designed G-quad cut locations. Due to the difficulty in finding the same nanotube or 1D CO-01 area, before and after images were difficult if not impossible to obtain with AFM imaging and after multiple exposures to the rinsing technique.

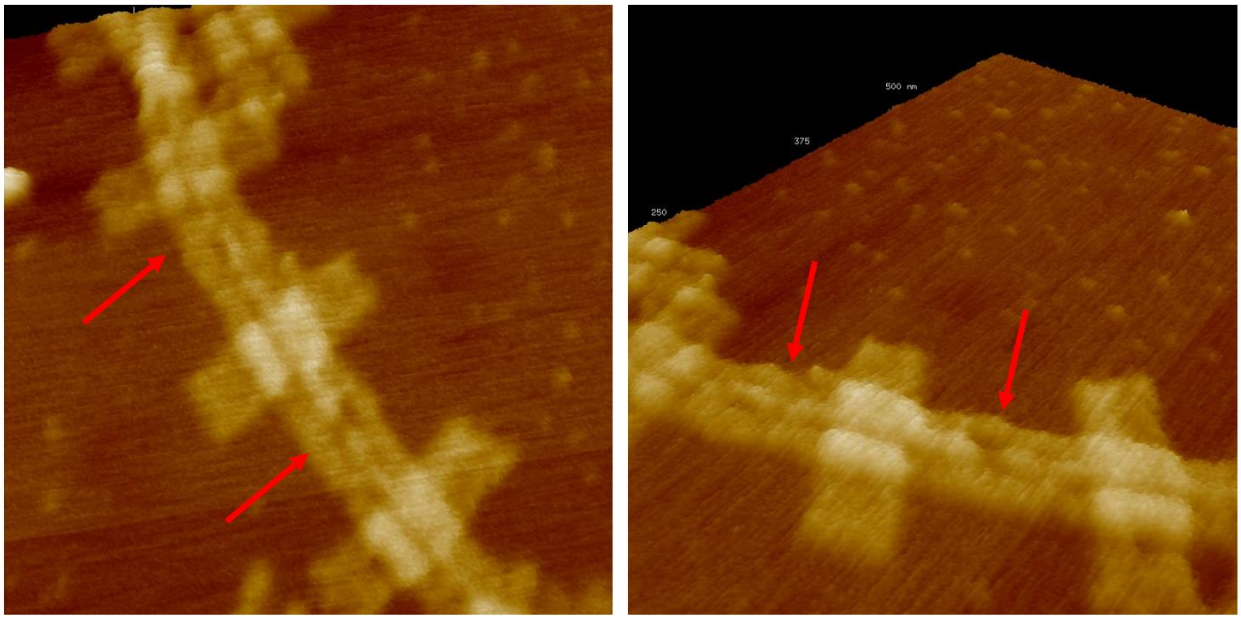

Figure 58: Possible Degradation of T_{40} Wrapped CNTs on CO-01 Surfaces after Two Hours of Reaction with 3 mM H_2O_2
A carbon nanotube positioned down the center of a 1D array of CO-01 imaged after incubation with 3 mM H_2O_2 for two hours. The red arrows are pointing to areas of indentation, or perceived degradation of CNTs at G-quad locations.

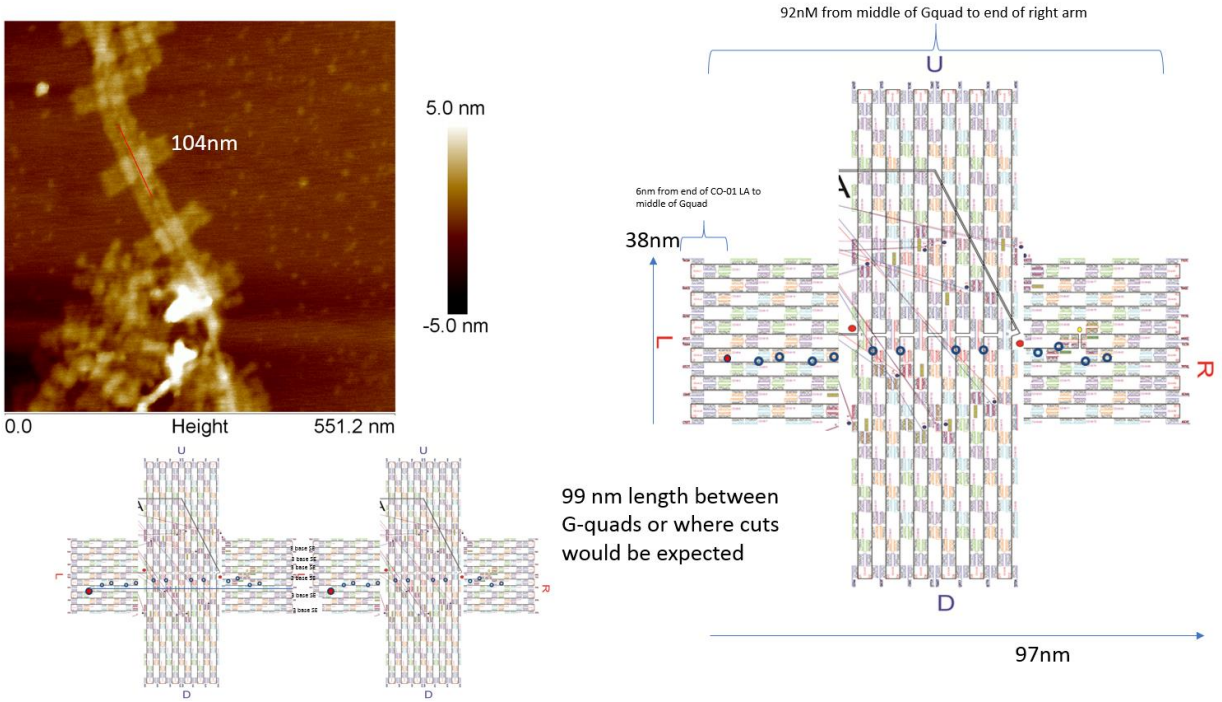

Figure 59: Analysis of Possible Degradation of CNTs on a 1D CO-01 Array
Measurements and calculations of observed and theoretical distances between possible G-quad induced cuts.

Studies of Catalyzed Oxidation of CNTs Bound to Pre-immobilized 0D Origami via Biotin-Streptavidin Bridging

Tests of H_2O_2 oxidation of CNTs immobilized via surface sequential depositions on CO-01 via biotin streptavidin interactions were performed as an additional step following the surface depositions. After CNT attachment to pre-immobilized CO, hemin was added for an hour, rinsed, and then H_2O_2 was introduced for two hours. Samples were washed and imaged using AFM. Two different results were observed following H_2O_2 reacting with biotin streptavidin immobilized CNT bearing constructs (shown in Figure 60). Nanotubes were either A) apparently cut at the G-quad location as designed, or B) the CNTs were possibly partially cut then due to mechanical forces arising from the nanotube's affinity for mica or the strength of the rinsing process, the nanotube remained connected to the origami edges, but detached from the streptavidin binding it to the center of the origami. Similar analysis of another example of

possible cutting, where the CNT did not remain in the center of the origami is shown in Figure 61. This displacement of the CNT may result from gas formation as H_2O_2 is catalyzed to oxidize the carbon in the CNT.

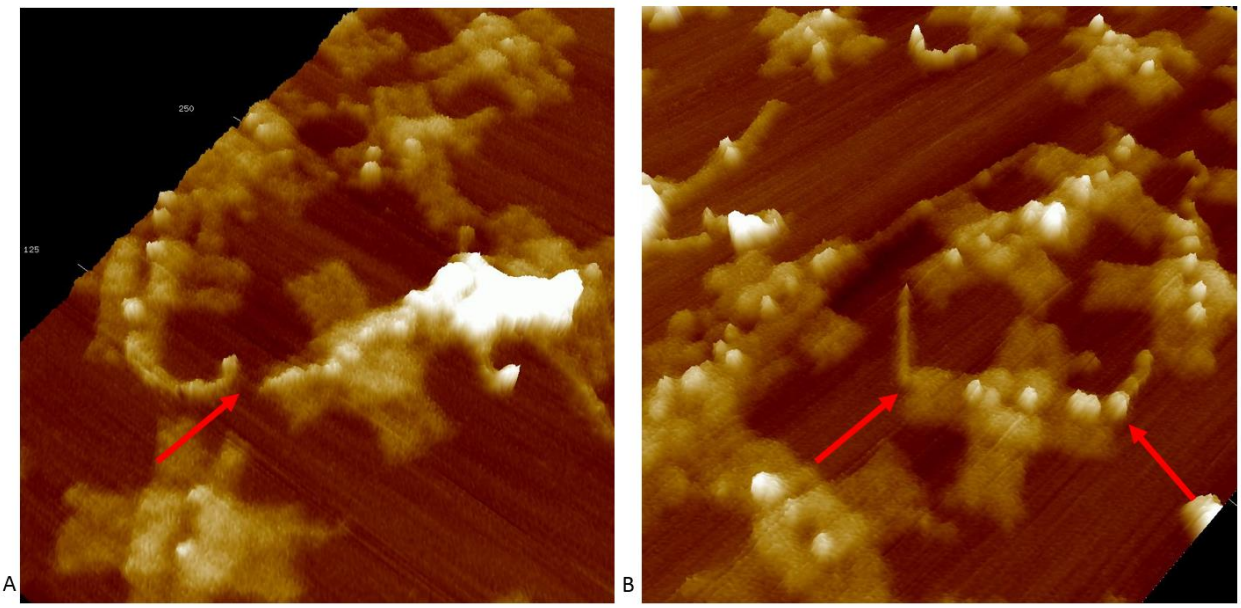

Figure 60: Potential Degradation of TAT-Biotin Wrapped CNTs on CO-01 Surfaces After Two Hour Reaction with 3 mM H_2O_2
These two AFM images are two different examples of modifications of 0D CO-01 containing biotin docking sites with TAT wrapped CNTs, shown here in 3D, after oxidation reactions. A) Appears to show one nanotube bridging between two origami that has been cut by one of the G-quads but remained intact across the middle. B) Shows nanotubes extending from the left and right arms of CO-01, but missing from the center.

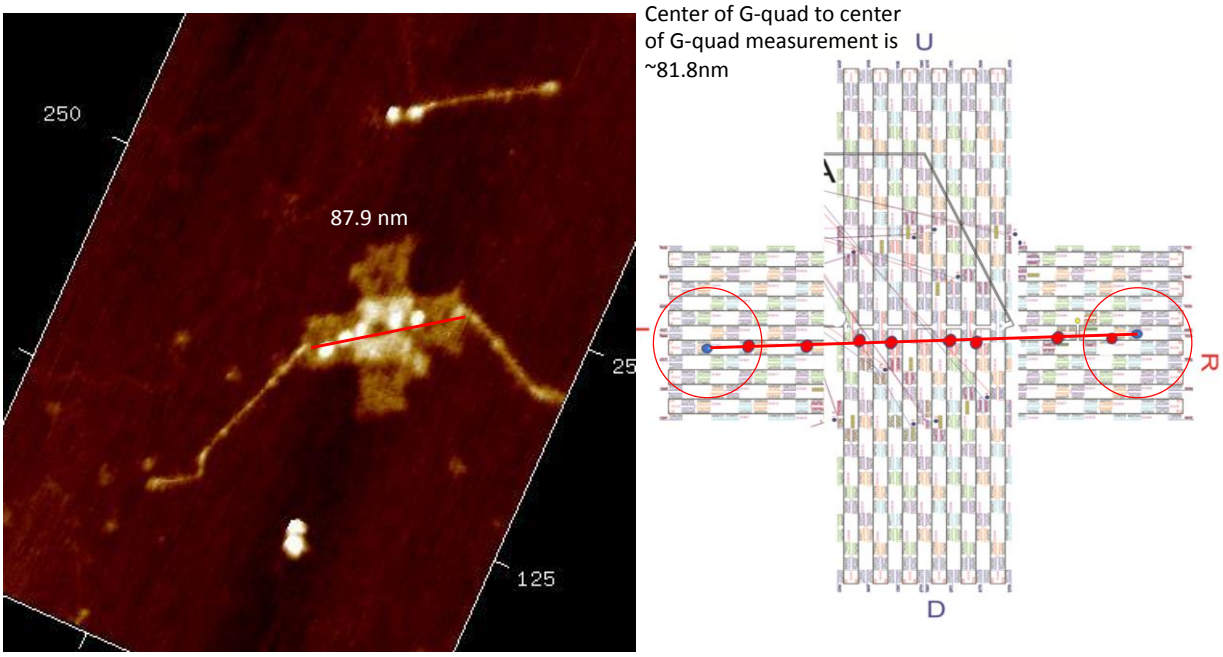

Figure 61: Analysis of Possible Degradation of CNTs on a 0D CO-01
Measuring the distance between the locations of the ends of two CNTs on the CO-01, provided a value of approximately 87.9 nm. The nominal distance from the center of one G-quad to the center of the other G-quad is ~81.8 nm. Taking into consideration the linker length expanding the reach of the G-quad, a difference of 6.1 nm is possible.

While H_2O_2 oxidation tests were studied and there is evidence that cutting or degradation of nanotubes was present, there is still no definitive evidence that cutting of nanotubes was performed through DNAzyme activity and visualized through AFM alone. Further tests would need to be performed.

CHAPTER 6
EXTENDED DISCUSSION

CNT Wrapping

CNTs have the ability to interact with some specificity selectively to a $(TAT)_4$ sequence and nonselectively to T_{40} ssDNA. The evidence of the binding is presented when referring back to Figure 27, through the solubilization process. Had the DNA not interacted properly with the CNTs, the CNTs would have remained insoluble in water and would not solubilize into a homogenous dark shaded mixture, and would have stayed separated as a poorly suspended mixture of agglomerated CNTs dispersed in $NaCl/H_2O$. Further evidence was presented in absorbance peaks of solubilized 6, 5-SWCNTs which coincided with literature values of 6,5-SWCNT absorbance peaks. When analyzing the absorbance spectra, there were correlations between literature values of 9,5-SWCNTs, another chirality of semiconducting CNTs, and visible peaks that did not align with 6,5-SWCNT peaks, indicating even though solubilized, there was still the presence of non-6,5-SWCNT impurities in the solution. The final confirmation that CNTs wrapped with DNA properly was the appearance of immobilization onto CO surfaces in general. Had the nanotubes not wrapped in DNA to some degree, they would not have interacted individually with Origami arrays.

CNT/CO Immobilization

When considering the reaction between CNTs wrapped in T_{40} ssDNA and CO with $(TAT)_{10}$ docking sites, for both surface and solution functionalization techniques, what is believed to be happening is similar to the chelating effect, where the $(TAT)_{10}$ DNA, which is specific for 6,5-SWCNTs is expected to displace the T_{40} wrapping through the chelating effect to allow functionalization of CO with CNT. The CO/CNT immobilization via biotin-streptavidin interactions has utilized the strongest known non-covalent interaction between a protein and a

ligand to functionalize the CNTs onto the CO surface. The advantage of biotin-streptavidin interactions is the strength of the interaction, but also the ability to perform both in solution and surface binding without the need for the thermal anneal step that the DNA mediated binding requires.

When CO/CNT functionalization was allowed to proceed in solution, notable tangling was observed, which prevents clear visualization of CO/CNT complexes for both binding approaches (TAT-DNA and streptavidin-biotin). Since CNTs tend to aggregate and form ropes, many AFM images showed large masses of aggregate, and because both CNTs and DNA have been purified to the fullest extent capable with the tools utilized in our workspace, one is led to believe that the nanotubes and DNA interact so well with each other that they form these aggregations in solution which are then solidified when deposited on a prepared mica slide.

Reactions in which surface bound CO were functionalized with CNTs were implemented as an approach to remove or limit the formation of aggregates. The reaction between surface immobilized 1D CO with $(TAT)_{10}$ docking sites and T_{40} wrapped CNTs avoided the formation of aggregations, but displayed little reaction between the CNTs and 1D CO, meaning either the CNTs preferred mica over DNA binding, or that linear arrays of CO pre-immobilized onto a surface presented too much steric or charge hindrance for CNT binding. The reaction between 0D CO with $(TAT)_{10}$ docking sites immobilized on mica and T_{40} wrapped CNTs again prevented the formation of aggregates, but decreased the degree of CO/CNT interactions and increased the observation of binding of apparent "carbon soot," or carbon impurities which still remain in the CNT samples. This "soot" could and likely does include very short CNTs that are unable to be resolved even with AFM. The decreased amount of functionalization between the origami (both 0D and 1D), and CNTs on mica surfaces is thought to be due to the fact that aside from the

carbon soot and other impurities, DNA wrapped CNTs have high affinity for mica surfaces which creates a competition between the DNA wrapped CNTs functionalizing DNA (CO) versus adsorbing to the mica surface.

Functionalization of surface immobilized CO with CNTs through streptavidin-biotin interactions was implemented to not only eliminate aggregation, but also to remove the need for a thermal treatment. The interaction of surface immobilized 0D CO with CNTs provided the clearest images of CNT/CO constructs without the interference of carbon soot or aggregation.

CNT H_2O_2 Oxidation Studies

While significant efforts were directed toward the observation of the interactions of H_2O_2 with the DNAzyme, not all studies were conclusive. Through DAB studies, the presence of localized precipitation at the intended location of the DNAzyme appears to have demonstrated that a large fraction of the DNAzymes were active as it catalyzed precipitation of DAB at a rapid pace. CNT oxidation studies performed with 0D and 1D constructs generated via solution phase functionalization techniques were inconclusive due to visibility issues resulting from aggregations. Oxidation studies of surface sequentially functionalized CO-01 employing biotin-streptavidin interactions for binding appeared to provide clearer evidence that oxidative cutting was proceeding to completion. This clearer visual evidence could be due to the fact that the aggregations have been eliminated, leaving a sharper view of the interactions between the origami and the nanotube. During the oxidation of surface immobilized CO-01 containing CNTs bridged with biotin-streptavidin docking sites, the disappearance of the nanotubes down the center of some CO-01 constructs but remaining in the locations between the G-quad and extending beyond the ends of the origami is possibly a result of the strong bond between DNA coated CNTs and mica. The rinsing may be so harsh that this leads to the displacement of the cut

CNT during the washing and imaging process after oxidation. Furthermore, finding the same CO-01 before and after H_2O_2 introduction has proven difficult or impossible to accomplish. Definitive proof that CNTs were cut through DNAzyme oxidation with H_2O_2 was not established through single molecule AFM imaging.

CHAPTER 7

CONCLUSIONS

CNT functionalization of CO has been demonstrated to be possible through the wrapping of CNTs in DNA and through staple modifications on the CO. AFM imaging demonstrating the functionalization of CO with CNTs provides confirmation that the DNA wrapping technique and the modifications on the CO are working as expected if at a lower yield than hoped for. The differences in concentration and impurities on the AFM images show that the electrodialysis and drop dialysis steps are further improving the utility of individual nanotubes.

For functionalization reactions performed in solution, it is believed that many functionalized origami products are formed and reside within the aggregations, rendering them not clearly visible via AFM imaging. While solution-based complexation provides the highest yields, and would be a preferred approach for further studies and CNT applications, due to the aggregation limitations, it is suggested that solution phase reactions do not provide a feasible method for preparing high numbers of high-quality assemblies amenable to AFM characterization. Complete assemblies were only viewable at high magnification on the outer edges of aggregates. Despite the aggregations, a large degree of functionalization was observed on the outer edges of aggregates. While this technique led to significant functionalization, the tangling between CNTs inhibited observation of well controlled products. Believing that 1D linear arrays had entangled the CNTs, 0D CO was employed in an effort to decrease aggregates. Use of 0D CO in solution did not eliminate the aggregates, and has approximately the same degree of functionalization as observed for 1D CO in solution.

Even though yield is greatly reduced, the occurrence of some successful functionalization of surface bound CO $(TAT)_{10}$ with T_{40} wrapped CNTs provides a starting point for future

platforms of origami bound CNTs. This approach does not appear to be as robust as one using SA-biotin interactions and shows evidence that it is prone to non-specific binding events, including unintended binding with the single stranded edges of the cross-origami arms.

Through surface immobilization techniques, the streptavidin-biotin interactions provided the least amount of aggregations, required no temperature gradient, and can be performed within hours. A disadvantage of surface reactions is that the CO is already adsorbed to the mica surface, limiting the mobility of CO, thus hindering its ability to properly co-align with CNTs of extended length. The size of streptavidin molecules obscures the view of the ~1 nm diameter CNT on the DO surface, thus limiting the accuracy of analysis of AFM images of CNT/DO complexes. Sequential surface reaction provides an advantageous approach for preparing carbon nanotube-DNA Origami complexes. Surface depositions eliminate aggregation and enable high resolution, high density experimentation on 6,5-SWCNTs immobilized on origami, addressing an important barrier to experimentation.

Tests involving DAB confirmed that the DNAzyme was active on CO, encouraging further investigation into the activity of DNAzymes with CNTs. H_2O_2 tests on DNAzymes and CNTs were inconclusive, but provided ambiguous but tantalizing evidence of CNT cutting through 1-2 electron oxidation catalyzed by DNAzymes in the presence of H_2O_2. The tests reported here help advance the use of DNA Origami in practical applications, as well as provide a starting point for advancement in carbon nanotube based scientific investigations.

AUTHOR CONTRIBUTIONS

Kathryn Pitton (KP), David Neff (DN) and Michael L. Norton (MLN) conceived and designed the experiments. KP performed the experiments. KP, DN, and MLN analyzed the data.

CONFLICTS OF INTEREST

The authors declare no conflict of interest. The funding sponsors had no role in the design, collection, analyses, or interpretation of the manuscript and the publication of results.

REFERENCES

1. Iijima, S., Helical microtubules of graphitic carbon. *Nature* **1991,** *354*, 56.
2. Rothemund, P. W. K., Folding DNA to create nanoscale shapes and patterns. *Nature* **2006,** *440*, 297.
3. Mangalum, A.; Rahman, M.; Norton, M. L., Site-Specific Immobilization of Single-Walled Carbon Nanotubes onto Single and One-Dimensional DNA Origami. *Journal of the American Chemical Society* **2013,** *135* (7), 2451-2454.
4. Zhao, Z.; Liu, Y.; Yan, H., DNA origami templated self-assembly of discrete length single wall carbon nanotubes. *Organic & biomolecular chemistry* **2013,** *11* (4), 596-8.
5. Burge, S.; Parkinson, G. N.; Hazel, P.; Todd, A. K.; Neidle, S., Quadruplex DNA: sequence, topology and structure. *Nucleic acids research* **2006,** *34* (19), 5402-15.
6. Alizadeh, N.; Salimi, A.; Hallaj, R., Hemin/G-Quadruplex Horseradish Peroxidase-Mimicking DNAzyme: Principle and Biosensing Application. *Advances in biochemical engineering/biotechnology* **2017**.
7. Liu, W.; Zhong, H.; Wang, R.; Seeman, N. C., Crystalline Two-Dimensional DNA-Origami Arrays. *Angewandte Chemie International Edition* **2011,** *50* (1), 264-267.
8. Kroto, H. W.; Heath, J. R.; O'Brien, S. C.; Curl, R. F.; Smalley, R. E., C60: Buckminsterfullerene. *Nature* **1985,** *318*, 162.
9. Seeman, N. C., Nucleic acid junctions and lattices. *Journal of theoretical biology* **1982,** *99* (2), 237-47.
10. Udomprasert, A.; Kangsamaksin, T., DNA origami applications in cancer therapy. *Cancer science* **2017,** *108* (8), 1535-1543.
11. Sanderson, K., Bioengineering: What to make with DNA origami. *Nature* **2010,** *464* (7286), 158-9.
12. Mann, C.; Hertel, T., 13 nm Exciton Size in (6,5) Single-Wall Carbon Nanotubes. *The Journal of Physical Chemistry Letters* **2016,** *7* (12), 2276-2280.
13. Wang, X.; Li, Q.; Xie, J.; Jin, Z.; Wang, J.; Li, Y.; Jiang, K.; Fan, S., Fabrication of Ultralong and Electrically Uniform Single-Walled Carbon Nanotubes on Clean Substrates. *Nano Letters* **2009,** *9* (9), 3137-3141.
14. Sigma-Adrich, Product Information Single-walled Carbon Nanotubes. Sigma-Aldrich: 2016.
15. Kitiyanan, B.; Alvarez, W. E.; Harwell, J. H.; Resasco, D. E., Controlled production of single-wall carbon nanotubes by catalytic decomposition of CO on bimetallic Co–Mo catalysts. *Chemical Physics Letters* **2000,** *317* (3), 497-503.
16. Dang, X.; Gu, L.; Qi, J.; Correa, S.; Zhang, G.; Belcher, A. M.; Hammond, P. T., Layer-by-layer assembled fluorescent probes in the second near-infrared window for systemic delivery and detection of ovarian cancer. *Proceedings of the National Academy of Sciences* **2016,** *113* (19), 5179-5184.
17. Kwon, Y. H.; Minnici, K.; Park, J. J.; Lee, S. R.; Zhang, G.; Takeuchi, E. S.; Takeuchi, K. J.; Marschilok, A. C.; Reichmanis, E., SWNT Anchored with Carboxylated Polythiophene "Links" on High-Capacity Li-Ion Battery Anode Materials. *Journal of the American Chemical Society* **2018,** *140* (17), 5666-5669.
18. Qian, Z. S.; Shan, X. Y.; Chai, L. J.; Ma, J. J.; Chen, J. R.; Feng, H., DNA nanosensor based on biocompatible graphene quantum dots and carbon nanotubes. *Biosensors and Bioelectronics* **2014,** *60*, 64-70.

19. Aqel, A.; El-Nour, K. M. M. A.; Ammar, R. A. A.; Al-Warthan, A., Carbon nanotubes, science and technology part (I) structure, synthesis and characterisation. *Arabian Journal of Chemistry* **2012,** *5* (1), 1-23.
20. Dresselhaus, M. S.; Dresselhaus, G.; Saito, R., Physics of carbon nanotubes. *Carbon* **1995,** *33* (7), 883-891.
21. Rahmandoust, M.; chsner, A., Buckling Behaviour and Natural Frequency of Zigzag and Armchair Single-Walled Carbon Nanotubes. *Journal of Nano Research* **2012,** *16*, 153--160.
22. AZoNano, W. by. Carbon Nanotubes - Structure, Naming and Properties of Carbon Nanotubes (Buckytubes) https://www.azonano.com/article.aspx?ArticleID=983 (accessed Jan 17, 2018).
23. Tu, X.; Manohar, S.; Jagota, A.; Zheng, M., DNA sequence motifs for structure-specific recognition and separation of carbon nanotubes. *Nature* **2009,** *460*, 250.
24. Maune, H. T.; Han, S. P.; Barish, R. D.; Bockrath, M.; Goddard, W. A., III; Rothemund, P. W.; Winfree, E., Self-assembly of carbon nanotubes into two-dimensional geometries using DNA origami templates. *Nat Nanotechnol* **2010,** *5* (1), 61-6.
25. Eskelinen, A.-P.; Kuzyk, A.; Kaltiaisenaho, T. K.; Timmermans, M. Y.; Nasibulin, A. G.; Kauppinen, E. I.; Törmä, P., Assembly of Single-Walled Carbon Nanotubes on DNA-Origami Templates through Streptavidin–Biotin Interaction. *Small* **2011,** *7* (6), 746-750.
26. Franklin, A. D.; Chen, Z., Length scaling of carbon nanotube transistors. *Nature Nanotechnology* **2010,** *5*, 858.
27. Kagan, V. E.; Konduru, N. V.; Feng, W.; Allen, B. L.; Conroy, J.; Volkov, Y.; Vlasova, I. I.; Belikova, N. A.; Yanamala, N.; Kapralov, A.; Tyurina, Y. Y.; Shi, J.; Kisin, E. R.; Murray, A. R.; Franks, J.; Stolz, D.; Gou, P.; Klein-Seetharaman, J.; Fadeel, B.; Star, A.; Shvedova, A. A., Carbon nanotubes degraded by neutrophil myeloperoxidase induce less pulmonary inflammation. *Nature Nanotechnology* **2010,** *5*, 354.
28. Ziegler, K. J.; Gu, Z.; Peng, H.; Flor, E. L.; Hauge, R. H.; Smalley, R. E., Controlled Oxidative Cutting of Single-Walled Carbon Nanotubes. *Journal of the American Chemical Society* **2005,** *127* (5), 1541-1547.
29. Xiang, Y.; Lu, Y., DNA as Sensors and Imaging Agents for Metal Ions. *Inorganic Chemistry* **2014,** *53* (4), 1925-1942.
30. Kong, D. M.; Cai, L. L.; Guo, J. H.; Wu, J.; Shen, H. X., Characterization of the G-quadruplex structure of a catalytic DNA with peroxidase activity. *Biopolymers* **2009,** *91* (5), 331-9.
31. Breaker, R. R.; Joyce, G. F., A DNA enzyme that cleaves RNA. *Chemistry & biology* **1994,** *1* (4), 223-9.
32. Breaker, Ronald R.; Joyce, Gerald F., The Expanding View of RNA and DNA Function. *Chemistry & biology* **2014,** *21* (9), 1059-1065.
33. Kasprowicz, A.; Stokowa-Sołtys, K.; Jeżowska-Bojczuk, M.; Wrzesiński, J.; Ciesiołka, J., Characterization of Highly Efficient RNA-Cleaving DNAzymes that Function at Acidic pH with No Divalent Metal-Ion Cofactors. *ChemistryOpen* **2016,** *6* (1), 46-56.
34. Atsumi, H.; Belcher, A. M., DNA Origami and G-Quadruplex Hybrid Complexes Induce Size Control of Single-Walled Carbon Nanotubes via Biological Activation. *ACS Nano* **2018,** *12* (8), 7986-7995.

35. Kosynkin, D. V.; Higginbotham, A. L.; Sinitskii, A.; Lomeda, J. R.; Dimiev, A.; Price, B. K.; Tour, J. M., Longitudinal unzipping of carbon nanotubes to form graphene nanoribbons. *Nature* **2009,** *458*, 872.
36. Gellert, M.; Lipsett, M. N.; Davies, D. R., Helix formation by guanylic acid. *Proceedings of the National Academy of Sciences of the United States of America* **1962,** *48*, 2013-8.
37. Sundquist, W. I.; Klug, A., Telomeric DNA dimerizes by formation of guanine tetrads between hairpin loops. *Nature* **1989,** *342* (6251), 825-9.
38. Ana-Maria Chiorcea-Paquim, A. M. O.-B., Redox Behaviour of G-quadruplexes. *Electrochimica Acta* **2014,** *126*, 162-170.
39. Guanine. https://pubchem.ncbi.nlm.nih.gov/compound/guanine (accessed Apr 2, 2019).
40. Patel, D. J.; Phan, A. T.; Kuryavyi, V., Human telomere, oncogenic promoter and 5'-UTR G-quadruplexes: diverse higher order DNA and RNA targets for cancer therapeutics. *Nucleic acids research* **2007,** *35* (22), 7429-55.
41. Rhodes, D.; Lipps, H. J., G-quadruplexes and their regulatory roles in biology. *Nucleic acids research* **2015,** *43* (18), 8627-8637.
42. Li, T.; Dong, S.; Wang, E., G-quadruplex aptamers with peroxidase-like DNAzyme functions: which is the best and how does it work? *Chemistry, an Asian journal* **2009,** *4* (6), 918-22.
43. Grenoble, D. C.; Drickamer, H. G., The effect of pressure on the oxidation state of iron. 3. Hemin and hematin. *Proceedings of the National Academy of Sciences of the United States of America* **1968,** *61* (4), 1177-1182.
44. Travascio, P.; Li, Y.; Sen, D., DNA-enhanced peroxidase activity of a DNA-aptamer-hemin complex. *Chemistry & biology* **1998,** *5* (9), 505-17.
45. Hemin. http://www.chemspider.com/Chemical-Structure.401223.html (accessed Apr 2, 2019).
46. Saito, K.; Tai, H.; Hemmi, H.; Kobayashi, N.; Yamamoto, Y., Interaction between the Heme and a G-Quartet in a Heme–DNA Complex. *Inorganic Chemistry* **2012,** *51* (15), 8168-8176.
47. Zhang, L.; Zhou, J.; Ma, F.; Wang, Q.; Xu, H.; Ju, H.; Lei, J., Single-Sided Competitive Axial Coordination of G-Quadruplex/Hemin as Molecular Switch for Imaging Intracellular Nitric Oxide. *Chemistry (Weinheim an der Bergstrasse, Germany)* **2019,** *25* (2), 490-494.
48. Cheng, X.; Liu, X.; Bing, T.; Cao, Z.; Shangguan, D., General Peroxidase Activity of G-Quadruplex−Hemin Complexes and Its Application in Ligand Screening. *Biochemistry* **2009,** *48* (33), 7817-7823.
49. Bohlen, O. V.; Halbach, O. V.; Kiernan, J. A. Diaminobenzidine induces fluorescence in nervous tissue and provides intrinsic counterstaining of sections prepared for peroxidase histochemistry. *Biotechnic & Histochemistry*1999, *74*(5), 236–243.
50. Alexa Fluor 546 Tyramide Reagent - Thermo Fisher Scientific. https://www.thermofisher.com/order/catalog/product/B40954 (accessed Mar 19, 2019).
51. Faget, L.; Hnasko, T. S., Tyramide Signal Amplification for Immunofluorescent Enhancement. *Methods in molecular biology (Clifton, N.J.)* **2015,** *1318*, 161-72.
52. Einarson, O. J.; Sen, D., Self-biotinylation of DNA G-quadruplexes via intrinsic peroxidase activity. *Nucleic acids research* **2017,** *45* (17), 9813-9822.
53. Stack, E. C.; Wang, C.; Roman, K. A.; Hoyt, C. C., Multiplexed immunohistochemistry, imaging, and quantitation: a review, with an assessment of Tyramide signal amplification, multispectral imaging and multiplex analysis. *Methods (San Diego, Calif.)* **2014,** *70* (1), 46-58.

54. Shumayrikh, N.; Huang, Y. C.; Sen, D., Heme activation by DNA: isoguanine pentaplexes, but not quadruplexes, bind heme and enhance its oxidative activity. *Nucleic acids research* **2015,** *43* (8), 4191-4201.
55. Rodríguez-López, J. N.; Lowe, D. J.; Hernández-Ruiz, J.; Hiner, A. N. P.; García-Cánovas, F.; Thorneley, R. N. F., Mechanism of Reaction of Hydrogen Peroxide with Horseradish Peroxidase: Identification of Intermediates in the Catalytic Cycle. *Journal of the American Chemical Society* **2001,** *123* (48), 11838-11847.
57. Majhi, P. R.; Shafer, R. H., Characterization of an unusual folding pattern in a catalytically active guanine quadruplex structure. *Biopolymers* **2006,** *82* (6), 558-69.
58. Nano, A., Advanced Nanoscale Characterization of Polymer Materials Using Phase Imaging with the Innova from Bruker. **2008**.
59. Bachilo, S. M.; Strano, M. S.; Kittrell, C.; Hauge, R. H.; Smalley, R. E.; Weisman, R. B., Structure-assigned optical spectra of single-walled carbon nanotubes. *Science (New York, N.Y.)* **2002,** *298* (5602), 2361-6.
60. Lee, A. J.; Wang, X.; Carlson, L. J.; Smyder, J. A.; Loesch, B.; Tu, X.; Zheng, M.; Krauss, T. D., Bright Fluorescence from Individual Single-Walled Carbon Nanotubes. *Nano Letters* **2011,** *11* (4), 1636-1640.
61. Hartschuh, A.; Pedrosa, H. N.; Peterson, J.; Huang, L.; Anger, P.; Qian, H.; Meixner, A. J.; Steiner, M.; Novotny, L.; Krauss, T. D., Single Carbon Nanotube Optical Spectroscopy. *ChemPhysChem* **2005,** *6* (4), 577-582.
62. Avidin-Biotin Interaction. https://www.thermofisher.com/us/en/home/life-science/protein-biology/protein-biology-learning-center/protein-biology-resource-library/pierce-protein-methods/avidin-biotin-interaction.html (accessed Mar 19, 2019).
63. Johnson, A. B.; Lewis, A. B.; DNA Replication Mechanisms. *Molecular Biology of the Cell. 4th edition. New York: Garland Science;* **2002.**
64. Livnah, O.; Bayer, E. A.; Wilchek, M.; Sussman, J. L., Three-dimensional structures of avidin and the avidin-biotin complex. *Proceedings of the National Academy of Sciences of the United States of America* **1993,** *90* (11), 5076-5080.
65. Schöppler, F.; Mann, C.; Hain, T. C.; Neubauer, F. M.; Privitera, G.; Bonaccorso, F.; Chu, D.; Ferrari, A. C.; Hertel, T., Molar Extinction Coefficient of Single-Wall Carbon Nanotubes. *The Journal of Physical Chemistry C* **2011,** *115* (30), 14682-14686.
66. Haroz, E. H., Bachilo, S. M., Weisman, R. B. & Doorn, S. K. , Curvature effects on the E33 and E44 exciton transitions in semiconducting single-walled carbon nanotubes. *Phys. Rev.* **2008,** *B* (77), 125405.
67. Schindelin, J.; Arganda-Carreras, I. & Frise, E. et al. (2012), "Fiji: an open-source platform for biological-image analysis", *Nature methods* **9(7)**: 676-682, PMID 22743772
68. Parslow A, Cardona A and Bryson-Richardson RJ (2014) Sample drift correction following 4D confocal time-lapse imaging. J Vis Exp. 2014 Apr 12;(86).

APPENDIX A: OFFICE OF RESEARCH INTEGRITY APPROVAL LETTER

MARSHALL UNIVERSITY.
www.marshall.edu

Office of Research Integrity

February 8, 2019

Kathryn Pitton
7 Pyramid Drive – Apt 704
Huntington, WV 25705

Dear Ms. Pitton:

This letter is in response to the submitted thesis abstract entitled *"Organizing 6,5-Carbon Nanotubes on DNA Origami Arrays."* After assessing the abstract, it has been deemed not to be human subject research and therefore exempt from oversight of the Marshall University Institutional Review Board (IRB). The Code of Federal Regulations (45CFR46) has set forth the criteria utilized in making this determination. Since the information in this study does not involve human subjects as defined in the above referenced instruction, it is not considered human subject research. If there are any changes to the abstract you provided then you would need to resubmit that information to the Office of Research Integrity for review and a determination.

I appreciate your willingness to submit the abstract for determination. Please feel free to contact the Office of Research Integrity if you have any questions regarding future protocols that may require IRB review.

Sincerely,

Bruce F. Day, ThD, CIP
Director

APPENDIX B: CO-01 AND CNT MODIFICATION STAPLES

CO-01

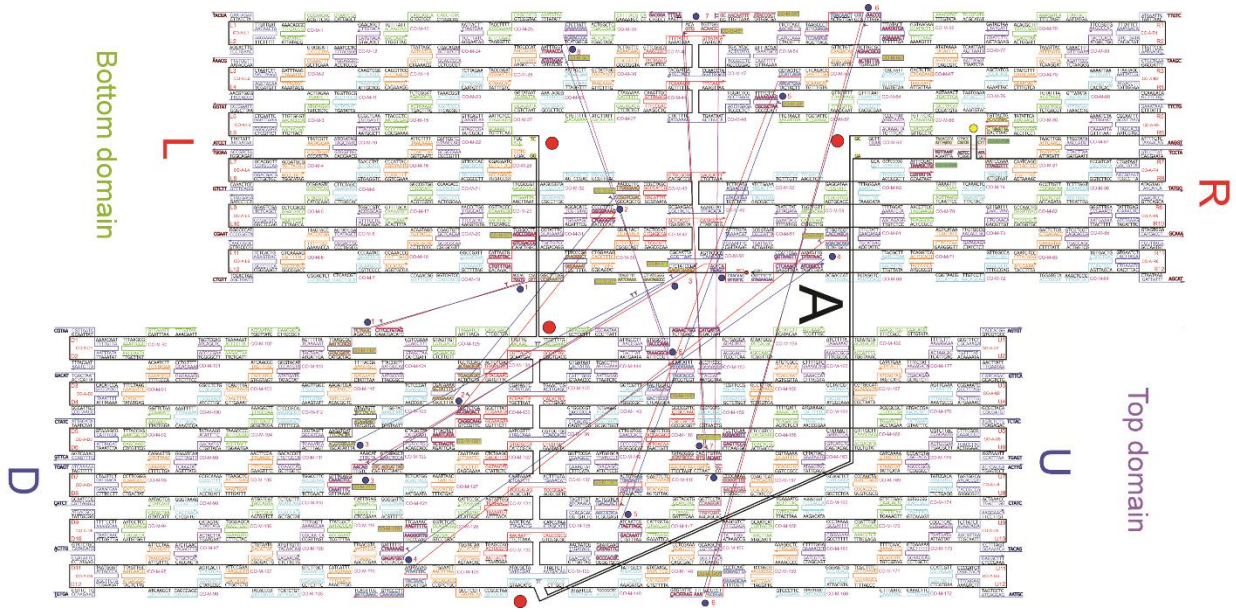

Figure 62: Structure of Cross Origami-01
The image illustrates the two planks of CO-01 moved from their signature crossed positions to reveal both orthogonal planks in full as well as the cross linkers[7]

DNA sequences for $(TAT)_{10}$ docking sites (IDT)

Name	Sequence
KPCO-M-9 (TAT)10	5'-GTGCCAAGGAAGATCGACATCCAGATATAT TAT TAT TAT TAT TAT TAT TAT TAT TAT-3'
CO-M-16-(TAT)10	5' – TAAGAAAAGATTGACCGTAATGGGCCAGTAT TAT TAT TAT TAT TAT TAT TAT TAT TAT – 3'
KPCO-M-10 short	5'-GGTTATAGCTATCTTACCGAATTGAGCGC-3'
CO-M-73-74-(TAT)10	5'-GAGATAGAACACCGCCTGCAACAAAATCAACAGTAGAAAAGTTTGAG TAT TAT TAT TAT TAT TAT TAT TAT TAT TAT – 3'
CO-M-74-Short-new	5' –TAA CAT TA – 3'
CO-M-81-(TAT)10-New	5' – ATTGAACCAATATAATCCTGATTGTCA TAT TAT TAT TAT TAT TAT TAT TAT TAT TAT – 3'
KPCO-M-21 (TAT)10	5'-TTCCCAGTGCTTCTGGTGCCGGAAGTGTAT TAT TAT TAT TAT TAT TAT TAT TAT TAT – 3'
KPCO-M-21-22new	5'-GGAACAAACGGCGGTAAGCAGATAGCCGAAACTGAAC -3'
KPCO-M-27-28(TAT)10	5'-CCATATTAATTAGACGGGAGAATTACAAAGTTACCGTC GGATTCTCCACCA TAT TAT TAT TAT TAT TAT TAT TAT TAT TAT– 3'
CO-M-69#-(TAT)10-New	5' – TTTGGATTATACCTGATAAATTGT TAT TAT TAT TAT TAT TAT TAT TAT TAT TAT – 3'
CO-M-62-(TAT)10 –New	5' – TATCTTTAAAATCCTTTGCCCGAACCG TAT TAT TAT TAT TAT TAT TAT TAT TAT TAT– 3'
CO-M-62 –Short-New	5' –CGACCTGC – 3'
CO-M-133-(TAT)10	5' – CTCAGAGCACCGCCACCCTCAGAGATTAAGCA TAT TAT TAT TAT TAT TAT TAT TAT TAT TAT– 3'
CO-M-136-Modi-fordocking12	5' – ATAAAGCCGCAAAGAATTAGCAAACCACCACC – 3'
CO-M-134-(TAT)10	5' – CATTTGGGATTATCACCGTCACCGGTCATTGC TAT TAT TAT TAT TAT TAT TAT TAT TAT TAT – 3'
CO-M-135-Modi-fordocking12	5' – CTGAGAGTCTACAAAGGCTATCAGACTTGAGC – 3'
CO-M-130-(TAT)10	5' – CAACCATCCGATAGTTGCGCCGACTTTAAGAA TAT TAT TAT TAT TAT TAT TAT TAT TAT TAT – 3'
CO-M-139-Modi-fordocking12	5' – CTGGCTCAAATTACCTTATGCGATAATGACAA – 3'
CO-M-131-(TAT)10	5' – CCACAGACACAAACTACAACGCCTGATAGCGT TAT TAT TAT TAT TAT TAT TAT TAT TAT TAT – 3'
CO-M-138-Modi-fordocking12	5' – CCAATACTTAAAATGTTTAGACTGGTAGCATT – 3'

Table 8: CO-01 Staples for $(TAT)_{10}$ Modifications

DNA sequences for all twelve locations of docking sites for CNT functionalization. All staples from 5'-3'

DNA sequences for Biotin docking sites (IDT)

Name	Sequence
KPCO-M-9 Biotin	5'-GTGCCAAGGAAGATCGACATCCAGATATTTT/5Biosg/-3‘
CO-M-81-Biotin	5' – ATTGAACCAATATAATCCTGATTGTCA TTTT/5Biosg/ – 3'
KPCO-M-21 Biotin	5'-TTCCCAGTGCTTCTGGTGCCGGAAGTGTTTT/5Biosg/ – 3'
KPCO-M-21-22new	5‘-GGAACAAACGGCGGTAAGCAGATAGCCGAAACTGAAC -3'
CO-M-69#-Biotin	5' – TTTGGATTATACCTGATAAATTGT TTTT/5Biosg/ – 3'
CO-M-69#-Short-New	5' –GTCGAAATCGTTATTA – 3'
CO-M-133-Biotin	5' – CTCAGAGCACCGCCACCCTCAGAGATTAAGCA TTTT/5Biosg/ – 3'
CO-M-134-Biotin	5' – CATTTGGGATTATCACCGTCACCGGTCATTGC TTTT/5Biosg/ – 3'
CO-M-135-Modi-fordocking12	5' – CTGAGAGTCTACAAAGGCTATCAGACTTGAGC – 3'
CO-M-130-Biotin	5' – CAACCATCCGATAGTTGCGCCGACTTTAAGAA TTTT/5Biosg/ – 3'
CO-M-131-Biotin	5' – CCACAGACACAAACTACAACGCCTGATAGCGT TTTT/5Biosg/ – 3'

Table 9: CO-01 Staples for Biotin Docking Modifications
DNA sequences for eight locations of docking sites for CNT immobilization. All staples from 5'-3'

DNA sequence for EAD2 G-quadruplex DNA (IDT)

Name	Sequence
CO-M-4gquad-ead2-mod	5'-AATAGCAATAGATGGGCGCATCGTACCCTGGGAGGGAGGGAGGGA-3'

Table 10: G-quadruplex DNA staple for CO-01 with Twelve Central $(TAT)_{10}$ Docking Sites
Staple modified in CO-01 that contained the 18-base sequence $EAD2^{65}$ that formed parallel G-quadruplex secondary structure tetrad

DNA sequence forP2M.S G-quadruplex DNA (IDT)

Name	Sequence
CO-M-4-Gquad-MOD-P2M.S	5'-AATAGCAATAGATGGGCGCATCGTACCTTTTTTTTTTTATTTATTATTATTATTTTGTGGGTAG GGCGGGTTGG-3'
CO-M-87 EAD2 MOD*	5'-GTGGGTAGGGCGGGTTGGTTTATTATTATTATTTATTTTTTTTTTTCATCAACCATACAAAAT ATAGATTTT-3'

Table 11: G-quadruplex DNA staple for CO-01 with Eight Biotin Tether Docking Sites
Staple modifications for P2M.S sequence for mixed hybrid G-quadruplex for CO-01 with eight central biotin docking sites
* Staple incorrectly named during ordering process. Should be CO-M-87 P2M.S MOD.

DNA Sequences for Right Arm Terminating Ends

Name	Sequence
CO-A-R1-5nt-T	5'-GTTAAATAAGAATAAAGTGTGATAAATAAGGCTTTTT-3'
CO-A-R2-5nt-T	5'-AAATCGTCGCTATTAAATAACCTTGCTTCTGTTTTTT-3'
CO-A-R3-5nt-T	5'-AAATAAAGAAATTGCGTTAGCACGTAAAACAGTTTTT-3'
CO-A-R4-5nt-T	5'-TATTCCTGATTATCAGAGCGGAATTATCATCATTTTT-3'
CO-A-R5-5nt-T	5'-TGCTGAACCTCAAATAATCTAAAGCATCACCTTTTTT-3'
CO-A-R6-5nt-T	5'-ACATTGGCAGATTCACCTGAAATGGATTATTTTTTTT-3'

Table 12: ssDNA Sequences for Right Arm Terminating Ends
Staple modifications for terminating ends on the right arm of CO-01 consisting of six locations of $(PolyT)_{5.}$

DNA Sequences for Left and Right Arm 3-Base Overhang Sticky Ends

Name	Sequence
CO-A-L1-5nt-T	TCCTGAACAAGAAAAAATCAACAATAGATAAGTTTTT
CO-A-L2-5nt-T	TTGCACCCAGCTACAAAAGATTAGTTGCTATTTTTTT
CO-A-L3-5nt-T	AATAATAAGAGCAAGAGAATTGAGTTAAGCCCTTTTT
CO-A-L4-5nt-T	GTTTGAGGGGACGACGAACCGTGCATCTGCCATTTTT
CO-A-L5-5nt-T	CCCGGGTACCGAGGTCTCGACTCTAGAGGATCTTTTT
CO-A-L6-5nt-T	AGCTGATTGCCCTTCACAGTGAGACGGGCAACTTTTT
CO-A-R1-5nt-T	GTTAAATAAGAATAAAGTGTGATAAATAAGGCTTTTT
CO-A-R2-5nt-T	AAATCGTCGCTATTAAATAACCTTGCTTCTGTTTTTT
CO-A-R3-5nt-T	AAATAAAGAAATTGCGTTAGCACGTAAAACAGTTTTT
CO-A-R4-5nt-T	TATTCCTGATTATCAGAGCGGAATTATCATCATTTTT
CO-A-R5-5nt-T	TGCTGAACCTCAAATAATCTAAAGCATCACCTTTTTT
CO-A-R6-5nt-T	ACATTGGCAGATTCACCTGAAATGGATTATTTTTTTT

Table 13: ssDNA Sequences for Left and Right Arm 3 Base Overhang Sticky Ends
Staple modifications for 3 base overhang sticky ends on the left and right arms of CO-01

6, 5-SWCNT DNA Wraps (IDT)

Name	Sequence
B-DNA TAT wrap CNT	5'-/5Biosg/TTTTATTATTATTATTTT/3Bio/-3'
T_{40} ssDNA	5'-TTTTTTTTTTTTTTTTTTTTTTTTTTTTTTTTTTTTTTTT-3'

Table 14: ssDNA Sequences for CNT Solubilization
This table shows the sequences of ssDNA used for solubilization of carbon nanotubes through wrapping. B-DNA TAT wrap provides a biotin on the 5' and 3' end with TAT sequences in the center, which wrapped the CNTs that will interact with the biotin-streptavidin CO-01. T_{40} ssDNA is the sequence that wraps the CNTs prepared for $(TAT)_{10}$ docking site CO-01.

APPENDIX C: SUPPLEMENTARY INFORMATION

Chirality and Diameter calculations for all carbon nanotubes :[20]

Name (symbol)	Formula	Value
Carbon-Carbon distance ($a_{C\text{-}C}$)		1.421 Angstroms
Length of unit vector (a)	$\sqrt{3_{a_{c-c}}}$	2.46 Angstroms
Chiral Vector ($\vec{C}$)	$\vec{C} = \overrightarrow{na_1} + \overrightarrow{ma_2}$ = (n,m)	n, m: integers
Chiral angle (θ)	$\sin\theta = \frac{\sqrt{3}m}{2\sqrt{n^2+m^2+nm}}$	$0 \leq \lvert\theta\rvert \leq 30°$
Circumference of nanotube (L)	$L = \lvert C_h\rvert = a\sqrt{n^2+m^2+nm}$	$0 \leq \lvert m\rvert \leq n$
Diameter of nanotube (d_1)	$d_1 = \frac{L}{\pi} = \frac{\sqrt{n^2+m^2+nm}}{\pi}a$	-

CNT Concentration Determination:

Using the UV-VIS option on a Nanodrop ND 1000, the CNTs are analyzed in a manner similar to the one used to quantitate DO using 2 µL of sample. The normalize and HiAbs functions are turned off and the absorbance values are set to 260 and 575 nm. Schöppler 2011 says that extinction coefficient of S1 exciton transition is 4400 /M x cm per carbon atom with 88 carbon atoms per nm of 6,5 CNT. The S1 (991nm) exciton is ~2.5 times greater than the S2 (575nm) so we estimated an extinction coefficient for the 575 nm peak at 1760 / M x cm per carbon atom. This gave us an estimated concentration of carbon atoms 0.1 = 1760 x 1 x concentration. Concentration = 60 µM carbon atoms. If there are 88 carbon atoms in 1 nm then there are 8800 in 100 nm so 60 µM /8800 ~ 7 nM of <u>100 nm CNT equivalents</u>

A_{575} @ 1mm = 0.1 so A_{575} @ 1cm = 1.0

60 µM Carbon Atoms

60 µM/8800 = ~0.0070 µM

Or 7 nM of 100 nm CNT equivalents

Mica deposition times of origami onto mica substrates:

1. CO-01 – 30 seconds
2. Diafiltered CO-01- 10 minutes
3. CO-01 + CNT – 2 minutes
4. CO-01 + Dialysis and Drop Dialysis CNT – 2 minutes
5. Diafiltered CO-01 + Dialysis and Drop Dialysis CNT – 15 minutes

APPENDIX D: LIST OF ABBREVIATIONS

6, 5-SWCNT….6, 5- single walled carbon nanotubes

0D CO-01…. Zero-dimensional single construct Cross Origami-01

1D CO-01…. first dimensional linear array Cross Origami-01

2D CO-01…. Second dimensional planar sheeted Cross Origami-01

Å…. Angstrom

ABTS….2,2'-azino-bis(3-ethylbenzothiazoline-6-sulfornic acid)diammonium salt

AFM…. atomic force microscopy

B-DNA…. Biotin ssDNA sequence

CD…. circular dichroism

CNT…. carbon nanotubes

CO-01…. Cross Origami-01

CO….Cross Origami

CO….Carbon monoxide

COB…. cross origami buffer/ and Tris-Acetate-EDTA/$MgCl_2$

COMOCAT…. cobalt molybdenum catalysis

Co-Mo/SiO_2…. cobalt molybdenum/silicon dioxide

DAB…. 3,3'-Diaminobenzidine

DMSO…. dimethyl sulfoxide

DNA…. deoxyribonucleic acid

DNAzyme…. G-quad/hemin complex

DO….DNA Origami

dsDNA…. double stranded DNA

EAD2…. G-quad of interest measuring 18 bases long

FRET….Fluorescence resonance energy transfer

G4…. G-quadruplex DNA

H_2O_2…. hydrogen peroxide

HA…. Harvard Apparatus

HBA….Hemin-binding aptamer

HIPCO…. high pressure carbon monoxide

HRP…. horseradish peroxidase

kDa…. kilo Dalton

KCl…. potassium chloride

KCOB…. potassium cross origami buffer

LA…. left arm

M13…. M13mp18 plasmid DNA

$MgCl_2$…. magnesium chloride

MWCNT…. multi-walled carbon nanotube

NaCl…. Sodium Chloride

Na_2HPO_4…. sodium phosphate dibasic

$NiCl_2$…. nickel chloride

nM…. 10^{-9} Molar

OD…. optical density

OE…. open ends

PPBT….poly[3-(potassium-4-butanoate) thiophene]

RA…. right arm

RNA…. ribonucleic acid

RCF….relative centrifugal force

SE…. sticky ends

ssDNA…. single stranded DNA

SWCNT…. single walled carbon nanotubes

T_{40}…. forty thymine ssDNA

$(TAT)_{10}$…. ten repeated sequences of thymine-adenine-thymine with one segment of an oligo

UV-VIS…. ultraviolet-visible

APPENDIX E: VITA

Kathryn A. Pitton
7 Pyramid Drive, # 704
Huntington, WV, 25705
(813) 389-9317
Kathrynpitton@gmail.com

May 2019

Education

August 2017- May 2019	Master of Science in Chemistry, Marshall University, Huntington, WV
January 2015- May 2017	Bachelor of Science in Chemistry, Florida Atlantic University, Boca Raton, FL
August 2010- December 2014	Bachelor of Science in Biology, Florida Atlantic University, Boca Raton, FL

Research

2017- Present **"**ORGANIZING 6, 5-SWCNT ONTO DNA ORIGAMI ARRAYS"

- Collaborators: Michael Norton, PhD; David Neff, MS.
- Research conducted at Marshall University Department of Chemistry as part of the requirement for the degree of Master of Science
- Funding: NSF Cooperative Agreement Number OIA-1458952.

Recent Presentations

Oral

March 2018	"Carbon Nanotube and Peroxidase Placement on DNA Origami" Presented to faculty and staff at Marshall University
April 2019	"Organizing 6, 5-SWCNT onto DNA Origami Arrays" Presented to faculty and staff at Marshall University

Poster

April 2019	"Multi-point Alignment of 6,5 Carbon Nanotubes on DNA origami Substrates" by Pitton, K.A.; Neff, D.; and Norton, M, PhD. Presented at ACS Spring 2019 National Meeting and Expo. Division of Colloid and Surface Chemistry. Fundamental research in Colloids, Surfaces, & Nanomaterials, Orlando, FL.
April 2019	"Multi-point Alignment of 6,5 Carbon Nanotubes on DNA origami Substrates" by Pitton, K.A.; Neff, D.; and Norton, M, PhD. Presented at ACS Spring 2019 National Meeting and Expo. Division of Colloid and Surface Chemistry. Sci-Mix, Orlando, FL.
April 2018	"Carbon Nanotube Placement on DNA Origami with Imaging and Characterization through Atomic Force Microscopy" by Pitton, KA; Neff, D.; and Norton, M, PhD. Presented at Marshall University College of Science industry day, Huntington, WV

February 2018	"Origami Platform for Optical Reporting" by Pitton, K.A.; Hensley, A; Neff, D; and Norton, M.L., PhD. Presented at the West Virginia University Institute of Water Security and Science Conference, Morgantown, WV